# Evaluation and Optimization of Dense Wireless Networks

Salman Malik

**THÈSE DE DOCTORAT DE**
**l'UNIVERSITÉ PIERRE ET MARIE CURIE**

Spécialité

**Informatique**

École doctorale Informatique, Télécommunications et Électronique (Paris)

Présentée par

**Salman MALIK**

Pour obtenir le grade de

**DOCTEUR de l'UNIVERSITÉ PIERRE ET MARIE CURIE**

Sujet de la thèse

# Evaluation et Optimisation des Réseaux Sans Fil Denses

devant le jury composé de

| | | |
|---|---|---|
| M. Philippe JACQUET | Bell Labs, Alcatel Lucent | Directeur de thése |
| M. Piyush GUPTA | Bell Labs, Alcatel Lucent | Rapporteur |
| M. Philippe ROBERT | INRIA Paris-Rocquencourt | Rapporteur |
| M. Jean WALRAND | UC Berkeley | Rapporteur |

**Evaluation and Optimization of Dense Wireless Networks**

**Abstract:** The main objective of this thesis is to analyze the performance of wireless networks under various scenarios: stationary, mobile, single-hop and multi-hop networks.
Our main focus in the first two parts of this thesis is on the geometric placement of simultaneous transmitters in the network.
In the first part, we study the impact of the placement of transmitters, by the medium access control scheme, on the performance of single-hop wireless network. We establish a general framework and study the optimal placement of transmitters in the network. Later we compare this optimal placement with placements obtained by random point processes such as Poisson point process, ALOHA, node coloring and CSMA. Our analysis allows us to evaluate the performance gains of a highly managed medium access control that would be required to implement the optimal placement of transmitters. For instance, we show that the capacity of this highly managed medium access control cannot be more than twice the capacity of a low managed medium access control such as ALOHA.
Later, we use analytical methods to evaluate the heuristics for optimizing the capacity and coverage in an existing cellular network by optimally locating additional base stations.
In the second part, we extend our analysis to multi-hop wireless network where we evaluate the optimum transmission range and network throughput capacity with various medium access control schemes. Our analyses in the first two parts of this thesis allow us to gain perspectives into the theoretical limits on the performance of an optimized medium access control in single-hop and multi-hop wireless network.
In the last part, we shift our focus to capacity-delay tradeoff in mobile wireless network. We propose a georouting scheme and study its scaling properties. Using a realistic mobility model and the information available at mobile nodes, our scheme achieves a delay which is bounded by a constant with network capacity that increases quasi-linearly when the number of nodes in the network increases and approaches infinity.
**Keywords:** wireless networks, mobile networks, cellular networks, medium access, ALOHA, node coloring, CSMA, routing, capacity, throughput, delay

# Contents

# Chapter 1

# Introduction

With increasing computing power and lowering costs of hardware, there has been an explosive growth in the number of devices that are equipped with wireless radios. Examples of these devices are mobile phones, laptops, computers, sensors, home appliances, consumer electronics, *etc*. Wireless radios allow these devices or nodes, as they are called in the terminology of computer networking, to form networks and communicate using electromagnetic waves, on the shared medium called *channel*, without the need of cables.

## 1.1 Types of Wireless Networks

Depending on the type of communication between nodes, wireless networks can be divided into two categories:

- single-hop wireless networks and
- multi-hop wireless networks.

In single-hop networks, nodes communicate with each other directly over one hop or, in other words, nodes only communicate with other nodes which are located within their respective neighborhoods. Examples of such networks are wireless networks which only allow nodes to send data to their destination nodes directly, *e.g.*, IEEE 802.11 wireless LANs where nodes communicate with Access Point (AP) or *smart home* networks or networks which consist of wired infrastructure as their backbone except the last hop which is wireless, *e.g.*, cellular data and voice networks and mobile IP. Figure 1.1 is an illustration of such networks.

Nodes in a network maybe spread in a large area and radio range of wireless nodes is limited which may not allow them to transmit data directly to their destinations. Therefore, nodes must use intermediate relays to deliver their data. Such networks are called multi-hop wireless networks where nodes not only transmit their own data but also serve as relay for other nodes. Examples are *ad hoc* and *mesh* networks. The ad hoc networking of wireless

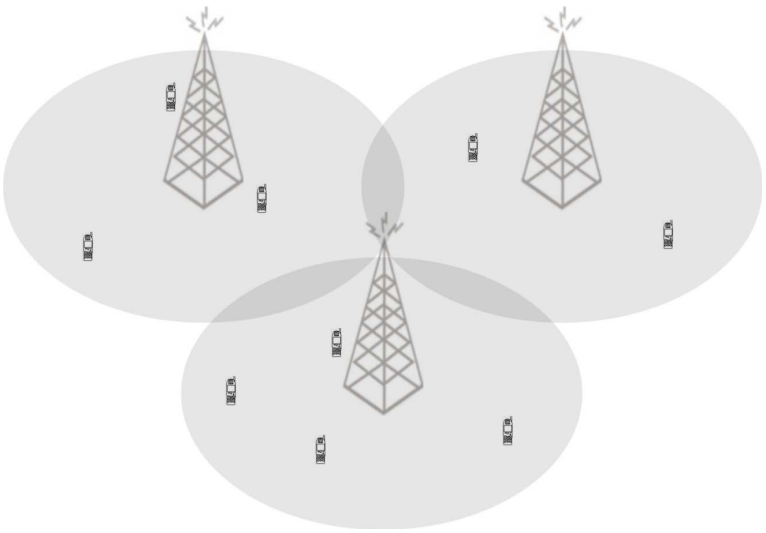

Figure 1.1: An illustration of the basic scheme of cellular (single-hop) networks. Base stations are connected via wired infrastructure and mobile phones connect with their respective base stations via wireless links.

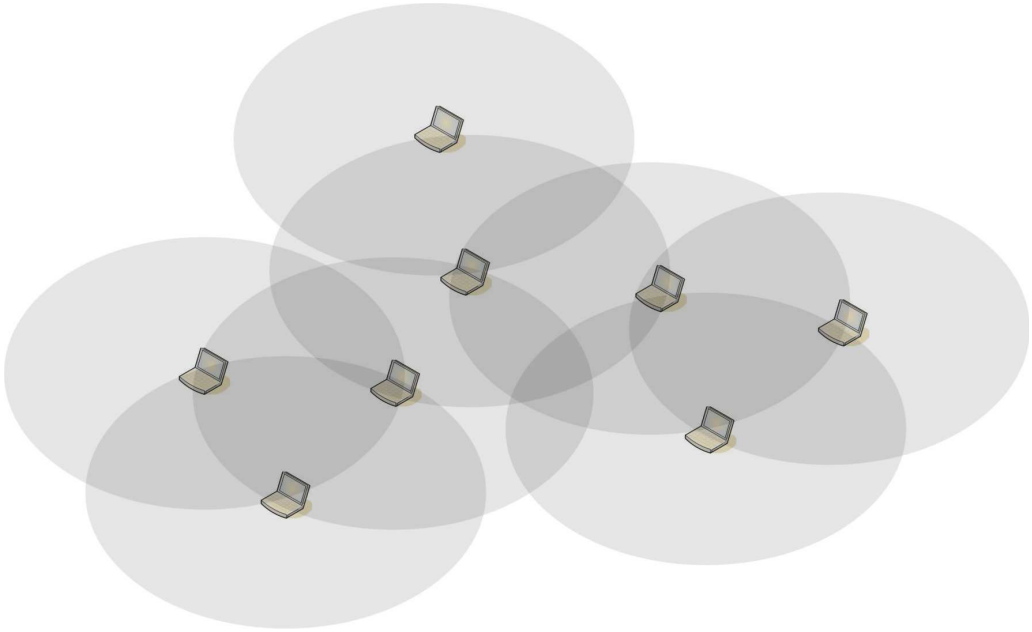

Figure 1.2: An illustration of ad hoc (multi-hop) networks.

devices lacks any wired infrastructure or a centralized coordinator to harmonize the access to the shared medium. Moreover, nodes can be *mobile* and therefore update their links to other nodes frequently and the network is self-configuring. In contrast, nodes in mesh networks are

usually *fixed* or *immobile* and are usually a part of a networking infrastructure. However, they also use multi-hop communication to transmit or relay data to their destination nodes. Figure 1.2 shows an example of multi-hop wireless ad hoc networks.

## 1.2 The Problem

The goal of designing medium access control (MAC) schemes or protocols for wireless networks is to allow nodes to efficiently share the channel. Simultaneous transmitters should be selected in such a way that improves the *spatial reuse* in the network, *i.e.*, the shared medium should be used simultaneously by transmitters which are spatially separated in such a way that they do not interfere with each other's transmissions. In other words, permanent spatial clustering of simultaneous transmitters should never occur in the wireless network. In order to achieve this goal, MAC schemes generally use an exclusion rule to prevent nodes which are located near to each other from transmitting simultaneously.

The task of designing MAC schemes can be a challenging problem because of the difficulties posed by various types of wireless networks. To name a few: dynamic network topology, lack of any centralized control, energy constraints, channel characteristics, mobility of nodes, radio hardware limits, *etc.* are some of the issues faced by network and protocol designers. These challenges influence the design and protocol overhead of MAC schemes in various ways, *e.g.*:

- protocol overhead to implement MAC schemes in various types of wireless networks, *e.g.*, intercommunication required between nodes for the distributed implementation of the protocol,
- scaling properties of the MAC scheme when the number of nodes in the network increases,
- energy efficiency, *e.g.*, minimizing the number of transmissions required for the functioning of the protocol, *etc*.

Therefore, the performance improvement by achieving higher degree of spatial reusability in wireless networks may come at a significantly higher design complexity, *e.g.*, additional protocol overhead, *etc.* or inefficient energy usage by nodes.

The choice of a MAC scheme also requires a deeper understanding of its performance. For example, frequency division multiple access (FDMA) achieves spectral separation of transmissions. However, scarcity of available wireless spectrum coupled with an insatiable desire of higher bandwidth makes the use of spectral separation techniques in large and dynamic wireless networks almost impractical because of the lack of any centralized control, limited available spectrum or inadequate achievable performance (*e.g.*, low capacity and/or high latency). Time division multiple access (TDMA) can improve the spatial reuse, resulting in better performance while sharing the same spectrum, but they are also complex to implement in networks

without centralized control. Code division multiple access (CDMA) assigns a code to each transmitter and allows multiple nodes to transmit simultaneously. However, its implementation in large networks maybe difficult because of the large number of required codes. In CDMA networks, the signal-to-noise plus interference ratio (SINR) is artificially augmented thanks to the rejection (of unwanted signals) properties of CDMA. Indeed this would be equivalent to considering a lower SINR threshold parameter than required. But since we consider general SINR threshold parameter, this is covered by the general framework of our thesis. Random access schemes like ALOHA and carrier sense multiple access (CSMA) may not require significant overhead but they may have their own drawbacks. For example, simple ALOHA may degrade the performance because a node transmits without any coordination with other transmitters. In order to minimize collisions, CSMA requires that a node senses the medium before transmission. This can result in higher performance but it is also more demanding on the physical layer. Moreover, a simple CSMA based scheme may suffer from problems like hidden node and exposed node problems.

In this thesis, the terminologies of MAC scheme and spatial distribution of simultaneous transmitters are strongly interlinked as we will use realistic models of various above mentioned MAC schemes to derive the accurate models of spatial distributions of simultaneous transmitters. These models should precisely capture how their corresponding MAC schemes allow nodes in the network to transmit on the channel. We will investigate the performance of various types of wireless networks with these models of spatial distributions of simultaneous transmitters and draw our conclusions for the design of efficient schemes and protocols for large and dynamic networks.

### 1.2.1 Single-hop Wireless Networks

Now the first question arises, what is the most optimal MAC scheme or the most optimal spatial distribution of simultaneous transmitters for single-hop wireless networks? This question needs to be answered to have a quantitative measure of the performance of various MAC schemes. We discussed in §1.2 that, in addition to performance, there are other issues as well to consider for the design and implementation of MAC schemes in wireless networks. Hopefully, our analyses will provide us with new insights into the performance of various MAC schemes and compliment the efforts of network or protocol designers in their investigation of the trade-offs involving these factors for designing new schemes for single-hop networks.

Cellular networks are also a type of single-hop networks where network area is divided into *cells* and each cell is served by a base station which is also responsible for the resource management, like bandwidth allocation, *etc.*, among the mobile phone users in that cell. Depending on the demographic distribution or non-uniform geographic distribution of users, base stations are positioned to avoid congestion at the locations of high density of users. However, the density of users may also change over time, *e.g.*, because of the development of a new commercial area *etc.* which may lead to congestion and insufficient available bandwidth. In other

words, the current bandwidth resources may not be able to sustain the increasing number of users anymore and this may require installation of new base stations in these areas. Therefore, we need to find where should be the most optimal positions for the additional base stations? This requires capacity and coverage dimensioning of the *area of interest* where additional base stations shall be placed.

### 1.2.2 Multi-hop Wireless Networks

Determining the *end-to-end* throughput capacity in multi-hop wireless networks with randomly distributed nodes is a challenging problem as nodes have to transmit their own data as well as act as a relay for the data of other nodes. If each node sends data to a randomly selected destination node, the article [Gupta & Kumar 2000] has already shown that, for a MAC scheme which allows spatial and temporal scheduling of simultaneous transmissions, the throughput capacity is $O(\sqrt{n/\log n})$[1] where $n$ is the number of nodes in the network. However, here we are also interested in quantifying the throughput capacity with various MAC schemes to find the most optimal MAC scheme for multi-hop networks. We expect that by analyzing the relationship between the spatial distributions of simultaneous transmitters and multi-hop throughput capacity, our results will also provide deeper insights for the designers of protocols for multi-hop networks.

### 1.2.3 Mobile Multi-hop Wireless Networks

So far, we have not discussed the packet delivery delay as it is almost *negligible* because, in networks with fixed nodes, packets are transmitted or relayed immediately like *hot potatoes*, *i.e.*, without delay between store and forward. The article [Grossglauser & Tse 2002] has shown that, by exploiting the mobility of nodes in the network, capacity can be increased to $O(n)$. However, this improvement in capacity comes with a significantly higher delay which scales as $O(\sqrt{n})$. There has been other studies to improve this capacity-delay tradeoff in wireless networks with mobile nodes but mostly with the models for the mobility of nodes which are not very realistic. We will discuss these works in detail in Chapter 2. In this work, we will see if we can benefit from a realistic model of the mobility of nodes and their geographic information to improve the capacity-delay tradeoff in mobile wireless networks.

## 1.3 Organization of this Thesis and Our Contributions

In this section, we will present the organization of thesis and our contributions.

[1] We recall the following notation: (i) $f(n) = O(g(n))$ means that there exists a constant $c$ and an integer $N$ such that $f(n) \leq cg(n)$ for $n > N$. (ii) $f(n) = \Theta(g(n))$ means that there exists two constants $c_1$ and $c_2$ and an integer $N$ such that $c_1 g(n) \leq f(n) \leq c_2 g(n)$ for $n > N$.

We will discuss some of the related works on performance analysis of MAC schemes in wireless networks in Chapter 2. In Chapter 3, we will discuss the network models that we will use in our analyses throughout this work. We will also discuss the models of various MAC schemes that we will use to derive the models of spatial distributions of simultaneous transmitters.

Rest of the thesis is divided into the following three parts.

### 1.3.1 Part 1: Single-hop Wireless Networks

In the first part, we will address the capacity in single-hop wireless networks.

In Chapter 4, we will introduce the concept of *local capacity* in single-hop wireless networks and evaluate it for various MAC schemes. We will also construct models of spatial distributions of simultaneous transmitters under various MAC schemes and our goal is to identify the most optimal scheme and also to see how does it compare with other, more practical MAC schemes like ALOHA, node coloring and CSMA based schemes.

In Chapter 5, we will develop an algorithm to find the locations of $K$ additional base stations in the area of interest to optimize capacity and coverage of an existing cellular network.

### 1.3.2 Part 2: Multi-hop Wireless Networks

In this part, we will extend our analysis to multi-hop wireless networks.

In Chapter 6, we will analyze the optimum normalized transmission range of various MAC schemes. Transmission range has an impact on the number of hops required to relay a packet to its destination and therefore its analysis is important to investigate the throughput capacity of multi-hop networks.

In Chapter 7, we will evaluate the throughput capacity of multi-hop wireless networks with various MAC schemes.

### 1.3.3 Part 3: Mobile Multi-hop Wireless Networks

In this part of the thesis, we will extend our analysis to networks with mobile nodes.

In Chapter 8, we will present a scheme where nodes exploit the knowledge of their own location and the location of the final destination and a realistic mobility model to achieve a capacity-delay tradeoff where average packet delivery delay is bounded and capacity scales *quasi-linearly* with increasing number of nodes in the network.

# Chapter 2

# Capacity of Wireless Networks

The assessment of the capacity of wireless networks is a challenging task and significant research efforts have been made to study this problem. The difficulty posed by this problem comes from the fact that it has to take into account the following three main aspects:

- propagation of electromagnetic waves through medium,
- geometry of wireless network, *i.e.*, the positioning of nodes in the network and
- extraction of information from received signals.

In this chapter, we will discuss some of the important related works and find out how they address the above mentioned aspects of this problem.

## 2.1 Capacity of Single-hop Wireless Networks

In one of the first analyses, the article [Nelson & Kleinrock 1984] studied the capacity of wireless network with slotted ALOHA and despite using a very simple geometric model for the reception of signals, the result is very similar to what can be obtained under a realistic SINR based interference model where a signal is received only if its SINR is above a desired threshold. Under a similar geometric model and assuming that all nodes are within range of each other, the article [Kleinrock & Tobagi 1975] evaluated CSMA scheme and compared it with slotted ALOHA in terms of throughput (bit-rate). The article [Blaszczyszyn *et al.* 2010] used simulations to analyze CSMA and compared it with ALOHA, both slotted and un-slotted. For simulations, the authors of this article assumed Poisson distributed transmitters with density $\lambda$. Each transmitter sends packets to its assigned receiver located at a fixed distance of $a\sqrt{\lambda}$, for some $a > 0$.

The articles [Weber *et al.* 2005, Weber *et al.* 2010] introduced the concept of *transmission capacity* which is defined as the maximum number of successful transmissions per unit area at

a specified *outage probability*, *i.e.*, the probability that the SINR at the receiver is below a certain threshold. The authors of these articles studied the transmission capacity of ALOHA and CDMA schemes under the assumption that simultaneous transmitters form a homogeneous Poisson point process and, as in the article [Blaszczyszyn *et al.* 2010], they also assumed that the receivers are located at fixed distance from their transmitters. The fact that the receivers are not a part of the network or node distribution model and are located at a fixed distance from their transmitters is a simplification. An accurate model of wireless network should consider that the transmitters, transmit to receivers which are randomly located within their neighborhood. Although, the article [Weber *et al.* 2005] also analyzed the case where receivers are located at a random distance but it was assumed that the transmitters employ transmit power control such that the signal power at their intended receivers is some fixed value.

Poisson point process can only accurately model an ALOHA based scheme where transmitters are independently and uniformly distributed in the network area. However, with MAC schemes based on exclusion rules, like node coloring or CSMA, modeling simultaneous transmitters as Poisson point process leads to an inaccurate representation of the distribution of signal level of interference. On the other hand, correlation between the location of simultaneous transmitters makes it extremely difficult to develop a tractable analytical model and derive the closed-form expression for the distribution of interference and probability of successful reception. Some of the proposed approaches are as follows. In Chapter 18 of the book [Baccelli & Blaszczyszyn 2009], the authors used a Matérn point process for CSMA scheme whereas the article [Busson & Chelius 2009] proposed to use Simple Sequential Inhibition (*SSI*) or an extension of *SSI* called $SSI_k$ point process. In articles [Hasan & Andrews 2007, Kaynia & Jindal 2008], simultaneous interferers are modeled as Poisson point process and outage probability is obtained by excluding or suppressing some of the interferers in the guard zone around a receiver. The article [Ganti *et al.* 2011] analyzed transmission capacity in networks with *general* node distributions under a restrictive hypothesis that density of interferers is very low and, asymptotically, approaches zero. The authors of this article derived bounds of high-SINR transmission capacity with ALOHA using Poisson point process and CSMA using Matérn point process. Other related works include the analysis of single-hop throughput and capacity with slotted ALOHA, in networks with random and deterministic node placement, and TDMA, in one-dimensional line-networks only, in the article [Haenggi 2009].

## 2.2 Capacity of Multi-hop Wireless Networks

Most of the works we have discussed so far, analyze the capacity of wireless network by taking into account only the simultaneous single-hop transmissions. However, when source and destination nodes are randomly distributed in the network area, packets are usually transported through multiple relays towards their respective destinations. Therefore, these analyses may not give an accurate assessment of the performance of wireless network using multi-hop com-

munication.

Though computing the end-to-end capacity of wireless network is an extremely challenging task because of the possible impact of routing protocol on the hop length and spatial distribution of simultaneous transmitters, there have been significant attempts to overcome the above mentioned limitations. In the seminal work of the article [Gupta & Kumar 2000], the authors used a spatial and temporal scheme for scheduling transmissions in the network and derived the scaling laws on the capacity when the number of nodes increases and approaches infinity. They showed that if nodes in the network transmit at constant rate, the effective radius of successful transmission scales as $O(1/\sqrt{n})$. Therefore, if nodes transmit to their nearest neighbors only, there can be $O(n)$ simultaneous transmissions in the network with bit rate per source-destination pair of $O(1)$ which is independent of $n$ and the network capacity scales as $O(n)$.

In case of multi-hop communication, Gupta & Kumar also introduced the concept of *transport capacity* which measures the sum of the end-to-end throughput of the network multiplied by the end-to-end distance and showed that if nodes are optimally located and traffic patterns are also optimally assigned, the network transport capacity scales as $O(\sqrt{n})$ or, in other words, bit-rate per source destination pair in multi-hop networks is upper bounded by $O(1/\sqrt{n})$. However, if nodes are randomly distributed, they showed that the throughput obtainable by each node for a randomly chosen destination drops to $O(1/\sqrt{n \log n})$ where the $\log n$ factor comes from the fact that the network must be connected or, in other words, at least one route or path must exist between all pairs of nodes *with high probability (w.h.p.)* which approaches one as $n$ approaches infinity. We can also obtain this result as follows. Let us assume that $p_n$ is the transmission rate of each node, *i.e.*, the proportion of time each node is active and transmitting. Therefore, the effective radius of transmission is given by

$$r_n = \sqrt{\frac{\kappa}{np_n}}\,, \tag{2.1}$$

when $n$ increases and approaches infinity, for some constant $\kappa > 0$ which depends on the protocol and physical layer parameters, interference model, *etc*. Therefore, the average number of relays a packet has to traverse to reach its destination will be $h_n = O(1/r_n)$. Consequently, $np_n$ must be divided by $h_n$ to get the useful network throughput capacity

$$\frac{np_n}{h_n} = O(\sqrt{p_n n})\,.$$

From the article [Gupta & Kumar 1998], we know that in order to ensure connectivity in a network, so that every source is able to communicate with its randomly chosen destination, $p_n$ must satisfy the limit

$$p_n \leq O\left(\frac{1}{\log n}\right)\,,$$

and this leads to Gupta & Kumar's throughput capacity of $O(\sqrt{n/\log n})$.

The articles [Xue & Kumar 2006, Franceschetti *et al.* 2007] have shown that, even in case of randomly distributed nodes, the throughput capacity in wireless network can be increased to an upper bound of $O(\sqrt{n})$ and the $\log n$ factor can be overcome by constructing a complex system of *highways* of nodes to transport data and using different transmission ranges for different transmissions. The authors of these articles used techniques from percolation theory to show that a system of horizontal and vertical highways can be formed in a network of randomly distributed nodes. Each highway is accessed by an $O(\sqrt{n})$ number of nodes and these highways can then use time sharing scheme to carry data over short hops (of length bounded by a constant) at constant bit-rate which gives the $O(1/\sqrt{n})$ rate of communication per node. Other nodes use single-hops of longer length of $O(\log \sqrt{n})$ when data is to be pushed on these highways or delivered from these highways to destination nodes. In other related works, the article [Baccelli *et al.* 2006] gave a detailed analysis on the optimal probability of transmission for ALOHA which optimizes the spatial density of progress, *i.e.*, the product of simultaneously successful transmissions per unit of space by the average range of each transmission. Instead of considering the average range of transmission, the authors of the article [Weber *et al.* 2008] proposed a variant where each transmitter selects its longest feasible edge and then identifies a packet in its buffer whose next hop is the associated receiver. Similarly, the article [Andrews *et al.* 2010] evaluated the random transport capacity of wireless network without taking into account any particular routing protocol and under the strong assumptions that simultaneous interferers form a Poisson point process and relays are equally spaced on a straight line between a source and its destination.

An important aspect of the multi-hop communication is the transmission range of a transmitter as it has an impact on the hop-length as well as the probability of successful transmission: both factors have critical impact on the capacity of multi-hop wireless network. There have been many studies on the transmission range under various constraints. For example, the article [Deng *et al.* 2007] studied the transmission range that achieves the most economical energy usage in an ad hoc network of uniformly distributed nodes. The works [Santi & Blough 2003, Santi 2005] analyzed the critical transmission range required for connectivity in stationary and mobile wireless ad hoc networks. The article [Takagi & Kleinrock 1984] determined the optimal transmission range of slotted ALOHA and CSMA schemes which maximizes the expected one-hop progress of a packet while considering the tradeoff between the probability of successful transmission and the progress of the packet. The authors assumed that all nodes use same transmit power and the range of transmission is controlled by tuning the density of simultaneous transmitters via parameters like probability of transmission (in case of ALOHA) and carrier sense threshold (in case of CSMA). The article [Zorzi & Pupolin 1995] determined the normalized optimum transmission range under the assumption that simultaneous interferers form a Poisson point process. In an important analysis in the article [Gomez & Campbell 2004], the authors studied the impact of variable transmission range, by controlling the transmit power, on network connectivity, capacity and energy efficiency. They showed that

routing in networks where transmitters have same transmission range can only achieve half of the traffic carrying capacity of networks where transmitters have variable transmission range.

## 2.3 Capacity of Wireless Networks with Multiple-Input-Multiple-Output Technology

The results we have discussed so far evaluate the capacity of wireless network by assuming that nodes are equipped with only one antenna and, at a time, a receiver can only receive data from one transmitter and signal from all other transmitters is considered as interference.

The communication performance in wireless network can be significantly improved by using multiple-input-multiple-output (MIMO) technology. The earliest ideas in this field were introduced in articles [Kaye & George 1970, Brandenburg & Wyner 1974] and further developed in works of [Paulraj & Kailath 1993, Foschini 1996, Telatar 1999]. Following these pioneering works, there have been many articles which improved on these ideas progressively and evaluated the performance of MIMO systems under various scenarios. Some of these analyses can also be found in articles like [Zheng & Tse 2003, Choi & Murch 2004, Chiani *et al.* 2010].

There can be two flavors of MIMO: *classical* MIMO and *cooperative* MIMO. In classical MIMO, nodes are equipped with multiple antennas and each transmitter uses *spatial multiplexing* to transmit multiple streams of data in parallel. This technology has been in use in standards like fourth generation (4G) Long Term Evolution (LTE) which are presented in detail in specifications [3GPP 2005, 3GPP2 2007], Worldwide Interoperability for Microwave Access (WiMAX) based on IEEE 802.16e in the specification [802.16e 2009] and IEEE 802.11 wireless LANs based on the specification [802.11n 2009]. The capacity of wireless network consisting of nodes using classical MIMO has been studied in articles like [Bölcskei *et al.* 2006, Chen & Gans 2006, Jiang *et al.* 2011], where the latest work extended the result of Gupta & Kumar and showed that the capacity scales as $O\left(m\sqrt{\frac{n}{\log n}}\right)$, where each node is equipped with $m$ antennas.

In the framework of pure *information theoretic* capacity, *i.e.* the *Shannon* capacity, information can be extracted from *all* parallel flows of data from simultaneous transmitters. The article [Jacquet 2009] evaluated the capacity in terms of information rate received by a randomly located node in a wireless network consisting of nodes distributed according to two dimensional $(2D)$ Poisson point process. In this article, the author assumed that the receivers are equipped with MIMO-like technology and, from the received signal, extract information of all parallel flows, generated (transmitted) by simultaneous transmitters in the network, at a rate depending on the SINR of each information flow. Under this assumption, the author showed that the received information rate depends only on the attenuation coefficient $\alpha > 2$ and is equal to $\frac{\alpha}{2}(\log 2)^{-1}$ bits per *Hertz*. Starting with the works of [Gupta & Kumar 2003, Xie & Kumar 2004], there has also been an interest in the information theoretic capacity scaling laws of wireless network and a steady stream of articles have been addressing this topic. Some

of these works can be found in articles like [Jovicic *et al.* 2004, Leveque & Telatar 2005, Ahmad *et al.* 2006]. In networks employing cooperative MIMO, nodes cooperate, by allowing to transmit (or receive) signal to (or from) multiple nodes, to deliver data to their destinations. Examples of various schemes using cooperative MIMO can be found in articles like [Aeron & Saligrama 2007, Ozgur *et al.* 2007, Niesen *et al.* 2009]. Using pathloss model for propagation of electromagnetic waves through medium and statistical fading models, all these articles present various bounds or scaling laws on information theoretic capacity of wireless network: some of these results show bit-rate per source-destination pair which decays to zero as the number of nodes in the network approaches infinity, others show slower decay and some are even able to show an *almost* constant bit-rate using schemes based on cooperative MIMO.

## 2.4 Capacity-Delay Tradeoff in Mobile Multi-hop Wireless Networks

In case of networks with immobile nodes, the packets are relayed immediately like *hot potatoes* and the packet delivery delay can be assumed negligible. So the question arises, what happens if nodes are allowed to move and how the mobility of nodes in the network has an impact on the capacity and delay? In the article [Grossglauser & Tse 2002], the authors showed that if nodes are mobile and follow *independent and identically distributed* (*i.i.d.*) ergodic motions in a square area, the throughput capacity can rise to $O(n)$ by using the mobility of nodes. Under their proposed *postman* routing scheme, a source node relays its packet to a random mobile relay node which transmits this packet to its destination node only when they come close together, *i.e.*, at a distance of $O(1/\sqrt{n})$. Therefore, the time it takes to deliver a packet to its destination would be $O(\sqrt{n}/v)$ where $v$ is the average speed of nodes. In contrast, in the analysis of Gupta & Kumar, where nodes are considered to be immobile, the packet delivery delay tends to be negligible because the packets are relayed toward their respective final destinations like *hot potatoes* but the network throughput capacity is also lower by a factor of $\sqrt{n \log n}$. It is also interesting to note that the article [Diggavi *et al.* 2005] showed that a constant throughput capacity per source-destination pair is also feasible even with a more restricted mobility model, *i.e.*, when nodes are allowed to move along line segments only.

The main difference between the proposed models in the works of Gupta & Kumar and Grossglauser & Tse is that, in the former case, nodes are immobile or static and packets are transmitted between nodes like *hot potatoes* while, in the latter case, nodes are mobile and relays are allowed to carry buffered packets while they move. Earlier, in this chapter, we discussed the result of Gupta & Kumar and also discussed their result on throughput capacity in multi-hop networks under the condition that the network must remain connected. In contrast, in the context of Grossglauser & Tse, the network does not need to be connected as the packets are mostly carried in the buffer of a mobile relay. Therefore, there is no limit on $p_n$ other than the requirement that it must be smaller than some $\varepsilon < 1$ that depends on the protocol and some

other physical parameters. Thus, in this case, $r_n$ is $O(1/\sqrt{n})$. In the first step of Grossglauser & Tse's *postman* routing scheme, the source transmits its packet to the closest mobile relay or keeps it until it finds one. In the second step, this mobile relay delivers the packet to its destination when it comes within range of the destination node. Such a packet delivery requires a transmission phase which also includes retries and acknowledgements so that the packet delivery can be eventually guaranteed. The proposed model of Grossglauser & Tse should require a positing system like global positioning system (GPS) and the knowledge of the effective transmission range $r_n$. The estimate of $r_n$ could be achieved via a periodic beaconing from each node. Each beacon also contains the position coordinates of its transmitter and any other node, on receiving this beacon, knows the typical distance for a successful reception. However, a relay cannot rely on beaconing in order to detect when it is in the reception range of the destination. The reason is that a node stays in the reception range of another node for a short time period of order $r_n/v = 1/\sqrt{n}$ and this cannot be detected via a periodic beaconing with bounded frequency since $p_n = O(1)$. In fact, the frequency of periodic beaconing should be of $O(\sqrt{n})$. We may also assume that the destination node is fixed and its cartesian coordinates are known by the mobile relays. Otherwise, if the destination node is mobile, there would be a requirement for this node to track its own coordinates and disseminate this information in the network. Some of these ideas are also proposed in articles like [Stojmenovic 1999, Li *et al.* 2000].

In our work, we will propose a *georouting* scheme and study the scaling properties of its capacity and delay characteristics. We will show that the packet delivery delay of our scheme is bounded by $O(1/v)$ and throughput per source-destination pair is $O\big(\frac{1}{\log n \log\log n}\big)$. The authors of the article [Gamal *et al.* 2004] also studied the throughput-delay tradeoff in wireless networks. If we take the notation of $\sqrt{a(n)}$ in their work to measure the average distance traveled toward the destination between two consecutive transmissions of the same packet, we will show that our scheme yields $\sqrt{a(n)} = \Theta(1/\log n)$. If we compare this with their result, we should have a throughput of $\Theta\big(\frac{1}{\log n\sqrt{n}}\big)$ but our scheme delivers a higher throughput by a factor of $\sqrt{n}\log\log n$. In fact, if $\ell$ is the average free space distance of the random walk, then our scheme yields $\sqrt{a(n)} = \Theta\big(\frac{1}{1/\ell+\log n}\big)$. The apparent contradiction comes from the fact that they consider a mobility model based on brownian motion. This corresponds to having $\ell = 0$ and, in this case, our scheme would be equivalent to the *hot potatoes* routing of Gupta & Kumar with $\sqrt{a(n)} = \Theta(r_n)$. Let us point out that the brownian motion mobility is an important yet worst case model and it is not realistic for mobility in real world situations such as urban area mobile networks. Throughput and delay trade-offs have also appeared in other articles as well. However, to improve delay at the expense of capacity, most of these works propose schemes that use *redundancy* where a packet is relayed to more than one node before a copy arrives at the destination. The article [Toumpis & Goldsmith 2004] assumes that nodes move according to an *i.i.d.* ergodic mobility model and proposed two schemes that also use redundancy. In the first scheme, the authors showed that, for a bounded delay, capacity of $O(n^{-\frac{1}{2}}(\log n)^{-\frac{3}{2}})$ per source-destination pair is achievable and, in the second scheme, for de-

lay bounded by $O(n^{\varepsilon})$, it can rise to $O(n^{\frac{(\varepsilon-1)}{2}}(\log n)^{-\frac{5}{2}})$ where $0 < \varepsilon < 1$. The article [Neely & Modiano 2005] also proposed redundancy schemes in cell partitioned network setting with nodes moving according to *i.i.d.* mobility model and showed a throughput and delay tradeoff of: $delay/throughput \geq O(n)$. The authors of this article proposed three schemes that can achieve throughput per source-destination pair of $O(1)$, $O(1/\sqrt{n})$ and $O(n^{-1}(\log n)^{-1})$, for delays of $O(n)$, $O(\sqrt{n})$ and $O(\log n)$ respectively. Under a less restrictive network setting and similar mobility model, the article [Lin & Sharrof 2004] achieved better tradeoff and showed that for bounded delay, throughput per source-destination pair can be $O(n^{-1}(\log n)^{-3})$.

Note that, on the practical side, many protocols have been proposed for multi-hop wireless networks. These protocols may be classified into topology-based and position-based protocols. In topology-based protocols, some of which are discussed in articles like [Perkins & Belding-Royer 1999, Haas *et al.* 2002, Clausen & Jacquet 2003], there is a need to maintain information on routing tables and these protocols may not work efficiently in environments with high frequency of topology changes. For this reason, there has been an increasing interest in position-based geographic routing protocols. In these protocols, a node needs to know its own position as well as the positions of its one-hop neighbors and its destination node. These protocols do not need control or management packets to exchange information about link statuses or to update routing tables. Examples of such protocols can be found in articles like [Hou & Li 1986, Navas & Imielinski 1997, Ko & Vaidya 1998, Basagni *et al.* 1998, Kranakis *et al.* 1999, Karp & Kung 2000]. However, in contrast to our work, these works do not study the scaling properties of capacity and packet delivery delay in the network and their trade-off under these protocols.

# Chapter 3

# Medium Access Control Schemes in Wireless Networks

Modeling of wireless channel interference is the most crucial step required for the performance analysis of wireless networks. An important factor that influences the statistics of interference is the geometry of simultaneously transmitting nodes, *i.e.*, the spatial distribution of simultaneous transmitters which in turn depends on the MAC scheme employed by nodes in the network. In other words, in order to accurately model interference with various MAC schemes, it is important to derive accurate models of the distributions of simultaneous transmitters that precisely capture how various MAC schemes allow nodes in the network to transmit on the channel.

In this chapter, first we will present our models and assumptions we have used throughout this thesis. Later, we will also discuss various MAC schemes and use their sufficiently accurate models to arrive at the spatial distributions of simultaneous transmitters with these schemes.

## 3.1 Models and Assumptions

In this section, we will discuss the models that we will use throughout this thesis.

### 3.1.1 Timing Model

MAC schemes in wireless networks can be divided into two categories: continuous time access and slotted access. In order to simplify our analysis and cope with the difficulties introduced by the continuous time medium access, our main focus in this work will be on the slotted medium access although many of our results can be applied to continuous time medium access as well.

In slotted medium access, time is divided into slots of equal duration and we consider an ideal timing model, operating with the following assumptions:

– nodes are synchronized,

– transmissions begin at the start of the slot,

– packets are of equal length and

– packet transmission time is equal to one slot.

Note that, in our timing model, we have assumed that the propagation delays, *i.e.*, the time it takes for the signals to travel from the transmitters to the receivers are negligible.

Within slotted medium access category, we distinguish slotted ALOHA, node coloring, CSMA and grid pattern based MAC schemes.

### 3.1.2 Network Model

Unless otherwise specified, we will consider a wireless network where nodes are uniformly distributed with density $\nu$ in a two-dimensional $(2D)$ area $\mathcal{A}$ with center at origin $(0,0)$. We denote the set of all nodes in the network by $\mathcal{N}$ and $n$ is the number of elements in this set. Note that, in practical scenarios and for simulation purposes, the network area $\mathcal{A}$ and the set $\mathcal{N}$ are finite but for theoretical analysis, the set $\mathcal{N}$ can be infinite but distributed with a uniform density $\nu$ in an infinite plane $\mathbb{R}^2$, *i.e.*, $\mathcal{A} = \mathbb{R}^2$.

In slotted medium access, at any given slot, simultaneous transmitters in the network are distributed like a set of points

$$\mathcal{S} = \{\mathbf{z}_1, \mathbf{z}_2, \ldots, \mathbf{z}_k, \ldots\} ,$$

where $\mathbf{z}_i \in \mathcal{A}$ is the location of transmitter $i$ and $\mathbf{z}_i = (x_i, y_i)$. The spatial distribution of simultaneous transmitters, *i.e.*, the set $\mathcal{S}$ depends on the MAC scheme employed by nodes. Therefore, we will not adopt any *universal* model for the locations of simultaneous transmitters and only assume that, in all slots, the set $\mathcal{S}$ has a spatially homogeneous density equal to $\lambda$.

### 3.1.3 Propagation Model

The channel gain between an arbitrary transmitter $i$ and a receiver located at point $\mathbf{z} \in \mathcal{A}$ is denoted by $\gamma_i(\mathbf{z})$, such that the received power at the receiver is $P_i\gamma_i(\mathbf{z})$.

We have the following expression for the channel gain $\gamma_i(\mathbf{z})$

$$\gamma_i(\mathbf{z}) = \frac{F_i(\mathbf{z})}{\|\mathbf{z} - \mathbf{z}_i\|^{\alpha}} , \tag{3.1}$$

where $F_i(\mathbf{z})$ is the *fading factor* which is a random variable that represents the variation in channel gain between transmitter $i$ and the receiver located at point $\mathbf{z}$, $\|\mathbf{z} - \mathbf{z}_i\|$ is the Euclidean distance between the transmitter and the receiver and $\alpha > 2$ is the attenuation coefficient.

The variation in channel gain $F_i(\mathbf{z})$ has two components:

– *fast* fading and

– *slow* fading or shadowing effects.

We assume that the value of $F_i(\mathbf{z})$ remains constant over the duration of a slot. However, it varies from slot to slot and, for the signal from transmitter $i$ to the receiver located at point $\mathbf{z}$, there will be correlation between these varying values because of the shadowing effects and, in this case, the mean value of $F_i(\mathbf{z})$ will be less than one. In this thesis, we will ignore the shadowing effects and we will consider that $F_i(\mathbf{z})$ is an *i.i.d.* random variable which is independent of the position of the transmitter and the receiver. We will also assume that it is independent of the distance between them which is a simplification. Therefore, we can drop the subscript and the argument $\mathbf{z}$ and denote $F \equiv F_i(\mathbf{z})$. For the probability distribution of $F$, we will consider the following two cases:

1. *no fading:* $F$ is constant and equal to one,

2. *Rayleigh fading:* $F$ is an *i.i.d.* random variable with an exponential distribution of mean equal to one.

### 3.1.4 Transmission Model

We consider that all nodes are equipped with only one antenna and the transmission from transmitter $i$ to a receiver located at point $\mathbf{z}$ is successful if and only if the following condition is satisfied

$$\frac{P_i \gamma_i(\mathbf{z})}{N_0 + \sum\limits_{j \neq i, \mathbf{z}_j \in \mathcal{S}} P_j \gamma_j(\mathbf{z})} \geq \beta \,, \tag{3.2}$$

where $N_0$ is the background noise (ambient/thermal) power which is assumed equal to zero and $\beta$ is the minimum SIR threshold required for successfully decoding the packet.

We consider that all transmitters transmit at the same unit nominal transmit power, *i.e.*,

$$P_i = 1 \,,$$

for $i = 0, 1, 2, \ldots, k, \ldots$.

Note that, here we have ignored the inter-symbol interference (ISI) caused by echoes which may allow the above condition to be satisfied but the packet may still be non-decodable at the receiver.

The ISI can be mitigated using *guard periods* and/or adaptive equalization at the receivers however, this is beyond the scope of this thesis and we will ignore its impact on whether the transmission can be received successfully or not.

Therefore, the SIR of transmitter $i$ at any point $\mathbf{z}$ is given by

$$S_i(\mathbf{z}) = \frac{\gamma_i(\mathbf{z})}{\sum\limits_{j \neq i, \mathbf{z}_j \in \mathcal{S}} \gamma_j(\mathbf{z})}\,, \tag{3.3}$$

where $\gamma_i(\mathbf{z})$ is given by (3.1).

### 3.1.5 Node Model

We consider that each node has a buffer which contains packets and a node transmits a packet from its buffer when it is allowed by its MAC layer to transmit on the channel. However, if no packet is available in the buffer, the node transmits a HELLO packet or a *junk* packet of length such that its transmission time is equal to the duration of a slot.

In case of single-hop networks, we will discuss further details of our model in §4.1.

Note that, in case of multi-hop networks, each node generates packets in its buffer which are to be transmitted to a randomly selected destination node and packets may have to be routed through multiple relays to reach their destinations. Therefore, the buffers may also carry the routed packets. The details of our model for multi-hop networks can be found in §7.1.

## 3.2 Slotted ALOHA Scheme

In slotted ALOHA based MAC scheme, nodes do not use any complicated managed transmission scheduling and transmit their packets independently of each other with a certain medium access probability. In this section, we will describe the model of slotted ALOHA and later we will also discuss our strategy to evaluate it.

### 3.2.1 High-Level Specification of the Scheme

Note that, for the purpose of evaluation and simulations of the MAC schemes, we will only describe a high-level specification of the protocols where we will omit the packet management and other issues related to synchronization and distributed implementation of protocols.

In case of slotted ALOHA scheme, we denote the probability of medium access by $p$ and for the construction of the set of simultaneous transmitters $\mathcal{S}$ in each slot, we will use the following model.

1. We denote the set of all nodes, which have a packet to transmit, by $\mathcal{M}$. Under our assumption that each node has a packet in its buffer ready to be transmitted or, otherwise, it transmits a HELLO or junk packet, we can initialize $\mathcal{M} = \mathcal{N}$ and $\mathcal{S} = \emptyset$.

2. Randomly select a node $i$ from $\mathcal{M}$ and toss a coin independently with bias $p$. If the outcome is *heads*, add the node $i$ to the set $\mathcal{S}$, *i.e.*,

$$\mathcal{S} = \mathcal{S} \cup \{\mathbf{z}_i\} .$$

3. Remove node $i$ from the set $\mathcal{M}$.

4. If set $\mathcal{M}$ is non-empty, repeat from step 2.

### 3.2.2 Model for Analytical Evaluation

In case of slotted ALOHA scheme, the set of simultaneous transmitters $\mathcal{S}$ in each slot can be given by a uniform Poisson distribution of mean equal to $\lambda$ transmitters per unit square area as is also the case in articles [Baccelli *et al.* 2006, Jacquet 2009, Weber *et al.* 2010].

Note that the evaluation of slotted ALOHA will be discussed in detail in §4.2, for single-hop networks, and in §6.3 and §7.2.1, for multi-hop networks.

## 3.3 MAC Schemes Based on Exclusion Rules

In this section, first we will discuss the models of MAC schemes based on exclusions rules and later we will discuss our strategy to evaluate these schemes.

### 3.3.1 High-Level Specification of the Schemes

Here we will discuss the models of the following MAC schemes:

- node coloring scheme where the exclusion rule is based on distance and
- CSMA based scheme where the exclusion rule is based on signal levels.

#### 3.3.1.1 Node Coloring Schemes

Node coloring schemes use a managed transmission scheme based on TDMA approach. The aim is to minimize the interference between transmissions that cause packet loss. These MAC schemes assign colors to nodes that correspond to periodic slots, *i.e.*, nodes that satisfy a spatial condition, either based on physical distance or distance in terms of number of hops, will be assigned different colors. This condition is usually derived from the interference models of wireless networks such as unit disk graph (UDG) models. For example, in order to avoid collisions at receivers, all nodes within $k$ hops are assigned unique colors where the typical value of $k$ is 2. A few practical implementations of node coloring schemes are as follows. In the article [Ramanathan 1997], authors proposed coloring based on RAND, MNF and PMNF

algorithms. In RAND, nodes are colored in a random order whereas MNF and PMNF prioritize nodes according to the number of their neighbors. NAMA protocol in the article [Bao & Garcia-Luna-Aceves 2001] colors nodes, in 2-hop neighborhood, randomly using a hash number. In SEEDEX, proposed in the article [Rozovsky & Kumar 2001], nodes use random seed number in 2-hop neighborhood to randomly elect the transmitter. FPRP protocol in the article [Zhu & Corson 2001] is a five-phase protocol where nodes contend to allocate slots in 2-hop neighborhood. DRAND is the distributed version of RAND and the article [Rhee *et al.* 2009] showed its better performance as compared to SEEDEX and FPRP. The article [Vergados *et al.* 2010] proposed a joint TDMA scheduling/load balancing algorithm for wireless multi-hop networks and shows that it can improve the performance in terms of multi-hop throughput and fairness. Most of these MAC schemes use unit disk graph based interference model. However, success of a transmission depends on whether the signal-to-interference plus noise ratio SINR at the receiver is above a certain threshold. Recently proposed, the protocol in the article [Derbel & Talbi 2010] is an example of a node coloring scheme which uses SINR based interference model. Note that extremely managed transmission scheduling in node coloring schemes has significant overhead, *e.g.*, because of the control traffic or message passing required to achieve the distributed algorithms that resolve color assignment conflicts.

In this work, instead of considering any particular scheme, we will present a model which ensures that transmitters use an exclusion distance in order to avoid the use of the same slot within a certain distance. This exclusion distance is defined in terms of euclidean distance $d$ which may be derived from the distance parameter of a typical TDMA-based protocol. Therefore, a slot cannot be shared within a distance of $d$ or, in other words, nodes transmitting in the same slot shall be located at a distance greater or equal to $d$ from each other.

Following is a model of node coloring schemes which constructs the set of simultaneous transmitters $\mathcal{S}$ in each slot. This is supposed to be done off-line so that transmission patterns periodically recur in each slot.

1. Initialize $\mathcal{M} = \mathcal{N}$ and $\mathcal{S} = \emptyset$.
2. Randomly select a node $i$ from $\mathcal{M}$ and add it to the set $\mathcal{S}$, *i.e*,
$$\mathcal{S} = \mathcal{S} \cup \{\mathbf{z}_i\} .$$
3. Remove node $i$ from the set $\mathcal{M}$.
4. Remove all nodes from the set $\mathcal{M}$ which are at distance less than $d$ from $i$.
5. If set $\mathcal{M}$ is non-empty, repeat from step 2.

Above described steps model a node coloring scheme that may have a centralized or distributed implementation and *randomly* selects nodes for coloring while satisfying the constraints of Euclidean distance. Under given constraints, this model selects all possible nodes

that can transmit simultaneously in each slot and should give the maximum capacity achievable with any node coloring scheme which *may not* prioritize nodes for coloring, *e.g.*, the DRAND protocol in the article [Rhee *et al.* 2009].

#### 3.3.1.2 CSMA Based Schemes

As compared to managed transmission schemes like node coloring, CSMA based schemes are simpler but are more demanding on the physical layer because, before transmitting on the channel, a node verifies if the medium is idle by sensing the signal level. If the detected signal level is below a certain threshold, medium is assumed idle and the node transmits its packet. Otherwise, it may invoke a random back-off mechanism and wait before attempting a retransmission. CSMA/CD (CSMA with collision detection) and CSMA/CA (CSMA with collision avoidance), which is also used in IEEE 802.11, are the modifications of CSMA for performance improvement. This is discussed in more detail in the book [Tanenbaum 2002].

We will adopt a model of CSMA based scheme where nodes contend to access medium at the beginning of each slot. In other words, nodes transmit only after detecting that medium is idle. We assume that nodes defer their transmission by a tiny back-off time, from the beginning of a slot, and abort their transmission if they detect that medium is not idle. We also suppose that detection time and receive to transmit transition times are negligible and, in order to avoid collisions, nodes use randomly selected (but different) back-off times. Therefore, the main effect of back-off times is in the production of a random order of nodes in competition.

For the evaluation of the performance of wireless networks with CSMA based scheme, we will use the following simplified construction of the set of simultaneous transmitters $\mathcal{S}$.

1. Initialize $\mathcal{M} = \mathcal{N}$ and $\mathcal{S} = \emptyset$.
2. Randomly select a node $i$ from $\mathcal{M}$ and add it to the set $\mathcal{S}$, *i.e.*,
$$\mathcal{S} = \mathcal{S} \cup \{\mathbf{z}_i\} .$$
3. Remove node $i$ from the set $\mathcal{M}$.
4. Remove all nodes from the set $\mathcal{M}$ which can detect a combined interference signal of power higher than the carrier sense threshold $\theta_{cs}$ from all transmitters already added to the set $\mathcal{S}$. For example, in the propagation model described in §3.1.3, if
$$\sum_{\mathbf{z}_i \in \mathcal{S}} \frac{F_i(\mathbf{z}_j)}{\|\mathbf{z}_i - \mathbf{z}_j\|^\alpha} \geq \theta_{cs} , \tag{3.4}$$
then remove node $j$ from $\mathcal{M}$.
5. If set $\mathcal{M}$ is non-empty, repeat from step 2.

These steps model a CSMA based scheme which requires that transmitters do not detect an interference of signal level equal to or higher than $\theta_{cs}$, during their back-off periods, before transmitting on the medium. At the end of the construction of set $\mathcal{S}$, some transmitters may experience interference of signal level higher than $\theta_{cs}$. However, this behavior is in compliance with a realistic CSMA based scheme where nodes, which started their transmissions, or, in other words, are already added to the set $\mathcal{S}$ do not consider the increase in signal level of interference resulting from later transmitters.

### 3.3.2 Model for Analytical Evaluation

We discussed in Chapter 2 that an accurate model of interference distribution, in case of exclusion schemes, is very hard to derive because of the correlation in the locations of simultaneous transmitters, *e.g.*, simultaneous transmitters separated by a certain minimum distance. We also mentioned a few approaches to model distribution of transmitters in exclusion schemes including Matérn point process in articles [Baccelli & Blaszczyszyn 2009, Ganti *et al.* 2011] or *SSI* point process in the article [Busson & Chelius 2009]. Classical Matérn point process is a location dependent thinning of Poisson point process such that the remaining points are at least at a certain distance $b > 0$ from each other. Instead of using distance, the approaches of Baccelli & Blaszczyszyn and Ganti *et al.* used received power level, a function of distance, in order to model CSMA based schemes. However, Busson & Chelius showed that Matérn point process may lead to an underestimation of the density of simultaneous transmitters and proposed an *SSI* point process in which a node can transmit or, in other words, can be added to the set of simultaneous transmitters $\mathcal{S}$ if it is at least at a certain distance $b > 0$ from all active transmitters (*i.e.*, the transmitters already in the set $\mathcal{S}$). *SSI* point process can be used to study node coloring schemes but may result in a flawed representation of the distribution of simultaneous transmitters with CSMA based schemes. In case of CSMA based schemes, a node senses the medium to detect if the signal level of interference is below a certain threshold and only transmits if it remains below that threshold during the randomly selected back-off period. Therefore, the *decision* of transmission depends on all nodes which are already active and transmitting on the medium. In order to address this inaccuracy of *SSI* point process model, Busson & Chelius also proposed an $SSI_k$ point process which ensures that a node, before transmitting on the medium, takes into account the interference from $k$ nearest active transmitters. In contrast, our model of CSMA takes into account the interference from all active transmitters. It is also relevant to mention that very few analytical results are available on *SSI* and $SSI_k$ point processes and most of the results are obtained via simulations.

In this work, we will evaluate the exclusion rules based MAC schemes by using a combination of analytical methods, described in Chapter 4 and 7, with Monte Carlo simulations of the models described in §3.3.1. We will chose the density of nodes or the set of nodes in the network, *i.e.* the set $\mathcal{N}$, such that no more active transmitters can be added to the set $\mathcal{S}$ after saturation. In other words, the point process of set $\mathcal{S}$ is independent of the point process of set

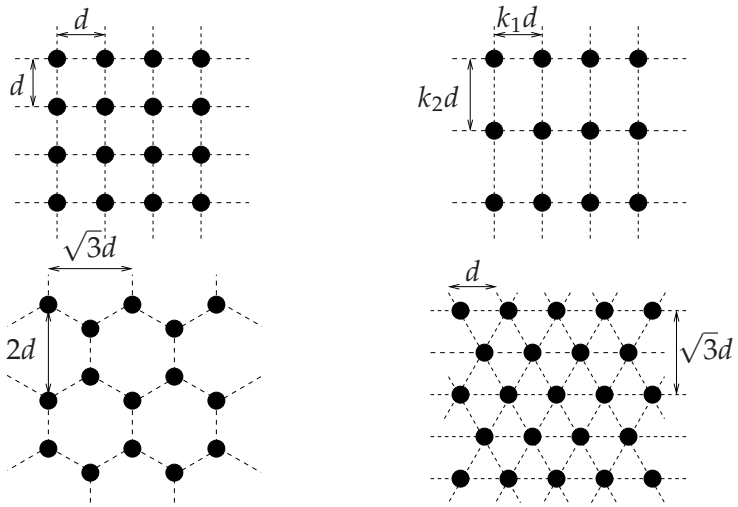


Figure 3.1: Square, Rectangular, Hexagonal and Triangular grid patterns. Note that $\frac{k_1}{k_2} < 1$.

$\mathcal{N}$.

We will discuss in detail the evaluation of these schemes in §4.3, for single-hop networks, and in §7.2.2, for multi-hop networks.

## 3.4 Grid Pattern Based Schemes

It can be argued intuitively that a good MAC scheme should optimize the spatial reuse by positioning the simultaneous transmitters in a regular grid pattern. Evaluation of grid pattern based MAC schemes is interesting as they can provide an *ideal* upper-bound on the performance, *e.g.*, under *no fading* channel model. However, their implementation is difficult because of the following reasons:

- limitations introduced by wave propagation characteristics like shadowing effects and
- irregular distribution of nodes (however, simultaneous transmitters can be base stations in cellular networks and their placement can be optimized).

In wireless networks, location aware nodes may be useful and if the node density is high, simultaneous transmitters can be selected in such a way that they closely resemble an ideal grid pattern. However, specification of a distributed MAC scheme that would allow grid pattern based positioning of simultaneous transmitters is beyond the scope of this thesis.

### 3.4.1 High-Level Specification of the Schemes

We consider the following model for the grid pattern based schemes. The set of nodes $\mathcal{N}$ is divided into $k$ partitions such that each partition is a grid (or closely resembles a grid) with

parameter $d$. The transmission process is a *round robin* scheduling on the $k$ partitions, *i.e.*, in each slot, a partition is randomly selected and all nodes in that partition transmit simultaneously. Note that the parameter $d$ defines the minimum distance between neighboring transmitters and it can be derived from the hop-distance parameter of a typical TDMA protocol. In our analyses, we have covered grid layouts of square, rectangle, hexagonal and triangle which are shown in Fig. 3.1.

Instead of handling the complication of the above described pattern fitting process that converges very slowly, we have devised the following strategy to evaluate grid pattern based schemes. We consider that the set $\mathcal{S}$ is a set of points arranged in a regular grid pattern. The basic mechanism for the construction of the set of simultaneous transmitters $\mathcal{S}$ under a grid pattern based scheme, in a network with randomly distributed nodes, is outlined in the following steps.

1. Initialize $\mathcal{M} = \mathcal{N}$ and $\mathcal{S} = \emptyset$.
2. Randomly select a node $i$ from $\mathcal{M}$ and add it to the set $\mathcal{S}$, *i.e.*,
$$\mathcal{S} = \mathcal{S} \cup \{\mathbf{z}_i\} .$$
3. Remove node $i$ from the set $\mathcal{M}$.
4. From the position of node $i$, construct a *virtual* grid pattern with parameter $d$. This virtual grid pattern should be one of the patterns we have mentioned above and it is also randomly rotated about the location of node $i$.
5. All nodes which overlap the points of the virtual grid, constructed in the above step, shall be added to the set $\mathcal{S}$.

For the theoretical analyses, we can assume that the density of nodes in the network is high and the points of the virtual grid always overlap existing nodes. However, for practical purposes and simulations, this may not be the case. Therefore, we will devise a scheme to distribute nodes uniformly in the network in such a way that the points of the virtual grid always overlap existing nodes. We will describe this model for the distribution of nodes, in case of simulations of grid pattern based schemes, in detail in §7.1. Note that the above steps are repeated in each slot to construct the set of simultaneous transmitters $\mathcal{S}$ and, in each slot, the virtual grid pattern is the same *modulo* a translation and/or rotation.

We will also discuss the evaluation strategy of grid pattern based schemes in more detail in §4.4, for single-hop wireless networks, and in §6.4 and §7.2.3, for multi-hop networks.

### 3.4.2 Model for Analytical Evaluation

We will discuss all analytical aspects of grid pattern based schemes in Chapter 4 where we will discuss the concept of reception areas and compute these areas using a numerical method

based on the demarcation of their boundaries. We will also introduce the model to compare these reception areas when the set of simultaneous transmitters are arranged in a grid pattern to when they are arbitrarily distributed and when continuous transformations are applied to the grid pattern.

# Part I

# Single-hop Wireless Networks

# Chapter 4

# Local Capacity in Wireless Networks

In this chapter, we will introduce a metric for the performance evaluation of wireless networks known as local capacity. Under the framework of local capacity, we quantify the average information rate received by a receiver node randomly located in the network. We will first discuss the mathematical model and the analytical tools and then apply these techniques to a wireless network to derive the local capacity of various MAC schemes discussed in Chapter 3 under *no fading* channel model. Our goal is to identify the most optimal scheme and also to see how does it compare with other schemes. Later, we will also discuss the impact of channel fading on the local capacity of various MAC schemes.

## 4.1 Model and Assumptions

In this chapter, we will consider a wireless network where nodes are uniformly spread in the network area $\mathcal{A}$.

We call the reception area of transmitter $i$ at location $\mathbf{z}_i \in \mathcal{A}$, the area of the plane $\mathcal{A}_i(\mathcal{S}, \beta, \alpha)$ where this transmitter is received with SIR at least equal to $\beta$.

Under *no fading* channel model, $\mathcal{A}_i(\mathcal{S}, \beta, \alpha)$ can be defined as

$$\mathcal{A}_i(\mathcal{S}, \beta, \alpha) = \{\mathbf{z} : \gamma_i(\mathbf{z}) \geq \beta \sum_{j \neq i, \mathbf{z}_j \in \mathcal{S}} \gamma_j(\mathbf{z})\} . \tag{4.1}$$

We recall from §3.1.3 that the background noise (ambient/thermal) power $N_0$ is assumed negligible and equal to zero and the channel gain $\gamma_i(\mathbf{z})$ under *no fading* channel model is given by

$$\gamma_i(\mathbf{z}) = \frac{1}{\|\mathbf{z} - \mathbf{z}_i\|^{\alpha}} .$$

In case of fading, one cannot define $\mathcal{A}_i(\mathcal{S}, \beta, \alpha)$ deterministically. Therefore, we will define

it as

$$|\mathcal{A}_i(\mathcal{S},\beta,\alpha)| = \int \Pr(\gamma_i(\mathbf{z}) \geq \beta \sum_{j\neq i,\mathbf{z}_j\in\mathcal{S}} \gamma_j(\mathbf{z}))d\mathbf{z}^2 \,,$$

where the integration is over the network area $\mathcal{A}$.

Note that $|\mathcal{A}_i|$ is the size of the surface area of $\mathcal{A}_i$, $\Pr(\gamma_i(\mathbf{z}) \geq \beta \sum_{j\neq i,\mathbf{z}_j\in\mathcal{S}} \gamma_j(\mathbf{z}))$ is the probability that the signal from transmitter $i$ is received successfully at point $\mathbf{z}$ and we recall from (3.1) that under fading

$$\gamma_i(\mathbf{z}) = \frac{F_i(\mathbf{z})}{\|\mathbf{z}-\mathbf{z}_i\|^\alpha} \,,$$

where $F_i(\mathbf{z})$ is an *i.i.d.* random variable which represents the fading of signal from transmitter $i$ to receiver located at point $\mathbf{z}$.

Note that the area $\mathcal{A}_i(\mathcal{S},\beta,\alpha)$ also contains the point $\mathbf{z}_i$ since here the SIR is infinite.

We define the average surface area $\sigma(\lambda,\beta,\alpha)$ of $\mathcal{A}_i(\mathcal{S},\beta,\alpha)$ as

$$\sigma(\lambda,\beta,\alpha) = \mathbb{E}[|\mathcal{A}_i(\mathcal{S},\beta,\alpha)|] \,.$$

Our principal performance metric is local capacity which is defined as the average information rate received by a receiver which is randomly located in the network.

Consider a receiver at a random location $\mathbf{z} \in \mathcal{A}$ in the network. Let $N(\mathbf{z},\beta,\alpha)$ denote the number of reception areas it belongs to and we can write

$$\int N(\mathbf{z},\beta,\alpha)d\mathbf{z}^2 = \sum_{i\in\mathcal{N}} |\mathcal{A}_i(\mathcal{S},\beta,\alpha)| \,.\, 1_{i\in\mathcal{S}} \,.$$

Therefore, we have the following identity

$$\mathbb{E}[N(\mathbf{z},\beta,\alpha)]|\mathcal{A}| = \mathbb{E}[|\mathcal{A}_i(\mathcal{S},\beta,\alpha)|] \sum_{i\in\mathcal{N}} \Omega_i(n) \,,$$

where $\Omega_i(n)$ is the average slot occupancy rate of node $i$, *i.e.*, the proportion of slots it is active to transmit on the medium. Note that, in case of slotted ALOHA, $\Omega_i(n)$ is equal to the probability of medium access $p$. We get

$$\mathbb{E}[N(\mathbf{z},\beta,\alpha)]|\mathcal{A}| = \sigma(\lambda,\beta,\alpha) \sum_{i\in\mathcal{N}} \Omega_i(n) \,,$$

we also know that $\sum_{i\in\mathcal{N}} \Omega_i(n) = \lambda|\mathcal{A}|$, which gives

$$\begin{aligned} \mathbb{E}[N(\mathbf{z},\beta,\alpha)]|\mathcal{A}| &= \lambda\sigma(\lambda,\beta,\alpha)|\mathcal{A}| \\ \mathbb{E}[N(\mathbf{z},\beta,\alpha)] &= \lambda\sigma(\lambda,\beta,\alpha) \,. \end{aligned} \tag{4.2}$$

This identity has also been proved in articles [Baccelli & Blaszczyszyn 2000, Jacquet 2009]. $\mathbb{E}[N(\mathbf{z},\beta,\alpha)]$ represents the average number of transmitters from which a receiver, randomly located in the network, can receive with SIR at least equal to $\beta$. Under the hypothesis that a node can only receive at most one packet at a time, *e.g.*, when $\beta > 1$, then $N(\mathbf{z},\beta,\alpha) \leq 1$. The average information rate received by the receiver $c(\beta,\alpha)$ is therefore equal to $\mathbb{E}[N(\mathbf{z},\beta,\alpha)]$ multiplied by the nominal capacity. *Without loss of generality* (*w.l.o.g.*), we assume *unit* nominal capacity and we will derive

$$c(\beta,\alpha) = \mathbb{E}[N(\mathbf{z},\beta,\alpha)] = \lambda\sigma(\lambda,\beta,\alpha)\,. \tag{4.3}$$

Note that the local capacity is averaged on time and on any receiver which is randomly located in the network. It is also independent of $\lambda$ as it is invariant for any *homothetic* transformation of the set of transmitters. We will derive the local capacity of wireless network with slotted ALOHA, node coloring, CSMA and grid pattern based MAC schemes. We will also show that maximum local capacity can be achieved with grid pattern based schemes. Wireless networks of grid topologies are studied in literature, *e.g.*, the articles [Liu & Haenggi 2005,Hong & Hua 2007] compared these networks with network consisting of randomly distributed nodes. In contrast to these works, we assume that wireless network consists of randomly distributed nodes and only the simultaneous transmitters form a regular grid pattern. In our model, we have abstracted out the multi-hop aspect of communication and this allows us to focus on the *localized* capacity. Our model also captures a realistic scenario of nearby-neighbor communication in wireless networks where each transmitter can transmit to a receiver which is randomly located in its neighborhood or reception area.

Note that, in our model, we will consider the asymptotic case where $\mathcal{A} = \mathbb{R}^2$ in order to ignore the border effects. However, we will need to come back to finite (but large) $\mathcal{A}$ when we will discuss the multi-hop and mobile networks in Chapter 7 and Chapter 8.

## 4.2 Slotted ALOHA Scheme

In case of slotted ALOHA scheme, as discussed in §3.2, the set of simultaneous transmitters, in each slot, can be given by a uniform Poisson distribution of mean equal to $\lambda$ transmitters per unit square area.

Using (3.2) with $N_0 = 0$ and $P_i = 1$ (for $i = 0, 1, \ldots, k, \ldots$), we can write

$$F_i(\mathbf{z})\|\mathbf{z}-\mathbf{z}_i\|^{-\alpha} \geq \beta \sum_{j\neq i, \mathbf{z}_j\in\mathcal{S}} F_j(\mathbf{z})\|\mathbf{z}-\mathbf{z}_j\|^{-\alpha}\,,$$

or

$$\mathcal{W}(\mathbf{z},\{\mathbf{z}_i\}) \geq \beta\mathcal{W}(\mathbf{z},\mathcal{S}-\{\mathbf{z}_i\})\,,$$

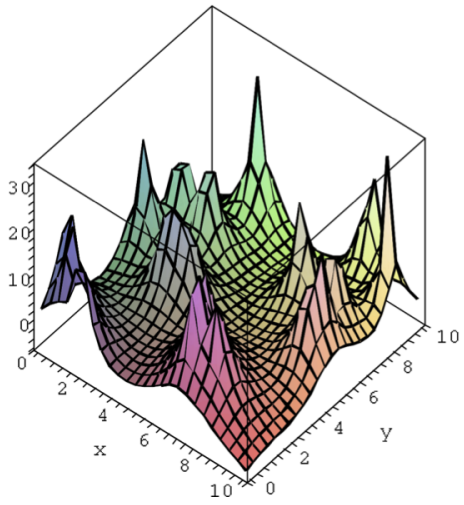


Figure 4.1: Signal Levels (in dB's) for a random network with attenuation coefficient $\alpha = 2.5$.

where

$$\mathcal{W}(\mathbf{z}, \mathcal{S}) = \sum_{\mathbf{z}_j \in \mathcal{S}} F_j(\mathbf{z}) \|\mathbf{z} - \mathbf{z}_j\|^{-\alpha} = \sum_{\mathbf{z}_j \in \mathcal{S}} F \|\mathbf{z} - \mathbf{z}_j\|^{-\alpha} .$$

We recall that, in case of *no fading*, $F$ is constant and equal to one and, in case of *Rayleigh fading*, $F$ is an *i.i.d.* random variable with an exponential distribution of mean equal to one.

In this section, we will use some of the results from the article [Jacquet 2009], to derive the local capacity of slotted ALOHA.

### 4.2.1 Reception Areas

Figure 4.1 shows the function $\mathcal{W}(\mathbf{z}, \mathcal{S})$ for $\mathbf{z}$ varying in the plane with $\mathcal{S}$, an arbitrary set of Poisson distributed transmitters. Figure 4.1 uses $\alpha = 2.5$. It is clear that closer the receiver is to the transmitter, larger is the SIR. For each value of $\beta$ we can draw an area, around each transmitter, where its signal can be received with SIR greater or equal to $\beta$. Figure 4.2 shows reception areas for the same set $\mathcal{S}$, as in Fig. 4.1, for various values of $\beta$. As can be seen, the reception areas do not overlap for $\beta > 1$ since there is only one dominant signal. For each value of $\beta$ we can draw, around each transmitter, the area where its signal is received with SIR greater or equal to $\beta$. Our aim is to find the average size of this area and how it is a function of $\lambda$, $\beta$ and $\alpha$.

$\mathcal{W}(\mathbf{z}, \mathcal{S})$ depends on $\mathcal{S}$ and hence is also a random variable. The random variable $\mathcal{W}(\mathbf{z}, \mathcal{S})$ has a distribution which is invariant by translation and therefore does not depend on $\mathbf{z}$. Therefore, we denote $\mathcal{W}(\lambda) \equiv \mathcal{W}(\mathbf{z}, \lambda)$. Let $w(\mathcal{S})$ be its density function. The set $\mathcal{S}$ is given by a $2D$ Poisson process process with intensity $\lambda$ transmitters per slot per unit square area and Laplace

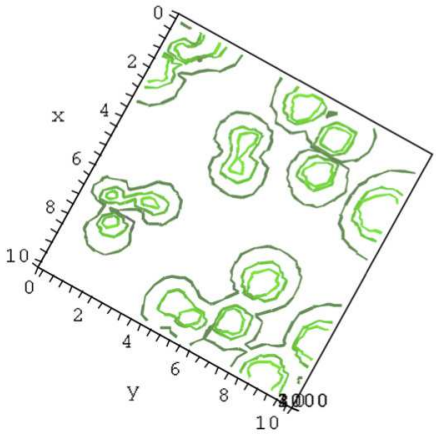


Figure 4.2: Distribution of reception areas for various value of SIR. $\beta = 1, 4, 10$ for situation of Fig. 4.1.

transform of $w(\mathcal{S})$, denoted by $\tilde{w}(\theta, \lambda)$, can be computed exactly. The Laplace transform

$$\tilde{w}(\theta, \lambda) = \mathbb{E}[\exp(-\theta \mathcal{W}(\lambda))] \,,$$

satisfies the identity

$$\tilde{w}(\theta, \lambda) = \exp\left(-\pi\lambda\mathbb{E}[F^{\frac{2}{\alpha}}]\Gamma(1-\frac{2}{\alpha})\theta^{\frac{2}{\alpha}}\right) \,, \tag{4.4}$$

where $\Gamma(.)$ is the Gamma function.

In case of *Rayleigh fading*

$$\mathbb{E}[F^{\frac{2}{\alpha}}] = \Gamma(1+\frac{2}{\alpha}) \,,$$

otherwise, under *no fading*, $\mathbb{E}[F^{\frac{2}{\alpha}}] = 1$. Note that in all cases, $\tilde{w}(\theta, \lambda)$ is of the form $\exp(-\lambda C\theta^{\gamma})$ where $\gamma = \frac{2}{\alpha}$, and the expression of $C$ in case of $2D$ map is $C = \pi\mathbb{E}[F^{\frac{2}{\alpha}}]\Gamma(1-\gamma)$.

From the above formula and by applying the inverse Laplace transformation, we get

$$P(\mathcal{W}(\lambda) < x) = \frac{1}{2i\pi}\int_{-i\infty}^{+i\infty} \frac{\tilde{w}(\theta, \lambda)}{\theta} e^{\theta x} d\theta \,,$$

Expanding $\tilde{w}(\theta,\lambda) = \sum_{n\geq 0} \frac{(-C\lambda)^n}{n!}\theta^{n\gamma}$, we get

$$P(\mathcal{W}(\lambda) < x) = \frac{1}{2i\pi}\sum_{n\geq 0}\frac{(-C\lambda)^n}{n!}\int_{-i\infty}^{+i\infty}\theta^{n\gamma-1}e^{\theta x}d\theta \,,$$

By bending the integration path towards negative axis

$$\frac{1}{2i\pi}\int_{-i\infty}^{+i\infty}\theta^{n\gamma-1}e^{\theta x}d\theta = \frac{e^{i\pi n\gamma}-e^{-i\pi n\gamma}}{2i\pi}\int_{0}^{\infty}\theta^{n\gamma-1}e^{-\theta x}d\theta = \frac{\sin(\pi n\gamma)}{\pi}\Gamma(n\gamma)x^{-n\gamma} \,,$$

we get,

$$P(\mathcal{W}(\lambda) < x) = \sum_{n\geq 0}\frac{(-C\lambda)^n}{n!}\frac{\sin(\pi n\gamma)}{\pi}\Gamma(n\gamma)x^{-n\gamma} \,, \tag{4.5}$$

with the convention that $\frac{\sin(\pi n\gamma)}{\pi}\Gamma(n\gamma) = 1$ for $n = 0$.

Let $p(\lambda, r, \beta, \alpha)$ be the probability to receive a signal at distance $r$ with SIR at least equal to $\beta$. Therefore, we have

$$p(\lambda, r, \beta, \alpha) = \int \psi(u) P\left(\mathcal{W}(\lambda) < \frac{r^{-\alpha}}{\beta}e^{u}\right) du \,,$$

where $\psi(u)$ is the probability density function of the fading factor $F \equiv e^u$. The average size of the reception area around an arbitrary transmitter with SIR at least equal to $\beta$ is

$$\sigma(\lambda, \beta, \alpha) = 2\pi \int p(\lambda, r, \beta, \alpha) r dr \,.$$

Using integration by parts, the article [Jacquet 2009] has shown that the average size of the reception area around an arbitrary transmitter $i$ with SIR at least equal to $\beta$ satisfies the identity

$$\sigma(\lambda, \beta, \alpha) = \frac{1}{\lambda}\frac{\sin(\frac{2}{\alpha}\pi)}{\frac{2}{\alpha}\pi}\beta^{-\frac{2}{\alpha}} \,. \tag{4.6}$$

Note that the average reception area $\sigma(\lambda, \beta, \alpha)$ is independent of the fading factor $F$.

$\sigma(\lambda, \beta, \alpha)$ is inversely proportional to the density of transmitters $\lambda$ and the product $\lambda\sigma(\lambda, \beta, \alpha)$ is a function of $\beta$ and $\alpha$. We notice that when $\alpha$ approaches infinity, $\sigma(\lambda, \beta, \infty)$ approaches $1/\lambda$. This is due to the fact that when $\alpha$ is very large, all nodes other than the closest transmitter tend to contribute as a negligible source of interference and consequently the reception areas turn to be the Voronoi cells around every transmitter. This holds for all values of $\beta$. The average size of Voronoi cell being equal to the inverse density of the transmitters $1/\lambda$ we get the asymptotic result. Note that when $\beta$ grows as $\exp(O(\alpha))$, we have

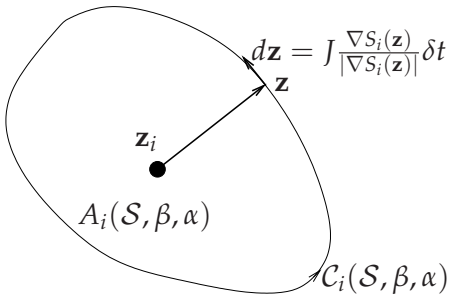


Figure 4.3: Computation of the reception area of transmitter $i$.

$\sigma(\lambda,\beta,\alpha) \approx \frac{1}{\lambda}\exp(-\frac{2}{\alpha}\log(\beta))$, which suggests that the typical SIR as $\alpha$ approaches infinity is of the order of $\exp(O(\alpha))$. Secondly, as $\alpha$ approaches 2, $\sigma(\lambda,\beta,2)$ approaches zero because $\sin(\frac{2}{\alpha}\pi)$ approaches zero. Indeed, in this case, the contribution of remote nodes tends to diverge and makes the SIR approach to zero. This explains why $\sigma(\lambda,\beta,2)$ approaches to zero for any fixed value of $\beta$.

### 4.2.2 Local Capacity

In this case, the analytical expressions (4.3) and (4.6) lead to

$$c(\beta,\alpha) = \mathbb{E}[N(\mathbf{z},\beta,\lambda)] = \sigma(1,\beta,\alpha)\,. \tag{4.7}$$

## 4.3 MAC Schemes Based on Exclusion Rules

In order to evaluate the local capacity of node coloring and CSMA based schemes, we will use our models, which we discussed in §3.3.1.1 and §3.3.1.2, in our Monte Carlo simulations along with the analytical method we will develop in the following section.

### 4.3.1 Reception Areas

Deriving an accurate analytical closed-form expression for the probability distribution of signal level with node coloring or CSMA based schemes does not seem tractable. Consequently, we also do not have a closed form expression for the average size of the reception area of an arbitrary transmitter. In this section, we will develop an analytical method to compute the average reception area of an arbitrary transmitter with node coloring or CSMA based schemes. Note that the value of $d$, in case of node coloring scheme, or $\theta_{cs}$, in case of CSMA based scheme, can be tuned to obtain an average transmitter density of $\lambda$.

Figure 4.3 is the figurative representation of the reception area $A_i(\mathcal{S},\beta,\alpha)$ of an arbitrary transmitter $i$. Our aim is to compute its size $|A_i(\mathcal{S},\beta,\alpha)|$. If $\mathcal{C}_i(\mathcal{S},\beta,\alpha)$ is the closed curve that

forms the boundary of $A_i(\mathcal{S}, \beta, \alpha)$ and $\mathbf{z}$ is a point on $\mathcal{C}_i(\mathcal{S}, \beta, \alpha)$, we have

$$|\mathcal{A}_i(\mathcal{S}, \beta, \alpha)| = \frac{1}{2} \int\limits_{\mathcal{C}_i(\mathcal{S},\beta,\alpha)} \det(\mathbf{z} - \mathbf{z}_i, d\mathbf{z}) \,, \tag{4.8}$$

where $\det(\mathbf{a}, \mathbf{b})$ is the determinant of vectors $\mathbf{a}$ and $\mathbf{b}$ and $d\mathbf{z}$ is the vector tangent to $\mathcal{C}_i(\mathcal{S}, \beta, \alpha)$ at point $\mathbf{z}$. $\det(\mathbf{z} - \mathbf{z}_i, d\mathbf{z})$ is the cross product of vectors $(\mathbf{z} - \mathbf{z}_i)$ and $d\mathbf{z}$ and gives the area of the parallelogram formed by these two vectors.

Note that (4.8) remains true if $\mathbf{z}_i$ is replaced by any interior point of $A_i(\mathcal{S}, \beta, \alpha)$.

The SIR of transmitter $i$ at point $\mathbf{z}$ is given by (3.3). We assume that at point $\mathbf{z}$

$$S_i(\mathbf{z}) = \beta \,.$$

On point $\mathbf{z}$ we can also define the gradient of $S_i(\mathbf{z})$, denoted by $\nabla S_i(\mathbf{z})$, as

$$\nabla S_i(\mathbf{z}) = \begin{bmatrix} \frac{\partial}{\partial x} S_i(\mathbf{z}) \\ \frac{\partial}{\partial y} S_i(\mathbf{z}) \end{bmatrix} .$$

The vector $d\mathbf{z}$ is co-linear with $J\frac{\nabla S_i(\mathbf{z})}{|\nabla S_i(\mathbf{z})|}$ where $J$ is the anti-clockwise rotation of $3\pi/2$ (or clockwise rotation of $\pi/2$) given by

$$J = \begin{bmatrix} 0 & 1 \\ -1 & 0 \end{bmatrix} .$$

Therefore, we can fix $d\mathbf{z} = J\frac{\nabla S_i(\mathbf{z})}{|\nabla S_i(\mathbf{z})|}\delta t$ and in (4.8)

$$\det(\mathbf{z} - \mathbf{z}_i, d\mathbf{z}) = (\mathbf{z} - \mathbf{z}_i) \times J\frac{\nabla S_i(\mathbf{z})}{|\nabla S_i(\mathbf{z})|}\delta t = -(\mathbf{z} - \mathbf{z}_i).\frac{\nabla S_i(\mathbf{z})}{|\nabla S_i(\mathbf{z})|}\delta t \,,$$

where $\delta t$ is assumed to be infinitesimally small. The sequence of points $\mathbf{z}(k)$ computed as

$$\begin{aligned} \mathbf{z}(0) &= \mathbf{z} \\ \mathbf{z}(k+1) &= \mathbf{z}(k) + J\frac{\nabla S_i(\mathbf{z}(k))}{|\nabla S_i(\mathbf{z}(k))|}\delta t \,, \end{aligned} \tag{4.9}$$

gives a discretized and numerically convergent parametric representation of $\mathcal{C}_i(\mathcal{S}, \beta, \alpha)$ by finite elements.

Therefore, 4.8 reduces to

$$|\mathcal{A}_i(\mathcal{S}, \beta, \alpha)| \approx -\frac{1}{2}\sum_k (\mathbf{z}(k) - \mathbf{z}_i).\frac{\nabla S_i(\mathbf{z}(k))}{|\nabla S_i(\mathbf{z}(k))|}\delta t \,, \tag{4.10}$$

assuming that we stop the sequence $\mathbf{z}(k)$ when it loops back on or close to the point $\mathbf{z}$.

The initial point

$$\mathbf{z}(0) = \mathbf{z} \,,$$

can be found using Newton's method. First approximate value of $\mathbf{z}$, required by Newton's method, can be computed assuming only one interferer nearest to the transmitter $i$ as discussed in the Appendix A.1.

The negative sign in (4.10) is automatically negated by the dot product of vectors $(\mathbf{z}(k) - \mathbf{z}_i)$ and $\nabla S_i(t, \mathbf{z}(k))$.

### 4.3.2 Local Capacity

The value of

$$\sigma(\lambda, \beta, \alpha) = \mathbb{E}[|\mathcal{A}_i(\mathcal{S}, \beta, \alpha)|] \,,$$

is computed using the Monte Carlo simulations and, therefore,

$$c(\beta, \alpha) = \mathbb{E}[N(\mathbf{z}, \beta, \alpha)] = \lambda\sigma(\lambda, \beta, \alpha) \,.$$

The local capacity $c(\beta, \alpha)$ is invariant for any homothetic transformation of $\lambda$ and, therefore, it is also independent of the values of MAC schemes parameters $\theta_{cs}$ or $d$.

## 4.4 Grid Pattern Based Schemes

In this section, we will discuss the optimality of grid patterns based schemes under *no fading* channel model. Later, we will also analyze the local capacity of such schemes.

### 4.4.1 Optimality of Grid Pattern Based Schemes

We consider a set of transmitters $\mathcal{S}$ and we will compare the reception areas when $\mathcal{S}$ is arbitrarily distributed in the network area $\mathcal{A}$ versus when $\mathcal{S}$ forms a regular grid pattern.

In order to simplify our analysis in this section, we define a function $s_i(\mathbf{z})$ as

$$s_i(\mathbf{z}) = \frac{\|\mathbf{z} - \mathbf{z}_i\|^{-\alpha}}{\sum_j \|\mathbf{z} - \mathbf{z}_j\|^{-\alpha}} \,.$$

The function $s_i(\mathbf{z})$ is similar to the SIR function $S_i(\mathbf{z})$, defined in (3.3), under *no fading* channel model except that the summation in the denominator factor also includes the numerator factor.

We also define a function $f(x)$ which can be continuous or integrable. For instance, here we will define it with the Heaviside step function as

$$f(x) = H[x - \beta'] \,,$$

for some given $\beta'$. Note that, in this case, the function is not continuous but we will not bother with this. For the following discussion, we can consider *w.l.o.g.* that the value of $\beta'$ is related to $\beta$ by

$$\beta' = \frac{\beta}{\beta + 1} .$$

Therefore, if transmitter $i$ is received successfully at location $\mathbf{z}$ or, in other words, with SIR greater or equal to $\beta$, then $s_i(\mathbf{z})$ is greater or equal to $\beta'$ and $f(s_i(\mathbf{z}))$ is equal to one.

We assume a virtual disk in the plane centered at $(0, 0)$ and of radius $R$. This allows us to express the density of set $\mathcal{S}$, denoted by $\nu(\mathcal{S})$, in terms of the number of transmitters covered by the disk of radius $R$ or area $\pi R^2$, when $R$ approaches infinity, and it is given by a limit as

$$\nu(\mathcal{S}) = \lim_{R \to \infty} \frac{1}{\pi R^2} \sum_i 1_{\|\mathbf{z}_i\| \leq R} .$$

We define

$$h(\mathbf{z}) = \sum_i f(s_i(\mathbf{z})) ,$$

so that $h(\mathbf{z})$ is equal to the number of transmitters that can be received successfully at $\mathbf{z}$ and its maximum value shall be one if $\beta > 1$. We define $\mathbb{E}[h(\mathbf{z})]$ by the limit

$$\mathbb{E}[h(\mathbf{z})] = \lim_{R \to \infty} \frac{1}{\pi R^2} \int\limits_{\|\mathbf{z}\| \leq R} h(\mathbf{z}) d\mathbf{z}^2 .$$

Note that the integration is network area $\mathcal{A}$ or, in other words, over the disk of radius $R$ where $R$ approaches infinity. We denote the reception area of an arbitrary transmitter $i$ as

$$\sigma_i = |\mathcal{A}_i(\mathcal{S}, \beta, \alpha)| = \int f(s_i(\mathbf{z})) d\mathbf{z}^2 ,$$

and we have

$$\mathbb{E}[h(\mathbf{z})] = \lim_{R \to \infty} \frac{1}{\pi R^2} \sum_i 1_{\|\mathbf{z}_i\| \leq R} \sigma_i = \nu(\mathcal{S}) \sigma ,$$

with

$$\sigma = \lim_{k \to \infty} \frac{1}{k} \sum_{i \leq n} \sigma_i .$$

As $R$ approaches infinity, $k$, *i.e.*, the number of transmitters in the set $\mathcal{S}$ covered by the disk of radius $R$ also approaches infinity.

Our objective is to optimize $\mathbb{E}[h(\mathbf{z})]$ whose definition is equivalent to the definition of $\mathbb{E}[N(\mathbf{z}, \beta, \alpha)]$ and therefore local capacity $c(\beta, \alpha)$ as well in expressions (4.2) and (4.3) respectively.

#### 4.4.1.1 First Order Differentiation

We denote the operator of differentiation *w.r.t.* $\mathbf{z}_i$ by $\nabla_i$. For $i \neq j$, we have

$$\nabla_i s_j = \alpha s_i s_j \frac{\mathbf{z} - \mathbf{z}_i}{\|\mathbf{z} - \mathbf{z}_i\|^2} ,$$

and

$$\nabla_i s_i = \alpha (s_i^2 - s_i) \frac{\mathbf{z} - \mathbf{z}_i}{\|\mathbf{z} - \mathbf{z}_i\|^2} .$$

Therefore,

$$\begin{aligned}
\nabla_i h(\mathbf{z}) &= \nabla_i \sum_i f(s_i(\mathbf{z})) \\
&= f'(s_i(\mathbf{z}))\nabla_i s_i + \sum_{j \neq i} f'(s_j(\mathbf{z}))\nabla_i s_j \\
&= \alpha s_i \frac{\mathbf{z} - \mathbf{z}_i}{\|\mathbf{z} - \mathbf{z}_i\|^2} \Big( - f'(s_i(\mathbf{z})) + \sum_j s_j f'(s_j(\mathbf{z})) \Big) .
\end{aligned}$$

Although, we know that $\int h(\mathbf{z}) d\mathbf{z}^2 = \infty$ , we nevertheless have a finite $\nabla_i \int h(\mathbf{z}) d\mathbf{z}^2$. In other words, the sum $\sum_j \nabla_i \sigma_j$ converges for all $i$.

**Lemma 4.4.1.** *For all $j \in \mathcal{S}$,*

$$\sum_i \nabla_i \sigma_j = 0 .$$

*Indeed this would be the differentiation of $\sigma_j$ when all points in $\mathcal{S}$ are translated by the same vector. Similarly,*

$$\sum_i \nabla_i \int h(\mathbf{z}) dz^2 = 0 .$$

**Theorem 4.4.1.** *If the points in the set $\mathcal{S}$ are arranged in a grid pattern then*

$$\nabla_i \int h(\mathbf{z}) d\mathbf{z}^2 = \sum_j \nabla_i \sigma_j = 0 ,$$

*and grids patterns are* locally *optimal.*

*Proof.* If $\mathcal{S}$ is a set of points arranged in a grid pattern, then

$$\nabla_i \int h(\mathbf{z}) d\mathbf{z}^2 = \sum_j \nabla_i \sigma_j ,$$

would be identical for all $i$ and, therefore, would be null since

$$\sum_i \nabla_i \int h(\mathbf{z}) d\mathbf{z}^2 = 0 .$$

We could erroneously conclude that:

– all grid sets are optimal and

– all grid sets give the same $\mathbb{E}[h(\mathbf{z})]$.

In fact this is wrong. We could also conclude that $\sigma$ does not vary but this will contradict that $\nu(\mathcal{S})$ *must* vary. The reason of this error is that a grid set cannot be modified into another grid set with a *uniformly bounded transformation*, unless the two grid sets are just simply translated by a simple vector. □

However, we have proved that the grid sets are locally optimal within sets that can be uniformly transformed between each other. In order to cope with uniform transformation and to be able to transform a grid set to another grid set, we will introduce the linear group transformation.

#### 4.4.1.2 Linear Group Transformation

Here, we assume that the points in the plane are modified according to a continuous linear transform $M(t)$ where $\mathbf{M}(\mathbf{t})$ is a matrix with $\mathbf{M}(\mathbf{0}) = \mathrm{I}$, *e.g.*, $\mathbf{M}(\mathbf{t}) = \mathrm{I} + \mathbf{tA}$ where $\mathbf{A}$ is a matrix.

Without loss of generality, we only consider $\sigma_0$, *i.e.*, the reception area of the transmitter at $\mathbf{z}_0$ which is located at the origin. Under these assumptions, we have

$$\frac{\partial}{\partial t}\sigma_0 = \sum_i (\mathbf{A}\mathbf{z}_i . \nabla_i \sigma_0) = \mathrm{tr}\Big(\sum_i \mathbf{A}^T \mathbf{z}_i \otimes \nabla_i \sigma_0\Big) ,$$

where "." indicates the scalar product.

In other words, using the identity

$$\frac{\partial \mathrm{tr}(\mathbf{A}^T \mathbf{B})}{\partial \mathbf{A}} = \mathbf{B} ,$$

the derivative of $\sigma_0$ *w.r.t.* matrix $\mathbf{A}$ is exactly equal to

$$\mathbf{D} = \sum_i \mathbf{z}_i \otimes \nabla_i \sigma_0 ,$$

such that

$$\mathbf{D} = \begin{bmatrix} D_{xx} & D_{xy} \\ D_{yx} & D_{yy} \end{bmatrix} .$$

Therefore, we can write the following identity

$$\mathrm{tr}\Big(\mathbf{A}^T \frac{\partial}{\partial \mathbf{A}} \sigma_0\Big) = \frac{\partial}{\partial t} \sigma_0(t, \mathbf{A})\Big|_{t=0} ,$$

where $\sigma_0(t, \mathbf{A})$ is the transformation of $\sigma_0$ under $M(t)$, *i.e.*,

$$\sigma_0(t, \mathbf{A}) = \det(\mathrm{I} + \mathbf{tA})\sigma_0 \, .$$

We assume that $\mathbf{M}(\mathbf{t}) = (\mathbf{1} + \mathbf{t})\mathbf{I}$ with $\mathbf{A} = \mathrm{I}$, *i.e.*, the linear transform is homothetic.

**Theorem 4.4.2.** $\mathbf{D}$ *is symmetric and* $\mathrm{tr}(\mathbf{D}) = 2\sigma_0$.

*Proof.* Under the given transform,

$$\sigma_0(t, \mathbf{A}) = \sigma_0(t, \mathrm{I}) = (1 + t)^2\sigma_0 \, .$$

As a first property, we have

$$\mathrm{tr}(\mathbf{D}) = 2\sigma_0 \, ,$$

since the derivative of $\sigma_0$ *w.r.t.* identity matrix I is exactly $2\sigma_0$, *i.e.*,

$$\mathrm{tr}(\mathbf{A}^T\mathbf{D}) = \mathrm{tr}(\mathbf{D}) = \sigma_0'(0, \mathrm{I}) = 2\sigma_0 \, .$$

The second property that $\mathbf{D}$ is a symmetric matrix is not obvious. The easiest proof of this property is to consider the derivative of $\sigma_0$ *w.r.t.* the rotation matrix J given by

$$\mathrm{J} = \begin{bmatrix} 0 & -1 \\ 1 & 0 \end{bmatrix} \, ,$$

which is zero since J is the initial derivative for a rotation and reception area is invariant by rotation. Therefore,

$$\mathrm{tr}(\mathrm{J}^T\mathbf{D}) = D_{yx} - D_{xy} = 0 \, ,$$

which implies that $\mathbf{D}$ is symmetric. □

Note that $\mathbf{D}$ can also be written in the following form

$$\mathbf{D} = \sum_i \mathbf{z}_i \otimes \nabla_i\sigma_0 = \int d\mathbf{z}^2 \sum_i \mathbf{z}_i \otimes \nabla_i f(s_0(\mathbf{z})) \, .$$

Let $\mathbf{T}$ be defined as

$$\mathbf{T} = \int d\mathbf{z}^2 \sum_i (\mathbf{z} - \mathbf{z}_i) \otimes \nabla_i f(s_0(\mathbf{z})) \, ,$$

such that

$$\mathbf{D} = \int \sum_i \mathbf{z} \otimes \nabla_i f(s_0(\mathbf{z}))\mathbf{dz^2} - \mathbf{T} \, .$$

The purpose of these definitions will become evident from theorems 4.4.3 and 4.4.4.

**Theorem 4.4.3.** *We will show that* $\int \sum_i \mathbf{z} \otimes \nabla_i f(s_0) d\mathbf{z}^2$ *is equal to* $\sigma_0 I$ *and, therefore,*

$$\mathbf{D} = \sigma_0 I - \mathbf{T} \, .$$

*We will also prove that* $\mathbf{T}$ *is symmetric.*

*Proof.* From the definition of $\mathbf{T}$, we can see that the sum $\sum_i (\mathbf{z} - \mathbf{z}_i) \otimes \nabla_i f(s_0(\mathbf{z}))$ leads to a symmetric matrix since

$$\mathbf{T} = \alpha \int f'(s_0(\mathbf{z})) \Big( \frac{s_0^2 - s_0}{\|\mathbf{z} - \mathbf{z}_0\|^2} (\mathbf{z} - \mathbf{z}_0) \otimes (\mathbf{z} - \mathbf{z}_0) + \sum_{i \neq 0} \frac{s_0 s_i}{\|\mathbf{z} - \mathbf{z}_i\|^2} (\mathbf{z} - \mathbf{z}_i) \otimes (\mathbf{z} - \mathbf{z}_i) \Big) d\mathbf{z}^2 \, ,$$

and the left hand side is made of $(\mathbf{z} - \mathbf{z}_i) \otimes (\mathbf{z} - \mathbf{z}_i)$ which are symmetric matrices. This implies that $\mathbf{T}$ is also symmetric.

We can see that

$$\sum_i \nabla_i f(s_0(\mathbf{z})) = -\nabla f(s_0(\mathbf{z})) \, ,$$

and using integration by parts we have

$$\int \sum_i \mathbf{z} \otimes \nabla_i f(s_0(\mathbf{z})) d\mathbf{z}^2 = -1 \times \begin{bmatrix} \int x \frac{\partial}{\partial x} f(s_0(\mathbf{z})) dxdy & \int x \frac{\partial}{\partial y} f(s_0(\mathbf{z})) dxdy \\ \int y \frac{\partial}{\partial x} f(s_0(\mathbf{z})) dxdy & \int y \frac{\partial}{\partial y} f(s_0(\mathbf{z})) dxdy \end{bmatrix} = \begin{bmatrix} \sigma_0 & 0 \\ 0 & \sigma_0 \end{bmatrix} ,$$

which is symmetric and equal to $\sigma_0 \mathrm{I}$. The sum/difference of symmetric matrices is also a symmetric matrix and, therefore, $\mathbf{D}$ is a symmetric matrix and $\mathbf{D} = \sigma_0 \mathrm{I} - \mathbf{T}$. □

Now, we will only consider grid patterns and, by virtue of a grid pattern, we can have

$$\sigma = \sigma_0 = \int f(s_0(\mathbf{z})) d\mathbf{z}^2 \, ,$$

and

$$\mathbb{E}[h(\mathbf{z})] = \nu(\mathcal{S}) \sigma_0 \, .$$

Under homothetic transformation, $\nu(\mathcal{S})$ and $\sigma_0$ are transformed but $\nu(\mathcal{S})\sigma_0$ remains invariant.

**Theorem 4.4.4.** *If the pattern of the points in set* $\mathcal{S}$ *is optimal w.r.t. linear transformation of the set,* $\mathbf{D} = \sigma_0 I$ *and* $\mathbf{T} = 0$.

*Proof.* The derivative of $\sigma_0$ *w.r.t.* matrix $\mathbf{A}$ is exactly equal to $\mathbf{D}$. Similarly, under the same transformation

$$\frac{\partial}{\partial t} \nu(\mathcal{S}) = \frac{1}{\det(\mathrm{I} + \mathbf{A}t)} \nu(\mathcal{S}) \, ,$$

and for $\mathbf{A} = \mathrm{I}$, it can be written as

$$\nu'(\mathcal{S})(t, \mathrm{I}) = \frac{\nu(\mathcal{S})}{(1+t)^2} \, .$$

In any case, the derivative of $\nu(\mathcal{S})$ *w.r.t.* matrix $\mathbf{A}$ is exactly equal to $-\mathrm{I}\nu(\mathcal{S})$. We also know that if the pattern is optimal *w.r.t.* linear transformation, the derivative of $\nu(\mathcal{S})\sigma_0$ *w.r.t.* to matrix $\mathbf{A}$ shall be null. This implies that

$$\nu(\mathcal{S})\mathbf{D} - \mathrm{I}\nu(\mathcal{S})\sigma_0 = 0 \, ,$$

which leads to $\mathbf{D} = \sigma_0 \mathrm{I}$ and $\mathbf{T} = 0$. □

We know that $\mathbf{T}$ is symmetric and $\mathbf{T} = 0$. Thus, $\mathrm{tr}(\mathbf{T}) = 0$, *i.e.*, eigenvalues are invariant by rotation. When a grid is optimal, we must have $\mathbf{T} = 0$. In any case, the matrix $\mathbf{T}$ must be invariant *w.r.t.* isometric symmetries of the grid. On $2D$ plane, the grid patterns which satisfy this condition are square, hexagonal and triangular grids. The square grid is symmetric *w.r.t.* any horizontal or vertical axes of the grid and, in particular, with rotation of $\pi/2$ represented by J. Therefore, the eigen system must be invariant by rotation of $\pi/2$. This implies that the eigenvalues are the same and therefore null since $\mathrm{tr}(\mathbf{T}) = 0$. Same argument also applies for the hexagonal grid with the invariance for $\pi/3$ rotation and for the triangular pattern with invariance for $2\pi/3$ rotation.

### 4.4.2 Reception Areas

In grid pattern based schemes, the simultaneous transmitters, *i.e.*, the set $\mathcal{S}$ is a set of points arranged in a grid pattern. We consider that, for every slot, the grid pattern is the same *modulo* a translation and/or rotation. Based on our discussion in previous section, we will only cover the grid layouts of square, hexagonal and triangle as shown in Fig. 3.1. Grids are constructed from $d$ which defines the minimum distance between neighboring transmitters and can be derived from the hop-distance parameter of a typical TDMA-based protocol. The density of grid points $\lambda$ depends on $d$. However, the local capacity $c(\beta, \alpha)$ is independent of the value of $d$ or, for that matter, $\lambda$ as it is invariant for any homothetic transformation of the set of transmitters.

In this case also, we will compute the average reception area $\sigma(\lambda, \beta, \alpha)$ using the analytical method described in §4.3.1.

### 4.4.3 Local Capacity

The expression to derive the local capacity is

$$c(\beta, \alpha) = \mathbb{E}[N(\mathbf{z}, \beta, \alpha)] = \lambda\sigma(\lambda, \beta, \alpha) \, ,$$

where $\sigma(\lambda, \beta, \alpha)$ is the average of the surface size of the reception area of a transmitter with grid pattern based scheme. In case of *no fading*, reception areas of all transmitters are the same *modulo* a translation and/or rotation, and their surface area size is the same. However, in case of *Rayleigh fading*, $\sigma(\lambda, \beta, \alpha)$ can be computed using Monte Carlo simulations. We will also compute simple upper bounds on the local capacity of grid pattern based schemes in §4.6.

## 4.5 Evaluation and Results

In this section, we will perform detailed analysis of MAC schemes, we have discussed in this chapter, under *no fading* channel model. The values of SIR threshold $\beta$ and attenuation coefficient $\alpha$ depend on the underlying physical layer or system parameters and are usually fixed and beyond the control of network or protocol designers. However, to give the reader an understanding of the influence of these parameters on the local capacity $c(\beta, \alpha)$ of various MAC schemes, we assume that these parameters are variable.

### 4.5.1 Slotted ALOHA Scheme

In case of slotted ALOHA, the local capacity $c(\beta, \alpha)$ is computed from analytic expressions (4.6) and (4.7).

### 4.5.2 MAC Schemes Based on Exclusion Rules

In order to approach an infinite map, we will perform numerical simulations in a very large network spread over $2D$ square map with length of each side equal to 10000 meters.

We will use the following methodology to compute the local capacity of exclusion rules based MAC schemes:

- simulate the placement of nodes on the network area,
- with each placement, select the set of simultaneous transmitters $\mathcal{S}$ by using the model specified in §3.3.1.1, for node coloring schemes, and the model specified in §3.3.1.2, for CSMA based schemes, and
- analytically calculate the reception area of the transmitter, which is located nearest to the center of the network area, using the method described in §4.3.1.

We will describe the computation of the local capacity of these schemes in detail, in the following section.

#### 4.5.2.1 Simulations

For the evaluation of node coloring scheme, we set $d$ equal to 25 meters and, in case of CSMA based schemes, the value of carrier sense threshold $\theta_{cs}$ is set equal to $1 \times 10^{-5}$. Considering the practical limitations introduced by the bounded network area, we use the following Monte Carlo method to evaluate $\sigma(\lambda, \beta, \alpha)$. We *only* compute the size of the reception area of a transmitter located nearest to the center of the network area and $\sigma(\lambda, \beta, \alpha)$ is the average of results obtained with 1000 samples of node distributions. Similarly, $\lambda$ is also the average of the density of simultaneous transmitters obtained with these 1000 samples of node distributions. Note that the models of MAC schemes select simultaneous transmitters randomly and transmitters are uniformly distributed in the network area. Therefore, using Monte Carlo method, *i.e.*, a large number of samples of node distributions and, with each sample, only measuring the reception area of a transmitter located nearest to the center of the network area gives an accurate approximation of $\sigma(\lambda, \beta, \alpha)$ in an infinite map.

It can be argued that the density of simultaneous transmitters maybe higher on the boundaries of the network area. However, the network area is very large and we observed that the difference, in spatial density of simultaneous transmitters, on the boundaries and central region is negligible. We also know that the local capacity $c(\beta, \alpha)$ is independent of $\lambda$ which depends on $d$ or $\theta_{cs}$. If the node density is very low, it will also have an impact on the packing (density) of simultaneous transmitters in the network. Therefore, $\lambda$ should be maximized to the point where no additional transmitter can be added to the network under given values of $d$ or $\theta_{cs}$. This can be achieved by keeping the node density very high, *e.g.*, we observed that the node density of one node per square meter is sufficient and further increasing the node density does not increase $\lambda$. In order to keep away the border effects, values of $d$ or $\theta_{cs}$ are chosen such that $\lambda$ is sufficiently high and border effects have minimal effect on the central region of the network.

### 4.5.3 Grid Pattern Based Schemes

For the evaluation of grid pattern based schemes, transmitters are spread in the network area in square, hexagonal or triangular grid pattern.

#### 4.5.3.1 Simulations

For all grid patterns, we set $d$ equal to 25 meters although it will have no effect on the validity of our conclusions as the local capacity $c(\beta, \alpha)$ is independent of $\lambda$. To keep away border effects, we will compute the size of the reception area of transmitter $i$, located in the center of the network area: $\mathbf{z}_i = (x_i, y_i) = (0, 0)$. The network area is large enough so that the reception area of transmitter $i$ is close to its reception area in an infinite map. The value of $\lambda$ depends on the type of grid pattern and it is computed using the Voronoi tessellation, discussed in the book [Aurenhammer & Klein 2000], of the network map such that each transmitter is located in

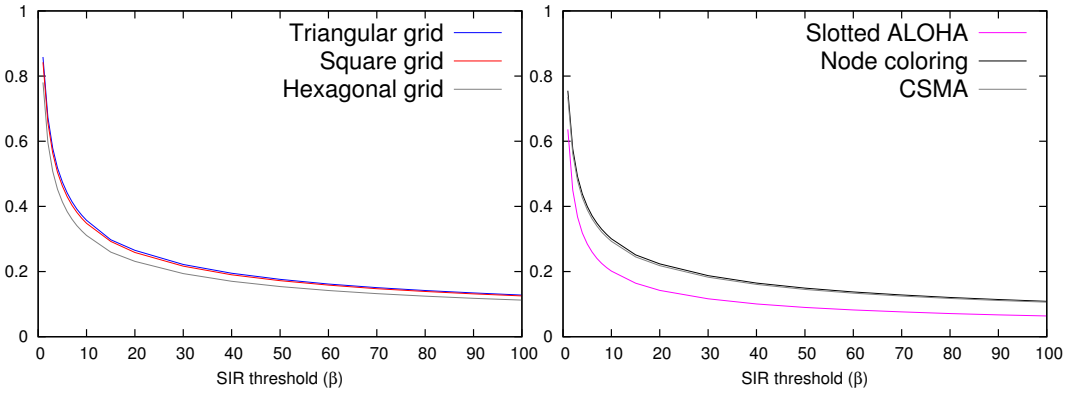


(a) $\beta$ is varying and $\alpha$ is fixed at 4.0.

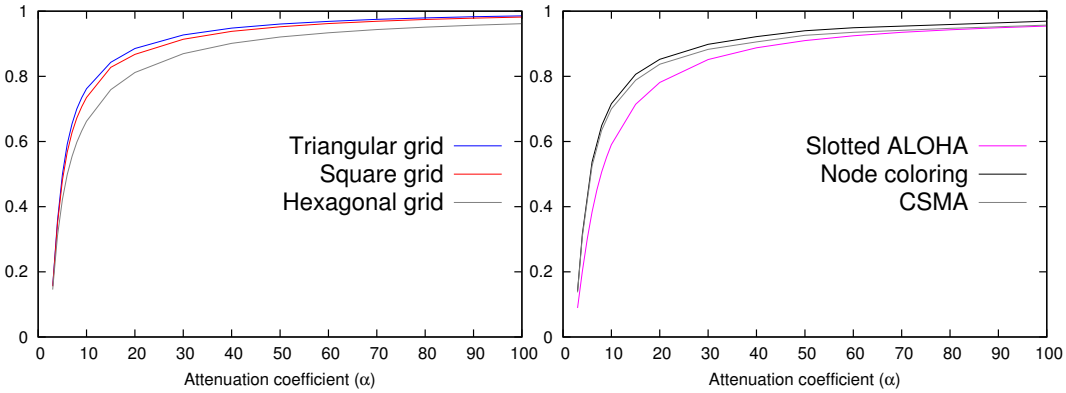


(b) $\beta$ is fixed at 10.0 and $\alpha$ is varying.

Figure 4.4: Local capacity $c(\beta, \alpha)$ of slotted ALOHA, node coloring, CSMA and grid pattern (triangular, square and hexagonal) based schemes under *no fading*.

a convex polygon whose area depends on the type of the grid. For example, in case of square grid pattern, Voronoi tessellation of the network map shows that each transmitter is located in a square region of area $d^2$ and we can derive the value of $\lambda$ to be equal to $\frac{1}{d^2}$. Similarly, in case of hexagonal and triangular grid pattern, the value of $\lambda$ is equal to $\frac{4}{3\sqrt{3}d^2}$ and $\frac{2}{\sqrt{3}d^2}$ respectively.

### 4.5.4 Summary of Results

Figure 4.4(a) shows the comparison of local capacity $c(\beta, \alpha)$ with slotted ALOHA, node coloring, CSMA and grid pattern based schemes with $\beta$ varying and $\alpha = 4.0$. Similarly, Fig. 4.4(b) shows the comparison of these MAC schemes with $\beta = 10.0$ and $\alpha$ varying. We know that as $\alpha$ approaches infinity, reception area around each transmitter turns to be a Voronoi cell with an average size equal to $1/\lambda$. Therefore, as $\alpha$ approaches infinity, $c(\beta, \alpha)$ approaches one. For slotted ALOHA scheme, (4.6) and (4.7) also arrive at the same result. For other MAC schemes,

we computed $c(\beta, \alpha)$ with $\alpha$ increasing up to 100 and from the results, we can observe that asymptotically, as $\alpha$ approaches infinity, $c(\beta, \alpha)$ approaching 1 is true for all schemes.

#### 4.5.4.1 Optimality of Grid Pattern Based Schemes

From the results, we can see that the maximum local capacity in wireless networks can be obtained with triangular grid pattern based scheme. In order to quantify the improvement in local capacity by triangular grid pattern based scheme over other more practical schemes, we perform a scaled comparison of slotted ALOHA, node coloring, CSMA and triangular grid pattern based schemes which is obtained by dividing the local capacity $c(\beta, \alpha)$ of all these schemes with the local capacity $c(\beta, \alpha)$ of triangular grid pattern based scheme. Figure 4.5 shows the scaled comparison with $\beta$ and $\alpha$ varying. It can be observed that triangular grid pattern based scheme can achieve, *at most*, double the local capacity of slotted ALOHA scheme. However, node coloring and CSMA based schemes can achieve almost $85 \sim 90\%$ of the optimal local capacity obtained with triangular grid pattern based scheme.

#### 4.5.4.2 Observations on Node Coloring Schemes

Triangular grid pattern based scheme can be visualized as an optimal node coloring which ensures that transmitters are exactly at distance $d$ from each other whereas, in case of random node coloring, transmitters are selected randomly and only condition is that they must be at a distance greater or equal to $d$ from each other. The exclusion region around each transmitter is a circular disk of radius $d/2$ with transmitter at the center. Note that the disks of simultaneous transmitters shall not overlap. The triangular grid pattern can achieve a packing density of $\pi/\sqrt{12} \approx 0.9069$. The packing density is defined as the proportion of network area covered by the disks of simultaneous transmitters. On the other hand, random packing of disks, which is the case in random node coloring, can achieve a packing density in the range of $0.54 \sim 0.56$ only as also pointed out in articles [Tanemura 1979, Busson & Chelius 2009]. We have seen in the results that even this sub-optimal packing of simultaneous transmitters by random node coloring scheme can achieve almost similar local capacity as obtained with optimal packing by triangular grid pattern based scheme.

#### 4.5.4.3 Observations on CSMA Based Schemes

We observe that the local capacity with CSMA based scheme is slightly lower (by approximately 3%) as compared to node coloring scheme and this is irrespective of the value of carrier sense threshold. The reason of slightly lower local capacity with CSMA based scheme is that the exclusion rule is based on carrier sense threshold, rather than the distance in-between simultaneous transmitters. With carrier sense based exclusion rule, CSMA based scheme may not allow to pack more transmitters, in each slot, that would have been possible with node col-

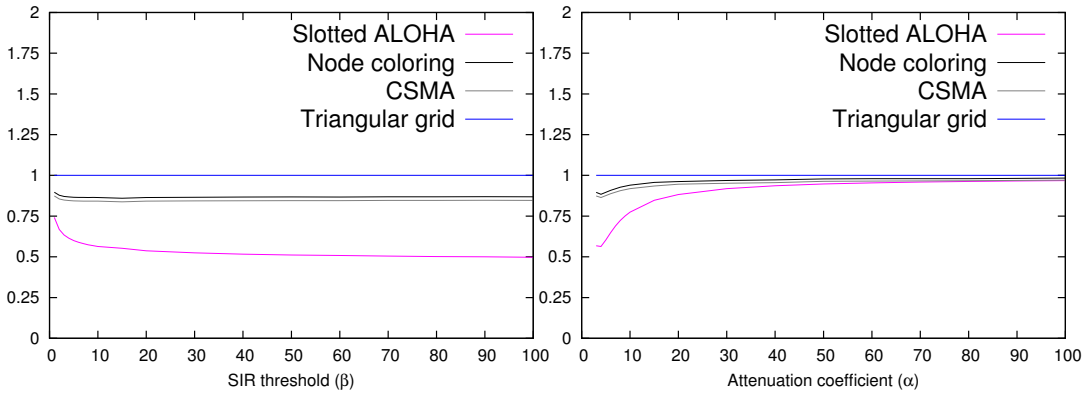


(a) $\beta$ is varying and $\alpha$ is fixed at 4.0. (b) $\beta$ is fixed at 10.0 and $\alpha$ is varying.

Figure 4.5: Scaled comparison of slotted ALOHA, node coloring, CSMA and triangular grid pattern based schemes under *no fading*.

oring scheme. In other words, CSMA may result in a lower packing density of simultaneous transmitters as compared to node coloring scheme. This can also be observed by comparing the densities of $SSI$ and $SSI_k$ point processes in the article [Busson & Chelius 2009] and also explains the slightly lower local capacity of CSMA based scheme as compared to node coloring scheme. As $\alpha$ approaches infinity, $\lambda$ with CSMA based scheme approaches the node density and reception area around each transmitter also becomes a Voronoi cell with an average size equal to the inverse of node density. In fact, asymptotically, as $\alpha$ approaches infinity, local capacity $c(\beta, \alpha)$ approaches one.

## 4.6 Impact of Fading on Local Capacity

In our evaluation in §4.5, we assumed the *no fading* channel model. However, in case of slotted ALOHA scheme, our results in (4.6) and (4.7) also show that fading has no impact on the local capacity. In this section, we will discuss the impact of fading on the MAC schemes, other than slotted ALOHA scheme, and we will show that when compared with the results under *no fading* channel model, fading will degrade the local capacity of these schemes.

For a receiver randomly located at point $\mathbf{z}$, variations in the signal level received from transmitters because of fading can be modeled as variations in their transmit power levels. First, we will show that under *high* fading, the transmitters with highest transmit power (or, in other words, the transmitters experiencing the highest fading) will form a sparse ALOHA pattern.

In this section, let $X$ be an *i.i.d.* random variable which models the fading on the channel and let us denote the cumulative distribution function of $X$ by $g(x)$, *i.e.*,

$$g(x) = \Pr(X \leq x) \, .$$

We denote the inverse of this cumulative distribution function by $g^{-1}(y)$.

**Theorem 4.6.1.** *For a given value $t$ and an arbitrary small value $\varepsilon < t$, if the probability distribution of the fading satisfies the identity*

$$\frac{g^{-1}(t)}{g^{-1}(t-\varepsilon)} \to \infty \,, \tag{4.11}$$

*we will have a network where the transmitters with highest transmit power will suppress other transmitters and will be sparsely distributed or, in other words, simultaneously active transmitters will form a sparse ALOHA pattern.*

*Proof.* Now at any point $\mathbf{z}$, the variations in the signal level of all transmitters $\mathbf{z}_i$ (for $i = 0, 1, 2, \ldots$,k,...) because of fading can be viewed as *i.i.d.* variations in their respective transmit power levels which follow the distribution of the random variable $X$.

For our discussion, we have the following properties for the distribution of the random variable $X$.

For a certain value $a$, we have

$$\Pr(X > a) = 1 - g(X \leq a) \to 0 \,,$$

and we relate $a$ and $t$ by

$$a = g^{-1}(t) \,.$$

Similarly, for a certain value $b$ we have

$$g^{-1}(t-\varepsilon) = b \,,$$

and from (4.11), we have

$$\frac{a}{b} \to \infty \,.$$

Therefore, we can write the following identity

$$\Pr(X > a).\frac{g^{-1}(t)}{g^{-1}(t-\varepsilon)} = \Pr(X > a).\frac{a}{b} \to \infty \,. \tag{4.12}$$

The identity (4.12) shows that the transmitters which appear to have very high transmit power (greater or equal to $a$), because of high fading, will be sparsely located because $\Pr(X > a) \to 0$ but, at a receiver at any point $\mathbf{z}$ in the plane, they will be received as if they are transmitting with unit power and their distances to the receiver have shrunk by at least the factor $1/(a)^{1/\alpha}$. Therefore, these sparsely located transmitters will appear to have a local density that approaches infinity at the point of the receiver. In other words, the reception areas of all transmitters with lower transmit power (equal or less than $b$) will shrink to the point of their own locations. Therefore, we will have a network where the active transmitters with very high transmit power, because of fading, will be uniformly and sparsely distributed in the network

and as they become sparser and sparser, the pattern of simultaneous transmitters converge to a sparse ALOHA pattern. Note that in case of grid pattern based scheme, they will form a sparse ALOHA pattern on the grid.

However, note that this holds only for fading which satisfies the property of (4.11). □

Now we will evaluate simple upper bounds on the local capacity of grid pattern based schemes under *no fading* and *Rayleigh fading* channel models.

**Theorem 4.6.2.** *The local capacity of grid pattern schemes is upper bounded by*

$$\hat{c}(\beta,\alpha) = \lambda\hat{\sigma}(\lambda,\beta,\alpha)\,, \tag{4.13}$$

*where*

$$\hat{\sigma}(\lambda,\beta,\alpha) \leq \pi\mathbb{E}[X^{\frac{2}{\alpha}}]\beta^{-\frac{2}{\alpha}}\Gamma\left(1-\frac{2}{\alpha}\right)d_{max}^2\,, \tag{4.14}$$

*where the value of $d_{max}$ depends on the grid pattern. In case of square grid pattern based scheme, $d_{max} = d/\sqrt{2}$ , where $d$ is the dimension of the grid. Similarly, in case of case of hexagonal and triangular grid pattern based schemes, $d_{max} = d$ and $d_{max} = d/\sqrt{3}$ respectively.*

*Proof.* In order to simplify our proof, we define the following function

$$W_i(\mathbf{z}) = \frac{\sum\limits_{j\neq i,\mathbf{z}_j\in\mathcal{S}} X_j\|\mathbf{z}-\mathbf{z}_j\|^{-\alpha}}{\|\mathbf{z}-\mathbf{z}_i\|^{-\alpha}}\,,$$

As $X_j$ is an *i.i.d.* random variable which is independent of the location of the transmitters and the receivers, we can drop the subscript and we will have

$$W_i(\mathbf{z}) = \frac{\sum\limits_{j\neq i,\mathbf{z}_j\in\mathcal{S}} \|\mathbf{z}-\mathbf{z}_j\|^{-\alpha}}{\|\mathbf{z}-\mathbf{z}_i\|^{-\alpha}}X\,.$$

If we take into account the interference from the nearest interferer only, we have a simple lower bound as

$$W_i(\mathbf{z}) \geq \frac{\|\mathbf{z}-\mu(\mathbf{z})\|^{-\alpha}}{\|\mathbf{z}-\mathbf{z}_i\|^{-\alpha}}X\,,$$

where $\mu(\mathbf{z})$ is the closest interferer $\mathbf{z}_j$ ($j \neq i$) to the point $\mathbf{z}$. Therefore, the upper bound on the probability to successfully receive the signal from transmitter $i$ at point $\mathbf{z}$ is

$$P(W_i(\mathbf{z}) < \beta') \leq \Pr\left(\frac{\|\mathbf{z}-\mu(\mathbf{z})\|^{-\alpha}}{\|\mathbf{z}-\mathbf{z}_i\|^{-\alpha}}X \;<\; \beta'\right),$$

where $\beta'$ is the inverse variation of SIR threshold $\beta$, *i.e.*, $\beta' = \frac{1}{\beta}$. We get

$$P(W_i(\mathbf{z}) < \beta') \leq \Pr\left(X < \beta' d_{max}^{\alpha} \|\mathbf{z} - \mathbf{z}_i\|^{-\alpha}\right),$$

where

$$d_{max} = \max \|\mathbf{z} - \mu(\mathbf{z})\|,$$

which depends on the grid pattern.

Therefore, we have

$$P(W_i(\mathbf{z}) \geq \beta') \leq 1 - \exp(-\beta' d_{max}^{\alpha} \|\mathbf{z} - \mathbf{z}_i\|^{-\alpha}).$$

Changing to the polar coordinates by using $r = \|\mathbf{z} - \mathbf{z}_i\|$, the upper bound on the average reception area $\hat{\sigma}(\lambda, \beta, \alpha)$ can be obtained as

$$\hat{\sigma}(\lambda, \beta, \alpha) \leq 2\pi \int_0^{\infty} (1 - \exp(-\beta' d_{max}^{\alpha} r^{-\alpha}))rdr.$$

Again, changing the variable $r^{-\alpha} = x$ which leads to $\frac{dx}{x} = -\alpha\frac{dr}{r}$, we get

$$\begin{aligned}
\hat{\sigma}(\lambda, \beta, \alpha) &\leq \frac{-2\pi}{\alpha} \int_0^{\infty} (1 - \exp(-\beta' d_{max}^{\alpha} x)) x^{-\frac{2}{\alpha}} \frac{dx}{x} \\
&\leq \frac{-2\pi}{\alpha} \int_0^{\infty} (1 - \exp(-x)) x^{-\frac{2}{\alpha}-1} dx \frac{1}{(\beta' d_{max}^{\alpha})^{-\frac{2}{\alpha}}} \\
&\leq \frac{-2\pi}{\alpha} \Gamma\left(-\frac{2}{\alpha}\right) \beta'^{\frac{2}{\alpha}} d_{max}^2 \\
&\leq \pi\Gamma\left(1 - \frac{2}{\alpha}\right) \beta'^{\frac{2}{\alpha}} d_{max}^2.
\end{aligned}$$

Replacing $\beta' = \frac{X}{\beta}$ and averaging over the probability density function of fading, we get

$$\begin{aligned}
\hat{\sigma}(\lambda, \beta, \alpha) &\leq \pi\mathbb{E}\left[\left(\frac{X}{\beta}\right)^{\frac{2}{\alpha}}\right] \Gamma\left(1 - \frac{2}{\alpha}\right) d_{max}^2 \\
&\leq \pi\mathbb{E}[X^{\frac{2}{\alpha}}]\beta^{-\frac{2}{\alpha}} \Gamma\left(1 - \frac{2}{\alpha}\right) d_{max}^2,
\end{aligned}$$

which completes the proof. □

We recall that in case of *Rayleigh fading*

$$E[X^{\frac{2}{\alpha}}] = \Gamma\left(1 + \frac{2}{\alpha}\right) ,$$

whereas, in case of *no fading*, $E[X^{\frac{2}{\alpha}}] = 1$.

Note that the value of $\lambda$ in case of square, hexagonal and triangular grid pattern based schemes is $\frac{1}{d^2}$, $\frac{4}{3\sqrt{3}d^2}$ and $\frac{2}{\sqrt{3}d^2}$ respectively. Therefore, using the respective values of $\lambda$ and $d_{max}$ of all grid pattern based schemes and (4.13) and (4.14), simple upper bounds on their local capacity can be derived. Note that, for $\alpha > 2$, the factor $\Gamma(1 + \frac{2}{\alpha})$ is less than one which means that, as compared to the results under *no fading* channel model, *Rayleigh fading* degrades the local capacity of grid pattern based schemes. However, as $\alpha$ approaches infinity, $\Gamma(1 + \frac{2}{\alpha})$ approaches one and the local capacity under *Rayleigh fading* approaches the local capacity under *no fading* channel model. Moreover, computations also show that, as compared to square and hexagonal grid pattern based schemes, the triangular grid pattern based scheme can achieve the highest local capacity under *Rayleigh fading* as it has the highest upper bound.

## 4.7 Conclusions

Our analysis shows that maximum local capacity in wireless networks can be achieved with grid pattern based schemes and our results show that triangular grid pattern outperforms square and hexagonal grids. Moreover, compared to simple slotted ALOHA, which does not use any protocol overhead, triangular grid pattern based scheme can only increase the local capacity by a factor of 2 or less whereas node coloring and CSMA based schemes can achieve almost similar local capacity as the triangular grid pattern based scheme.

The framework of local capacity assumes that nodes communicate with their nearby neighbors only and do not take into account the multi-hop communication in wireless networks. However, a MAC scheme which achieves higher local capacity should also be able to achieve higher end-to-end capacity in multi-hop networks. For example, consider that $\lambda$ is normalized across all schemes to one. Therefore, higher local capacity means higher $\sigma(1, \beta, \alpha)$ which has an impact on the average range of transmission and the number of hops required to reach the destination. In Chapter 6, we will evaluate the normalized maximum transmission range. It is important to mention that the analysis to establish exact bounds on end-to-end capacity with different schemes in multi-hop networks will be challenging as we will have to take into account the impact of various parameters like routing protocol, hop length and spatial distribution of simultaneous transmitters: all these factors can be interrelated. We will extend our capacity analysis to multi-hop wireless networks in Chapters 6, 7 and 8.

# Chapter 5

# Local Capacity and Coverage in Cellular Networks

In this chapter, we will study the problem of increasing the capacity and coverage of an existing cellular network by adding new base stations. We will consider a *sub-region* of an existing cellular network where the service provider wants to increase the bandwidth resources for the users as well as the coverage of the network and our goal is to find the optimal locations of $K$ additional base stations in this region. The addition of $K$ new base stations to the network may also impact the capacity and coverage of existing base stations which makes the problem very difficult to solve. In fact, we will show that this is an NP-Hard problem. In our approach, we will reduce this NP-hard problem to finding the points of minimum interference in an existing cellular network and we will propose heuristics that will select the locations for $K$ additional base stations from these points.

The article [Plastria 2001] gives an overview of the research about optimization approaches to the problem of locating one or more new facilities in an environment where other competing facilities already exist. Several other surveys on research in this area also appear in articles like [Gabszewicz & Thisse 1992, Eiselt *et al.* 1993, Drezner 1995, Eiselt & Laporte 1997]. In another article [Aboolian *et al.* 2007], the authors proposed greedy heuristics to optimize the locations of additional facilities that will compete, for customer demand, with each other and pre-existing facilities. The authors of this article also take into account the tradeoff issues like facility location and design, customer demand and profitability. The article [Buttazzo & Santambrogio 2005] studied the problem of locating services to optimize the transportation cost for the efficient planning of a city but their work does not consider pre-existing services or facilities. Our optimization criteria are the *performance* metrics of wireless cellular networks, *i.e.*, the optimization of capacity and coverage of an existing cellular network by locating a *given* number of additional base stations. In related works, the authors of the article [Kelif & Coupechoux 2009] analyzed the capacity and coverage of cellular networks where base stations are arranged in hexagonal cells. In the article [Altman *et al.* 2009], the authors assumed

that there are two competing service providers and they studied the uplink scenario of a cellular network where the users are placed on a line segment. The article [Prommak *et al.* 2004] formulated the problem of locating APs in IEEE 802.11 wireless LANs as constraint satisfaction problem where they considered the transmit power, frequency bands and location constraints. The authors of the article [Keung *et al.* 2010] introduced a simulated annealing algorithm for the optimal placement of base stations with the objective of maximizing the information collection within a constrained time. However, this objective may seem more suitable for wireless sensor networks.

## 5.1 The Context

Let us consider an existing cellular data network. In particular, let us put ourselves in the context of an LTE system, *e.g.*, an orthogonal frequency-division multiple access (OFDMA) system supporting fractional frequency reuse (FFR) for interference mitigation similar to the one used in articles [Stolyar & Viswanathan 2008, Stolyar & Viswanathan 2009]. This type of interference mitigation divides frequency and time resources into several resource sets. FFR in the context of OFDMA systems has been discussed in cellular networks standardization such as Third Generation Partnership Project (3GPP) and Third Generation Partnership Project 2 (3GPP2) which are presented in detail in specifications [3GPP 2005, 3GPP2 2007].

As we will consider the downlink case only, we can use the notation of the set of simultaneous transmitters $\mathcal{S}$ for the set of existing base stations in the cellular network, *i.e.*,

$$\mathcal{S} = \{\mathbf{z}_1, \mathbf{z}_2, \ldots, \mathbf{z}_k, \ldots\} ,$$

where $\mathbf{z}_i$ is the location of base station $i$. The density of set $\mathcal{S}$ is $\lambda$. Also, let us assume that the frequency band is divided into $B$ sub-bands

$$b \in \mathcal{F} = \{1, \ldots, B\} ,$$

and we denote the bandwidth of each sub-band by $W$. We consider that each sub-band consists of a fixed number $c$ of sub-carriers. Furthermore, time is divided into slots consisting of a number of OFDMA symbols and transmissions are scheduled to users by assigning a set of sub-carriers on specific slots. The time is slotted so that transmissions within each cell are synchronized and do not interfere with each other. To simplify the exposition, we assume that the resource sets span the entire time period however, extension to more general resource sets as discussed in articles [Stolyar & Viswanathan 2008, Stolyar & Viswanathan 2009] is also straightforward. We assume that there is no inter-carrier interference. Therefore a transmission in a cell, assigned to a sub-carrier of a sub-band, causes interference to only those users in other cells that are assigned to the same sub-carrier on the corresponding sub-band.

We denote the fraction of time an assignment algorithm allocates to the user located at

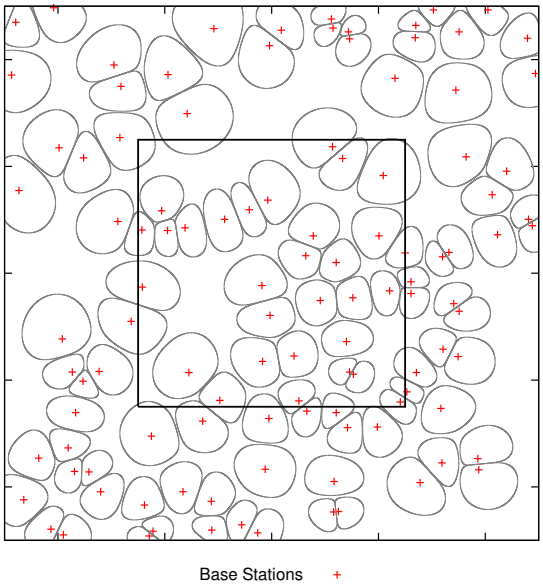


Figure 5.1: Area of interest $\mathcal{A}_{\mathcal{R}}$ is bounded by a square. $\beta = 1$ and $\alpha = 4.0$.

position $\mathbf{z}$ in sub-carrier $c$ of sub-band $b$ by $\tau^{(cb)}(\mathbf{z}) \in [0,1]$. Similarly, the nominal transmission rate, for the user located at position $\mathbf{z}$, in sub-carrier $c$ of sub-band $b$ is denoted by $R^{(cb)}(\mathbf{z}) \in [0,B]$, $B < \infty$. Therefore, the average rate a user located at position $\mathbf{z}$ actually receives is

$$c(\mathbf{z}) = \sum_{b}\sum_{c} \tau^{(cb)}(\mathbf{z}) R^{(cb)}(\mathbf{z}) \,.$$

Note that each base station $i$, $\mathbf{z}_i \in \mathcal{S}$, may need to allocate a set of sub-carriers and average transmission power $P_i^{(cb)}(\mathbf{z})$ if the user located at position $\mathbf{z}$ is to be assigned to sub-carrier $c$ of sub-band $b$. Let us denote the channel gain from the base station $i$ to a user located at position $\mathbf{z}$ on sub-carrier $c$ of sub-band $b$ by $\gamma_i^{(cb)}(\mathbf{z})$. Therefore, we can write the SINR of base station $i$, $\mathbf{z}_i \in \mathcal{S}$, as equal to

$$\frac{\gamma_i^{(cb)}(\mathbf{z}) P_i^{(cb)}(\mathbf{z})}{N_0 + \sum\limits_{j \neq i, \mathbf{z}_j \in \mathcal{S}} \gamma_j^{(cb)}(\mathbf{z}) P_j^{(cb)}(\mathbf{z})} \,. \tag{5.1}$$

## 5.2 Model and Assumptions

In order to simplify our analysis, we can ignore *w.l.o.g.* the subscripts $i, j$ and $b, c$ in (5.1) and make the following assumptions:

– the thermal/ambient noise power $N_0$ is negligible and equal to zero,

– $P_i^{(cb)}$ is constant and equal to one for all $i, b, c$ and

– we will ignore the fading and shadowing effects and assume that channel gain depends solely on the Euclidean distance and the attenuation coefficient $\alpha$.

Therefore, (5.1) reduces to the form

$$S_i(\mathbf{z}) = \frac{\|\mathbf{z} - \mathbf{z}_i\|^{-\alpha}}{\sum\limits_{j \neq i, \mathbf{z}_j \in \mathcal{S}} \|\mathbf{z} - \mathbf{z}_j\|^{-\alpha}} ,$$

which is the same expression as can be obtained under *no fading* channel model in §3.1.4. Note that, here $S_i(\mathbf{z})$ is the SIR of base station $i$ at a user located at point $\mathbf{z}$ in the network.

The available rate at the user becomes equal to the Shannon capacity given by

$$c(\mathbf{z}) = \sum_{\mathbf{z}_i \in \mathcal{S}} W \log_2(1 + S_i(\mathbf{z})) .$$

The coverage of a base station is defined as the set of all points in the network where *basic service* is provided with SIR at least equal to a certain threshold. In other words, the $\beta$-coverage area of a base station $i$ at location $\mathbf{z}_i \in \mathcal{S}$ is $\mathcal{A}_i(\mathcal{S}, \beta, \alpha)$ which represents the area where the transmission from this base station is received with SIR threshold greater or equal to $\beta$ and it is given by (4.1).

The coverage of the network is given by the union of the $\beta$-coverage areas of all base stations

$$\text{Coverage}(\lambda, \beta, \alpha) = \bigcup_{\mathbf{z}_i \in \mathcal{S}} \mathcal{A}_i(\mathcal{S}, \beta, \alpha) .$$

Note that we can compute the surface area of the $\beta$-coverage area of the base station $i$

$$\sigma_i = |\mathcal{A}_i(\mathcal{S}, \beta, \alpha)| ,$$

using the analytical method described in §4.3.1.

## 5.3 Scheme to Incorporate $K$ Additional Base Stations

In this section, we will discuss our scheme to incorporate $K$ additional base stations to the cellular network such that the capacity and coverage of the network is maximized with all base stations including the additional base stations as well.

### 5.3.1 Points of Maximum Capacity

Let us consider the case where we want to incorporate a new base station $l$, $\mathbf{z}_l \notin \mathcal{S}$. Then the new set of base stations will be given by

$$\mathcal{S}' = \mathcal{S} \cup \{\mathbf{z}_l\} .$$

Our goal is to find the location of $l$, $\mathbf{z}_l$.

The SIR at a user located at $\mathbf{z}$ and being served by a base station $i$ with $\mathbf{z}_i \in \mathcal{S}'$ is

$$S_i(\mathbf{z}) = \frac{\|\mathbf{z} - \mathbf{z}_i\|^{-\alpha}}{\sum\limits_{j \neq i, \mathbf{z}_j \in \mathcal{S}'} \|\mathbf{z} - \mathbf{z}_j\|^{-\alpha}} . \tag{5.2}$$

We want to compute the maximum of the capacity function obtained by adding a new base station which also depends on the locations of already existing base stations. We assume that the coordinates of existing base stations in the network are given and the distribution of users is uniform.

Therefore, the average capacity by adding the new base station is given by

$$\mathbb{E}[c(\mathbf{z})] = \frac{1}{\sigma^2_{\mathcal{R}}} \int\limits_{\mathcal{A}_{\mathcal{R}}} c(\mathbf{z})\, d\mathbf{z} , \tag{5.3}$$

with units bits per second per hertz per unit square kilometers (km) where $\sigma_{\mathcal{R}}$ is the surface area of the area of interest $\mathcal{A}_{\mathcal{R}}$ and

$$c(\mathbf{z}) = \sum_{\mathbf{z}_i \in \mathcal{S}'} W \log_2(1 + S_i(\mathbf{z})) . \tag{5.4}$$

The optima of this maximization problem are found at stationary points where the first derivative or the gradient of the objective function (5.3) is zero. An equation stating that the first derivative equals zero at an interior optimum is also called a "first-order condition". In other words, we want to study the behavior of the gradient of (5.3)

$$\nabla \mathbb{E}[c(\mathbf{z})] = \frac{1}{\sigma^2_{\mathcal{R}}} \nabla \left( \int\limits_{\mathcal{A}_{\mathcal{R}}} c(\mathbf{z})\, d\mathbf{z} \right) . \tag{5.5}$$

We can rewrite (5.4) as

$$c(\mathbf{z}) = \sum_{\mathbf{z}_i \in \mathcal{S}'} W \log_2(1 + S_i(\mathbf{z})) = \sum_{i \neq l, \mathbf{z}_i \in \mathcal{S}'} W \log_2(1 + S_i(\mathbf{z})) + W \log_2(1 + S_l(\mathbf{z})) .$$

In case of large cellular networks, when the number of base stations in the set $\mathcal{S}$ is very

large

$$\nabla \int_{\mathcal{A}_{\mathcal{R}}} \sum_{i \neq l, \mathbf{z}_i \in \mathcal{S}'} W \log_2(1 + S_i(\mathbf{z}))\, d\mathbf{z} \to 0\,,$$

and the relevant term in (5.5) is then given by

$$\nabla \int_{\mathcal{A}_{\mathcal{R}}} W \log_2(1 + S_l(\mathbf{z}))\, d\mathbf{z}\,. \tag{5.6}$$

Using Taylor series expansion, we know that

$$\log_2(1+x) = x - \frac{x^2}{2} + \frac{x^3}{3} - \dots\,,$$

and for small values of $x$, we can ignore the higher order terms. Therefore, in the low SIR regime, the problem of maximizing the existing capacity becomes equivalent to the problem of maximizing the SIR. In the high SIR regime, both quantities are also obviously related but we do not show a theoretical result here. However, simulation results suggest that even in this scenario we obtain a good approximation, *i.e.*, maximizing the capacity is equivalent to maximizing the SIR. Therefore, in this case, (5.6) reduces to

$$\nabla \int_{\mathcal{A}_{\mathcal{R}}} S_l(\mathbf{z})\, d\mathbf{z}\,,$$

and we know that

$$S_l(\mathbf{z}) = \frac{\|\mathbf{z} - \mathbf{z}_l\|^{-\alpha}}{\sum_{j \neq l, \mathbf{z}_j \in \mathcal{S}'} \|\mathbf{z} - \mathbf{z}_j\|^{-\alpha}} = \frac{u(\mathbf{z})}{g(\mathbf{z})}\,, \tag{5.7}$$

where $u(\mathbf{z}) = \|\mathbf{z} - \mathbf{z}_l\|^{-\alpha}$ and $g(\mathbf{z}) = \sum_{j \neq l, \mathbf{z}_j \in \mathcal{S}'} \|\mathbf{z} - \mathbf{z}_j\|^{-\alpha}$.

Therefore

$$\nabla S_l(\mathbf{z}) = \nabla \left( \frac{u(\mathbf{z})}{g(\mathbf{z})} \right) = \frac{g(\mathbf{z}) \nabla u(\mathbf{z}) - u(\mathbf{z}) \nabla g(\mathbf{z})}{g^2(\mathbf{z})}\,.$$

The problem of maximizing coverage in wireless data networks with $K$ additional base stations can be reduced to the classical maximum coverage problem in computer science which is also discussed in the book [Hochbaum 1997].

In maximum coverage problem, the inputs are several given sets and a number $K$. Note that these sets may have some elements in common. The goal is to select at most $K$ of these sets such that the maximum number of elements are covered, *i.e.*, the union of the selected sets has maximal size. Formally, the maximum coverage problem can be defined as follows.

**Inputs**: A number $K$ and a collection of sets

$$S = S_1, S_2, ..., S_m$$

**Objective**: Find a subset $S' \subseteq S$ of sets, such that $|S'| \leq K$ and the number of covered elements $\left| \bigcup_{S_i \in S} S_i \right|$ is maximized.

The problem of maximum coverage with $N$ given base stations and $K$ additional base stations can be reduced to the above described maximum coverage problem. In case of cellular networks, the set $S_i$ represents the base station $i$ and the elements of this set represents the users that this base station may cover with given SIR threshold $\beta$. Note that these sets may overlap for $\beta \leq 1$ but for $\beta > 1$, the coverage areas of the base stations do not overlap. The location of $K$ additional base stations shall be chosen so that the coverage of users, in the network, by $N + K$ base stations is maximum. This is analogous to selecting $K$ sets in maximum coverage problem which is an NP-hard problem.

Now returning back to the problem of maximizing capacity in the area of interest $\mathcal{A}_{\mathcal{R}}$, this problem is also NP-Hard as it can be considered as an extension of the maximum coverage problem to the case of users distributed in a network according to a continuous probability distribution.

If $\mathcal{A}_{\mathcal{R}}$ is large enough, we can consider $\int_{\mathcal{A}_{\mathcal{R}}} u(\mathbf{z}) d\mathbf{z}$ to be constant and therefore, in (5.7), we will only be interested in the behavior of $\nabla g(\mathbf{z})$.

### 5.3.2 Points of Minimum Interference

The signal level of the interference received at any location $\mathbf{z}$ on the two-dimensional plane is represented by the function

$$g(\mathbf{z}) = \sum_{j \neq l, \mathbf{z}_j \in \mathcal{S}'} \|\mathbf{z} - \mathbf{z}_j\|^{-\alpha} = \sum_{\mathbf{z}_j \in \mathcal{S}} \|\mathbf{z} - \mathbf{z}_j\|^{-\alpha} .$$

Note that $l$ is the additional base station whose location $\mathbf{z}_l$ has to be determined. There can be many local minima and to identify those points, we have used the following two-step approach:

1. subdivide the area of interest $\mathcal{A}_{\mathcal{R}}$ in the network by using the Delaunay triangulation scheme with the location of the base stations and

2. use the gradient descent method to locate the point of minimum interference in each triangle.

### 5.3.3 Delaunay Triangulation

A Delaunay triangulation for a set of points $\mathcal{S}$ in the two-dimensional plane, denoted by $\mathrm{DT}(\mathcal{S})$ is the triangulation or subdivision of the two-dimensional plane into triangles such that no point in $\mathcal{S}$ is inside the circumference of any triangle in $\mathrm{DT}(\mathcal{S})$. The Delaunay triangulation of a discrete set of points $\mathcal{S}$ corresponds to the dual graph of the Voronoi tessellation for $\mathcal{S}$.

We chose the Delaunay triangulation because we have the following properties.

**Proposition 5.3.1.** *Any local minimum interference over the region enclosed by the triangle* $\mathcal{T} \setminus \{p_1, p_2, p_3\}$ *is also a global minimum interference over this triangle.*

*Proof.* Consider the following function

$$g'(\mathbf{z}, \mathbf{z}_j) := \frac{1}{\|\mathbf{z} - \mathbf{z}_j\|^{\alpha}} ,$$

which is defined in the network except at point $\mathbf{z}_j$. Therefore, the total interference at point $\mathbf{z}$ is given by

$$g(\mathbf{z}) = \sum_{\mathbf{z}_j \in \mathcal{S}} g(\mathbf{z}, \mathbf{z}_j) .$$

□

Let us consider the triangle of vertices $p_1, p_2, p_3$ where the three vertices are the positions of three base stations

$$\mathcal{T} = \{\mathbf{z} : \mathbf{z} = \sum_{j=1}^{3} \lambda_j p_j ; 0 \leq \lambda_j \leq 1, j \in \{1,2,3\}, \sum_{j=1}^{3} \lambda_j = 1\} .$$

**Proposition 5.3.2.** *The function* $g'(\mathbf{z}, \mathbf{z_i})$ *and* $g(\mathbf{z})$ *is convex in* $\mathbf{z}$ *over the triangular region* $\mathcal{T} \setminus \{p_1, p_2, p_3\}$.

*Proof.* We first need to prove that $\frac{d^2 g'}{d\mathbf{z}^2}$ is positive.

Let $r_j = \|\mathbf{z} - \mathbf{z}_j\|$. The gradient of $g(\mathbf{z}, \mathbf{z}_j)$ is

$$\frac{dg'}{d\mathbf{z}} = -\alpha \|\mathbf{z} - \mathbf{z}_j\|^{-\alpha-1} \frac{\mathbf{z} - \mathbf{z}_j}{\|\mathbf{z} - \mathbf{z}_j\|} = -\alpha \frac{\mathbf{z} - \mathbf{z}_j}{\|\mathbf{z} - \mathbf{z}_j\|^{\alpha+2}} .$$

This means that

$$\frac{dg'}{dx} = -\alpha \frac{x - x_i}{r_i^{\alpha+2}} \quad \text{and} \quad \frac{dg'}{dy} = -\alpha \frac{y - y_i}{r_i^{\alpha+2}} ,$$

and

$$\begin{aligned} \frac{d^2 g'}{d\mathbf{z}^2} &= -\alpha \left( \frac{1}{\|\mathbf{z} - \mathbf{z}_j\|^{\alpha+2}} + (-\alpha - 2) \|\mathbf{z} - \mathbf{z}_j\|^{-\alpha-3} \frac{(\mathbf{z} - \mathbf{z}_j)^2}{\|\mathbf{z} - \mathbf{z}_j\|} \right) \\ &= -\alpha \left( \frac{1}{\|\mathbf{z} - \mathbf{z}_j\|^{\alpha+2}} - (\alpha + 2) \frac{(\mathbf{z} - \mathbf{z}_j)^2}{\|\mathbf{z} - \mathbf{z}_j\|^{\alpha+4}} \right) \\ &= \alpha(\alpha + 1) \frac{1}{\|\mathbf{z} - \mathbf{z}_j\|^{\alpha+2}} . \end{aligned}$$

Since there is no element of the set $\mathcal{S}$ which is included in the region $\mathcal{T} \setminus \{p_1, p_2, p_3\}$, the function $g'(\mathbf{z}, \mathbf{z}_j)$ is convex on $\mathcal{T} \setminus \{p_1, p_2, p_3\}$. Note that the sum of convex functions is also convex. Therefore, the function

$$g(\mathbf{z}) = \sum_{\mathbf{z}_j \in \mathcal{S}} g'(\mathbf{z}, \mathbf{z}_j) \,,$$

is also convex over the domain $\mathcal{T} \setminus \{p_1, p_2, p_3\}$ and any local minimum of a convex function is also its global minimum. Note that the fact that we are restricting our domain to be inside the triangular region helps us to determine that there is only one global minimum since the domain is a convex subset. □

### 5.3.4 Gradient Descent Method

Gradient descent method, discussed in Chapter 1 of the book [Bertsekas 1999], is based on the observation that if the real-valued function is defined and differentiable in a neighborhood of a point $\mathbf{z}^0$, then the function $g(\mathbf{z})$ decreases fastest if one goes from $\mathbf{z}^0$ in the direction of the negative gradient of $g$ at $\mathbf{z}^0$, *i.e.*, in the direction of $-\nabla g(\mathbf{z}^0)$. Since our objective is to find the minimum of $g$, we will use the gradient descent method. It follows that, if

$$\mathbf{z}^1 = \mathbf{z}^0 - \delta t \frac{\nabla g(\mathbf{z}^0)}{|\nabla g(\mathbf{z}^0)|} \,,$$

and therefore

$$\mathbf{z}^{k+1} = \mathbf{z}^k - \delta t \frac{\nabla g(\mathbf{z}^k)}{|\nabla g(\mathbf{z}^k)|} \,,$$

where $\delta t > 0$ is the step size. Note that $g(\mathbf{z}^{k+1}) < g(\mathbf{z}^k)$. First approximate location of minimum interference point $\mathbf{z}^0$ is the centroid of the triangle:

$$\mathbf{z}^0 = (x^0, y^0) = \left( \frac{x_{p_1} + x_{p_2} + x_{p_2}}{3}, \frac{y_{p_1} + y_{p_2} + y_{p_3}}{3} \right) ,$$

where $p_1, p_2$ and $p_3$ are the vertices of the triangle. In order to ensure that the points $\mathbf{z}^k$ $(k \geq 0)$ lie inside the triangle, we have used the method described in the article [Weisstein 2008].

### 5.3.5 Heuristics

Here we propose two heuristics to add $K$ additional base stations at the points of minimum interference identified by the gradient descent method.

Let $\mathcal{M}$ be the set of the location of these points of minimum interference.

1. *Heuristic 1:* The optimal position of an additional base station is found as follows.

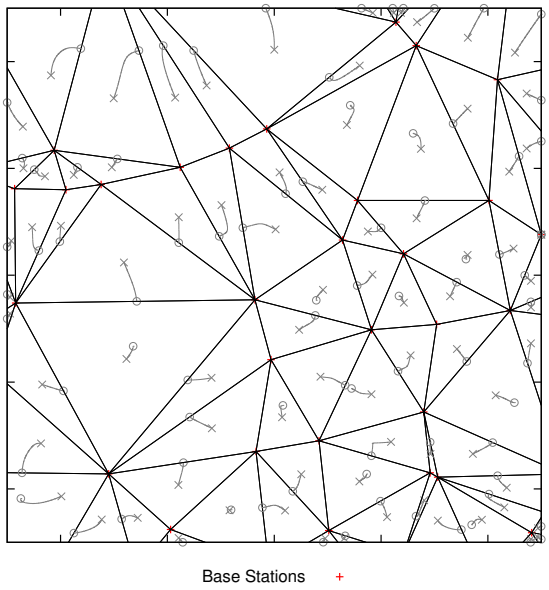


Figure 5.2: Finding points of local minimum interference in the area of interest $\mathcal{A}_{\mathcal{R}}$.

(a) Rank points in set $\mathcal{M}$ in the ascending order of interference or signal level received from all base stations in the set $\mathcal{S}$.

(b) Select the lowest ranked element $m$ from the set $\mathcal{M}$. The location of point $m$ shall become the position of an additional base station.

(c) Remove $m$ from the set $\mathcal{M}$, *i.e.*, $\mathcal{M} := \mathcal{M} - m$.

(d) For additional base stations, repeat from step (b).

2. *Heuristic 2:* Steps (a)-(c) of *Heuristic 2* are the same as in *Heuristic 1*. However, the addition of a base station at a point of minimum interference in set $\mathcal{M}$ may increase the interference at the remaining points in set $\mathcal{M}$, represented by $\{\mathcal{M} - m\}$. Therefore, after addition of a base station, we propose that the area of interest is re-triangulated to identify a new set $\mathcal{M}$ of points of minimum interference. In other words, in *Heuristic 2*, the points of minimum interference in the area of interest shall be identified before finding the location for the addition of each new base station.

   Note that the Delaunay triangulation in this case will be provided by the Bowyer-Watson algorithm, described in articles [Bowyer 1981, Watson 1981], which gives another approach for incremental construction. This also gives an alternative to edge flipping for computing the Delaunay triangles containing a newly inserted vertex.

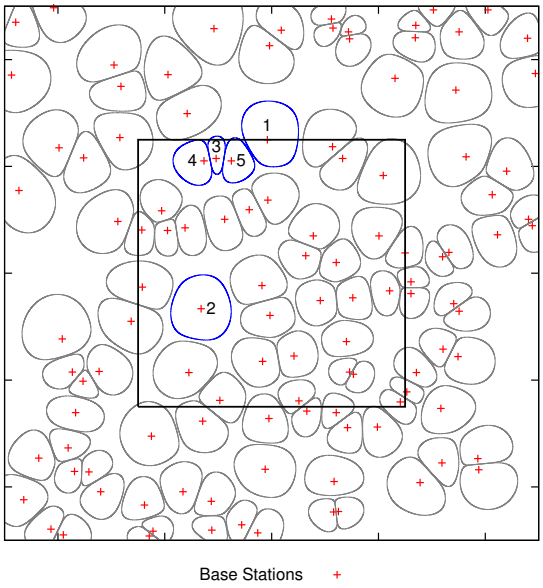


Figure 5.3: 5 base stations are added to the area of interest $\mathcal{A}_{\mathcal{R}}$ using *Heuristic 1*. The number indicates the order of addition to the network. $\beta = 1.0$ and $\alpha = 4.0$.

## 5.4 Evaluation and Results

We consider a cellular data network spread in an area of $10000 \times 10000$ square km and base stations are distributed in this area according to Poisson point process of intensity $\lambda = 1$ base stations per unit square km. We consider the attenuation coefficient $\alpha = 4.0$ and the coverage area of a base station is the area around this base station where it can be received with SIR at least equal to the SIR threshold $\beta = 1.0$. We assume that our area of interest $\mathcal{A}_{\mathcal{R}}$ lies in the center of this network and is a square area with each side of length 500 km.

### 5.4.1 Summary of Results

Figure 5.1 shows the $\beta$-coverage areas of the base stations distributed according to Poisson point process of intensity $\lambda = 1$. It also shows the area of interest $\mathcal{A}_{\mathcal{R}}$.

Figure 5.2 shows the process of the identification of the points of minimum interference in the area of interest $\mathcal{A}_{\mathcal{R}}$. Locations marked with a cross (x) show the first approximation of the points of minimum interference. Gradient descent method uses these first approximate positions to arrive at the final locations, marked with a circle (o), which is the true point of minimum interference in the region formed by the Delaunay triangle. Note that, in cases where a triangular region lies partially within the area of interest $\mathcal{A}_{\mathcal{R}}$, we are interested in identifying the point of minimum interference lying within the area of interest $\mathcal{A}_{\mathcal{R}}$.

Figures 5.3 and 5.4 shows the positioning of $K = 5$ additional base stations in the network

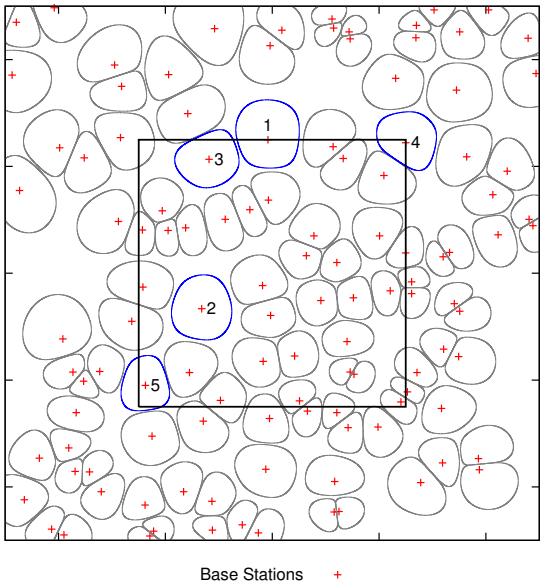


Figure 5.4: 5 base stations are added to the area of interest $\mathcal{A}_{\mathcal{R}}$ using *Heuristic 2*. The number indicates the order of addition to the network. $\beta = 1.0$ and $\alpha = 4.0$.

by using the approaches of *Heuristic 1* and *Heuristic 2* respectively. In order to show the improvement achieved by the two heuristics, we have computed the total area in the area of interest $\mathcal{A}_{\mathcal{R}}$ which lies within the coverage of any of the base stations in the newly formed set of base stations $\mathcal{S}'$. Note that the set $\mathcal{S}'$ also includes the additional base stations whose location is found using *Heuristic 1* and *Heuristic 2*.

In order to compute the capacity, we will numerically integrate (5.3) over the area of interest $\mathcal{A}_{\mathcal{R}}$. We will sub-divide $\mathcal{A}_{\mathcal{R}}$ into small sub-rectangles of size $\Delta x \times \Delta y$ and in each sub-rectangle, we will compute the capacity as

$$c(\mathbf{z}^k) = \sum_{i \in \mathcal{S}'} W \log_2(1 + S_i(\mathbf{z}^k)) \,,$$

where $\mathbf{z}^k = (x^k, y^k)$ is the center of the sub-rectangle $k$. Therefore, the average capacity can be numerically computed as

$$\mathbb{E}[c(\mathbf{z})] = \frac{1}{\sigma^2_{\mathcal{R}}} \int_{\mathcal{A}_{\mathcal{R}}} c(\mathbf{z})\, d\mathbf{z} = \frac{1}{\sigma^2_{\mathcal{R}}} \sum_k c(\mathbf{z}^k) \Delta x \Delta y \,.$$

Table 5.1 and 5.2 summarize the results obtained with both heuristics.

| | *Existing Network* | *Heuristic 1* | *Heuristic 2* |
|---|---|---|---|
| Capacity | 1.3559 | 1.5614 | 1.7007 |
| Percentage Increase | | 15.15% | 25.42% |

Table 5.1: Average capacity (bits/sec/Hetz/km$^2$) over the area of interest $\mathcal{A}_{\mathcal{R}}$.

| | *Existing Network* | *Heuristic 1* | *Heuristic 2* |
|---|---|---|---|
| Total coverage area | 168776 | 190501 | 204628 |
| Coverage percentage | 67,51% | 76,20% | 81,85% |
| Percentage Increase | | 12.87% | 21.25% |

Table 5.2: Coverage in the area of interest $\mathcal{A}_{\mathcal{R}}$.

## 5.5 Conclusions

We have studied the problem of optimally locating $K$ additional base stations in an existing cellular network. We showed that the problem of finding the optimal location of a set of new base stations is an NP-Hard problem. In our analysis, we considered a sub-region of an existing cellular data network where the service provider wants to increase the coverage and throughput of the users. We used interference gradient method to locate the points of minimum interference in the area of interest and proposed two heuristics to find the positions of additional based stations. Later, we evaluated the performance of these heuristics. In Chapter 9, we will discuss some extensions to this work.

# Part II

# Multi-hop Wireless Networks

# Chapter 6

# Transmission Range in Wireless Networks

In the first part of this thesis, we analyzed the local capacity of wireless networks with various MAC schemes and we only considered single-hop simultaneous transmissions. This abstraction of the multi-hop aspect of communication between nodes allowed us to concentrate on the localized capacity of wireless networks. However, the final destination of a packet may not be located within the transmission range of its source and the packet may have to be transported through multiple relays before delivery. Let us assume that $\overline{L}$ is the mean distance between a source and its destination node and $r_\lambda$ is the average transmission range of a transmitter in the network. Therefore, the average number of relays required to deliver a packet to its destination is $\overline{L}/r_\lambda$.

The framework of local capacity may not give a complete insight into the end-to-end throughput capacity of different MAC schemes in multi-hop wireless networks and this requires us to extend our analysis to take into account the multi-hop aspect of communication between nodes. In this chapter, we will evaluate the following parameters in multi-hop wireless networks consisting of randomly distributed nodes:

- normalized optimum transmission range and
- the minimized number of retransmissions required to transport a packet through multiple relays before delivery to its final destination.

We will measure these parameters for ALOHA based scheme where simultaneous transmitters are dispatched according to a uniform Poisson distribution and compare these results with various grid pattern based schemes where simultaneous transmitters are positioned in specific regular grid patterns. Note that, in this chapter, we will perform our analysis under *no fading* channel model only. However, in the next chapter, we will quantify throughput capacity which is inversely proportional to the average number of retransmissions required to deliver packets

in the network for various MAC schemes under *no fading* as well as *Rayleigh fading* channel models.

## 6.1 Model and Assumptions

For our analysis in this chapter, we consider a network which consists of nodes which are uniformly distributed in an infinite plane, *i.e.*, $\mathcal{A} = \mathbb{R}^2$. As we consider the *no fading* channel model only, the channel gain between a transmitter and a receiver depends only on the Euclidean distance between these two nodes and the attenuation coefficient $\alpha$.

We recall that these models are already described in detail in §3.1.

## 6.2 Normalized Optimum Transmission Range

The probability of successfully receiving a packet at distance $r$ from the transmitter is denoted by $p(\lambda, r, \beta, \alpha)$. Our aim is to find the value of $r$ which maximizes the quantity $rp(\lambda, r, \beta, \alpha)$. Therefore, the minimum number of retransmissions required to deliver a packet to its destination located at mean distance $\overline{L}$ is proportional to $\frac{\overline{L}}{rp(\lambda,r,\beta,\alpha)}$. This optimum transmission range of an arbitrary transmitter under a given density $\lambda$ of the set of simultaneous transmitters, *i.e.* the set $\mathcal{S}$, is denoted by $r_\lambda$. Because of an obvious homothetic invariance, we can also write

$$r_1 = \sqrt{\lambda} r_\lambda \, .$$

In this chapter, we will determine the optimum values of $r_1$ and $\frac{1}{rp(\lambda,r,\beta,\alpha)}$ with $\lambda = 1$, for slotted ALOHA and various grid pattern based schemes.

## 6.3 Slotted ALOHA Scheme

In this section, we will evaluate the optimum average transmission range of slotted ALOHA scheme.

### 6.3.1 Evaluation of Transmission Range

Using (4.5), the probability of successfully transmitting a packet at distance $r$, in case of slotted ALOHA scheme, can be written as

$$p(\lambda, r, \beta, \alpha) = P\left(\mathcal{W}(\lambda) < \frac{r^{-\alpha}}{\beta}\right) = \sum_{n \geq 0} \frac{(-C\lambda)^n}{n!} \frac{\sin(\pi n \gamma)}{\pi} \Gamma(n\gamma) \left(\frac{r^{-\alpha}}{\beta}\right)^{-n\gamma}, \qquad (6.1)$$

where, in case of *no fading*,

$$C = \pi \Gamma(1-\gamma) \, ,$$

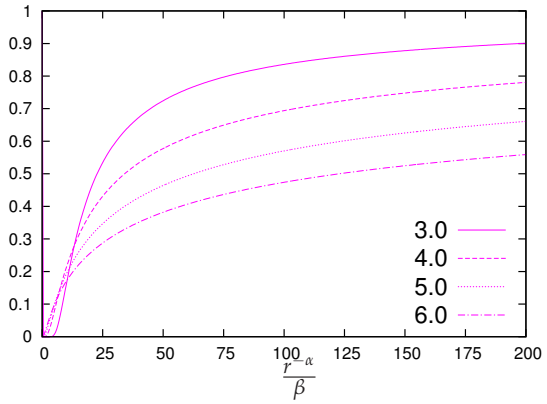


Figure 6.1: $P\left(\mathcal{W}(\lambda) < \frac{r^{-\alpha}}{\beta}\right)$ versus $\frac{r^{-\alpha}}{\beta}$ for $\lambda = 1$ and various values of $\alpha$.

and $\gamma = \frac{2}{\alpha}$. Figure 6.1 shows the plot of $P\left(\mathcal{W}(\lambda) < \frac{r^{-\alpha}}{\beta}\right)$ versus $\frac{r^{-\alpha}}{\beta}$ for $\lambda = 1$ and various values of $\alpha$.

Here, we will use simple algebra to show the homothetic invariance of $r_1$ which has also been proved in the article [Adjih *et al.* 2004].

**Theorem 6.3.1.** *$r_1 = \sqrt{\lambda} r_\lambda$, where $r_\lambda$ is the radius under the given density $\lambda$ of the set of simultaneous transmitters $\mathcal{S}$ such that*

$$P\left(\mathcal{W}(\lambda) < \frac{{r_\lambda}^{-\alpha}}{\beta}\right) = \int_0^{\frac{{r_\lambda}^{-\alpha}}{\beta}} w(x,\lambda)dx = p_0\,,$$

*where $p_0$ is a constant under given values of $\alpha$ and $\beta$.*

*Proof.* The signal level at any point in the plane with Poisson distributed transmitters is a random variable and the Laplace transform of its probability density is given by (4.4). Using the reverse Laplace transform we have

$$w(x,\lambda) = \frac{1}{2i\pi}\int_{-i\infty}^{+i\infty} \tilde{w}(\theta,\lambda)e^{\theta x}d\theta\,.$$

Inserting the expression from (4.4) in the above equation and commuting the integral signs because

$$\int_0^{\frac{{r_\lambda}^{-\alpha}}{\beta}} e^{\theta x}dx = \frac{e^{\theta\frac{{r_\lambda}^{-\alpha}}{\beta}} - 1}{\theta}\,,$$

yields

$$\frac{1}{2i\pi}\int_{-i\infty}^{+i\infty} \frac{e^{\theta\frac{{r_\lambda}^{-\alpha}}{\beta}} - 1}{\theta}\tilde{w}(\theta,\lambda)d\theta = p_0\,.$$

The change of variable $\lambda^{\frac{\alpha}{2}}\theta = \theta'$, makes $\lambda$ disappear from the $\tilde{w}(\theta, \lambda)$ expression

$$\frac{1}{2i\pi}\int_{-i\infty}^{+i\infty}\frac{e^{\theta' \frac{r_\lambda \sqrt{\lambda}^{-\alpha}}{\beta}} - 1}{\theta'}\tilde{w}(\lambda^{\frac{-\alpha}{2}}\theta', 1)d\theta' = p_0 \, .$$

Since $\tilde{w}(\lambda^{\frac{-\alpha}{2}}\theta', 1)$ is independent of $\lambda$ and $r_\lambda$ is multiplied by $\sqrt{\lambda}$, we get that $r_\lambda$ is simply proportional to $1/\sqrt{\lambda}$, *i.e.*, $r_\lambda = r_1/\sqrt{\lambda}$. □

Our objective is to derive the optimum value of $r_1$ which maximizes the function $rp(\lambda, r, \beta, \alpha)$ for $\lambda = 1.0$.

## 6.4 Grid Pattern Based Schemes

When activated by a grid pattern based scheme under *no fading* channel model, the reception areas of all transmitters remain the same, in every slot, *modulo* a translation and/or rotation. Therefore, by virtue of a grid pattern, we can consider *w.l.o.g.* the transmitter $i$ located at origin, *i.e.*,

$$\mathbf{z}_i = \mathbf{z}_0 = (x_0, y_0) = (0, 0) \, .$$

Let $r$ by the distance of point $\mathbf{z}$ from origin and the probability to receive a signal at distance $r$, from the transmitter $i$ at origin, with SIR at least equal to $\beta$ is

$$p(\lambda, r, \beta, \alpha) = 1, \quad \text{if } \mathbf{z} = (x, y) \text{ lies within the reception area of transmitter } i;$$
$$p(\lambda, r, \beta, \alpha) = 0, \quad \text{otherwise} \, .$$

Therefore, in case of grid pattern based schemes, we can define the optimum transmission range of a transmitter as equal to its maximum transmission range, *i.e.*, the maximum distance within its reception area at which it can transmit successfully and the minimum average number of retransmissions required to deliver a packet to its final destination at mean distance $\overline{L}$ becomes equal to $\overline{L}/r$.

As we discussed earlier, the purpose of our analyses of grid pattern based schemes is to establish bounds on the capacity in wireless networks. In this chapter also, we are interested in establishing an upper bound on the normalized transmission range and a lower bound on the number of retransmissions required to deliver a packet in wireless networks. That is why, we are interested in determining the maximum transmission range of a transmitter with various grid pattern based schemes. As we have introduced the notion of maximum transmission range, we will first briefly discuss the progression of a packet, towards its destination, in multi-hop wireless networks with grid pattern based schemes. Later we will present the numerical method we have used to determine the maximum transmission range in wireless networks with grid pattern based schemes.

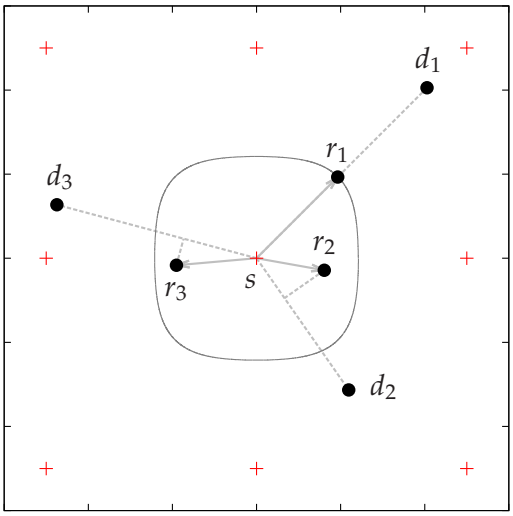


Figure 6.2: An example: node $s$ carries packets for destination nodes $d_1$, $d_2$ and $d_3$ and transmits the packet for the destination $d_1$ towards the relay $r_1$. Nodes in the network employ square grid pattern based scheme.

We define the *progress* of a packet as the distance between the transmitter and the receiver relay projected onto the line joining the transmitter and the final destination node of the transmitted packet. A node $j$ is said to be in transmitter $i$'s forward direction if the progress is non-negative when transmitter $i$ transmits packet to the receiver node $j$ successfully. Otherwise, node $j$ is said to be in the backward direction of transmitter $i$.

We assume that a transmitter in the network is also aware of the following parameters:

- its own cartesian coordinates,
- the cartesian coordinates of all destination nodes for which it is carrying a packet (this information can be contained in the packet itself) and
- the cartesian coordinates of all receiver nodes located within its reception area. In order to obtain this information, we may assume that a slot is sub-divided into management and data sub-slots and this information is collected during the management sub-slot and the packet is later transmitted during the data sub-slot. However, this specification is beyond the scope of this thesis and we only assume that this information is available at all transmitters.

Using this information, a transmitter can determine to transmit the packet with the largest forward progress (this condition maybe relaxed for the packets that can be delivered to their destination nodes immediately). This ensures that the number of hops required to reach the

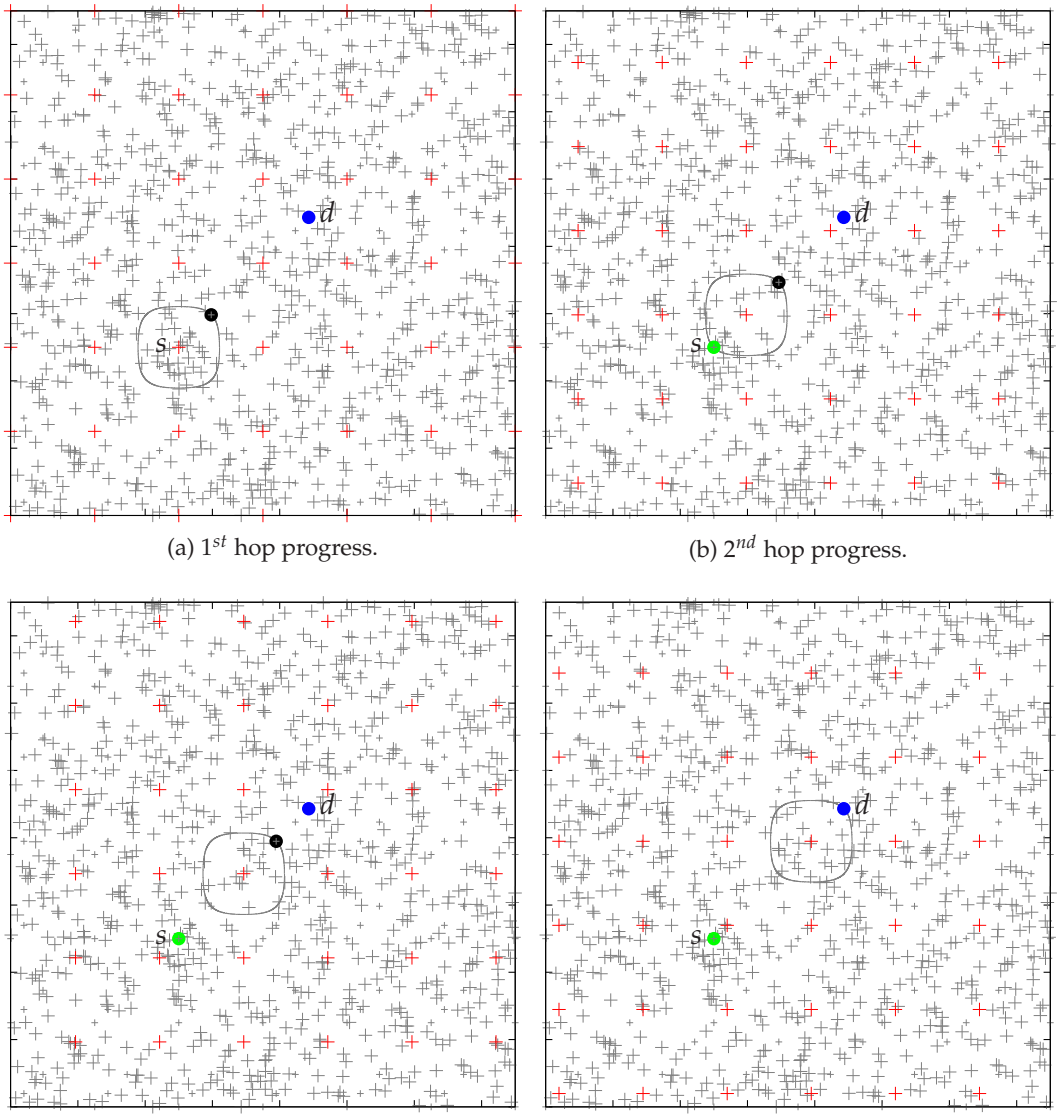


(a) $1^{st}$ hop progress.

(b) $2^{nd}$ hop progress.

(c) $3^{rd}$ hop progress.

(d) $4^{th}$ hop progress (packet delivered).

Figure 6.3: An example: progress of a packet from the source node $s$ towards the destination node $d$ with square grid pattern based scheme.

destination are minimized. Note that, we assume that a transmitter, when activated for transmission by the grid pattern based scheme, always has a packet to transmit. Consider the example in Fig. 6.2 where nodes in the network employ square grid pattern based scheme. This figure shows a set of simultaneous transmitters where the transmitter $s$ is carrying packets for the destination nodes $d_1$, $d_2$ and $d_3$. Note that, the closed curve bounding the node $s$ is the boundary of its reception area. As observed in the figure, the packet for destination $d_1$ has the

largest forward progress and, therefore, node $s$ transmits this packet to the relay node $r_1$.

Figure 6.3 is the figurative representation of the progress of a packet from node $s$ towards node $d$ in a network with randomly distributed nodes. In this case, nodes employ square grid pattern based scheme. Under this scheme, simultaneous transmitters, in each slot, are selected according to the rules specified in §3.4 and they form a regular square grid pattern which is *modulo* a translation and/or rotation. In the figure, the set of simultaneous transmitters are represented by the red color and the inactive nodes (potential receivers) are represented by the gray color. The source, destination and successful relay nodes are represented by green, blue and black colors respectively. When the source node $s$ is activated for transmission by the MAC scheme, it transmits the packet to the next relay. Similarly, Figures 6.3(b)-(d) show the progress of the packet from the successive relay nodes towards the final destination of the packet. The maximum forward progress of a packet is equal to the maximum transmission range achievable with the MAC scheme employed by nodes. As the density of nodes in the network increases and under the assumption that simultaneous transmitters always have packets to be transmitted in the direction of their maximum transmission range, the forward progress of the packets approach the maximum transmission range and packets travel in straight lines from their source nodes towards their destination nodes. If $\overline{L}$ is the mean distance between source and its destination node, we can see that the minimum number of hops required to reach the destination node is exactly equal to $\frac{\overline{L}}{r_\lambda}$, where $r_\lambda$ is the maximum transmission range under the given density of the set $\mathcal{S}$. In this chapter, we will evaluate the maximum transmission range of a transmitter with various grid pattern based schemes. We will cover the grid patterns of square, rectangular, hexagonal and triangle as shown in Fig. 3.1. For grid pattern based schemes, we are interested in the maximum transmission range and it is intuitive to assume that the rectangular grid pattern maybe able to achieve higher transmission range as compared to other grid patterns because transmitters along one dimension are far apart as compared to the other dimension. Therefore, under certain conditions, we maybe able to achieve better bounds on the network throughput capacity in multi-hop wireless networks with rectangular grid pattern based scheme. Our discussion in the following sections will help us in identifying those conditions. Note that, the density of the set of simultaneous transmitters $\lambda$ depends on parameter $d$. However, $r_1 = \sqrt{\lambda} r_\lambda$ is independent of the value of $d$ or, for that matter, $\lambda$ as it is invariant for any homothetic transformation of the set of simultaneous transmitters $\mathcal{S}$.

### 6.4.1 Evaluation of Transmission Range

The correlation between the location of simultaneous transmitters, in case of grid pattern based MAC schemes, makes it extremely difficult to develop a tractable analytical model and derive the closed-form expression for the distribution of signal levels and the maximum transmission range. Therefore, we will propose a numerical method to compute the maximum transmission range in wireless networks with grid pattern based schemes. The set of simultaneous transmitters, *i.e.* the set $\mathcal{S}$, is arranged in a grid pattern. We will cover grids of square, rectangular,

hexagonal and triangle patterns and, by consequence of the grid pattern, all transmitters have the same maximum transmission range *modulo* a translation and/or rotation. We will use the method of Lagrange multipliers, described in Chapter 17 of the book [Arfken 1985], to find the maximum transmission range of transmitter $i$ located at the origin while fulfilling the constraint of SIR threshold.

We can formulate our problem as follows.

$$\begin{aligned} \text{Maximize: } & D_i(\mathbf{z}) = \|\mathbf{z} - \mathbf{z}_i\| = \|\mathbf{z}\|, \\ \text{subject to: } & S_i(\mathbf{z}) = \beta \,, \end{aligned} \tag{6.2}$$

where $D_i(\mathbf{z})$ represents the Euclidean distance of point $\mathbf{z}$ from $\mathbf{z}_i$. The contour line of the function

$$D_i(\mathbf{z}) = \|\mathbf{z}\| = \kappa \,,$$

where $\kappa$ is a constant, is a circle in the plane with point $\mathbf{z}$ on its boundary at a given distance $\kappa$ from the origin. Similarly, the contour line of the SIR function

$$S_i(\mathbf{z}) = \frac{\|\mathbf{z} - \mathbf{z}_i\|^{-\alpha}}{\sum\limits_{j \neq i, \mathbf{z}_j \in \mathcal{S}} \|\mathbf{z} - \mathbf{z}_j\|^{-\alpha}} = \frac{\|\mathbf{z}\|^{-\alpha}}{\sum\limits_{j \neq i, \mathbf{z}_j \in \mathcal{S}} \|\mathbf{z} - \mathbf{z}_j\|^{-\alpha}} = \beta \,, \tag{6.3}$$

is the closed curve $\mathcal{C}_i(\beta, \alpha)$ that forms the boundary of the reception area $\mathcal{A}_i(\lambda, \beta, \alpha)$ of transmitter $i$. Our goal is to locate a point on the curve $\mathcal{C}_i(\beta, \alpha)$ which is furthest from the location of the transmitter $i$ and to determine its Euclidean distance from $\mathbf{z}_i$. Figure 4.3 is the figurative representation of these parameters. The contour lines of the functions $D_i(\mathbf{z})$ and $S_i(\mathbf{z})$ may be distinct but they will intersect or meet each other. In other words, while moving along the contour line of the function $S_i(\mathbf{z}) = \beta$, *i.e.*, along the curve $\mathcal{C}_i(\beta, \alpha)$, the value of $D_i(\mathbf{z})$ may vary. Only when the contour lines of functions $D_i(\mathbf{z})$ and $S_i(\mathbf{z})$ meet tangentially, *i.e.*, when the contour lines meet but do not cross each other that we do not increase or decrease the value of $D_i(\mathbf{z})$. The contour lines meet at the critical point where the tangent vectors of these contour lines are parallel and that point in the plane is the point of our interest. Note that, as the gradient of a function is perpendicular to the contour lines, the gradients of the functions $D_i(\mathbf{z})$ and $S_i(\mathbf{z})$ are also parallel at our point of interest.

We define the gradient of the function $D_i(\mathbf{z})$, $\nabla D_i(\mathbf{z})$, as

$$\nabla D_i(\mathbf{z}) = \begin{bmatrix} \frac{\partial}{\partial x} D_i(\mathbf{z}) \\ \frac{\partial}{\partial y} D_i(\mathbf{z}) \end{bmatrix} .$$

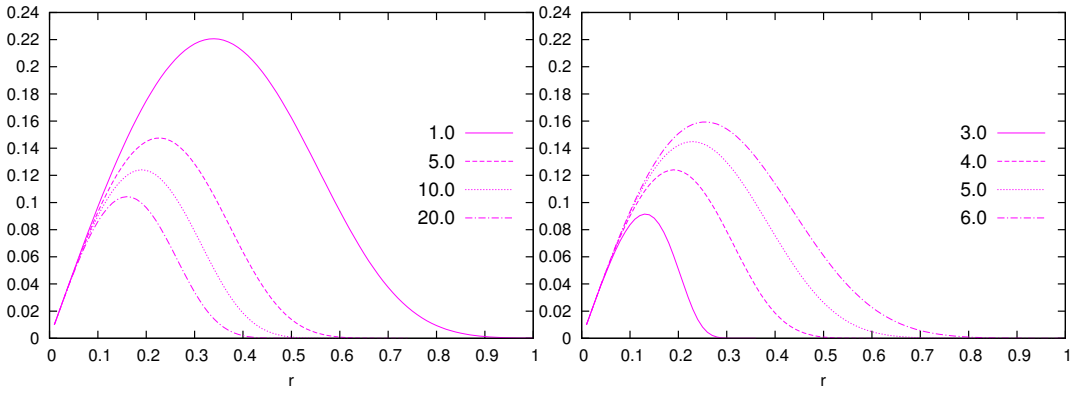


(a) $\beta$ is varying and $\alpha = 4.0$. (b) $\beta = 10.0$ and $\alpha$ is varying.

Figure 6.4: Optimizing $rp(\lambda, r, \beta, \alpha)$ with $\lambda = 1$ for slotted ALOHA scheme.

Similarly, the gradient of $S_i(\mathbf{z})$, $\nabla S_i(\mathbf{z})$, at point $\mathbf{z}$ on the curve $\mathcal{C}_i(\beta, \alpha)$, is

$$\nabla S_i(\mathbf{z}) = \begin{bmatrix} \frac{\partial}{\partial x} S_i(\mathbf{z}) \\ \frac{\partial}{\partial y} S_i(\mathbf{z}) \end{bmatrix}.$$

As it is extremely hard to derive close form expressions for the SIR function $S_i(\mathbf{z})$ and its gradient function when simultaneous transmitters are positioned in a specific grid pattern in the plane, we have to rely on the numerical method, described in §4.3.1, to obtain a discretized and numerically convergent representation of $\mathcal{C}_i(\beta, \alpha)$ by finite elements. We will use this discretized representation of $\mathcal{C}_i(\beta, \alpha)$ and compute the gradients of the functions $D_i(\mathbf{z})$ and $S_i(\mathbf{z})$ to determine the maximum transmission range. Equation (4.9) is a discretized representation of $\mathcal{C}_i(\beta, \alpha)$ and we will compute the gradients of the functions $D_i(\mathbf{z})$ and $S_i(\mathbf{z})$ at the sequence of points $\mathbf{z}(k)$ in (4.9) to determine the point where the gradients are parallel. This point will give the maximum transmission range of the transmitter $i$.

## 6.5 Evaluation and Results

In this section, we will perform detailed analysis of the MAC schemes, we have discussed in this chapter, under *no fading* channel model only.

### 6.5.1 Slotted ALOHA Scheme

In case of slotted ALOHA scheme, our goal is to identify the optimal value of $r$ which maximizes the value of $rp(\lambda, r, \beta, \alpha)$, which is computed from (6.1) with varying values of the parameters $\beta$ and $\alpha$ and $\lambda = 1$.

Figure 6.4 shows the plots of $rp(\lambda, r, \beta, \alpha)$ versus $r$, $\beta$ and $\alpha$ with $\lambda = 1$. In Fig. 6.4(a), $r$ and $\beta$ are varying and $\alpha$ is fixed at 4.0. Similarly, in Fig. 6.4(b), $r$ and $\alpha$ are varying and $\beta$ is fixed at 10.0. Note that, as we are only interested in the optimal value of $r$ which maximizes the value of $rp(\lambda, r, \beta, \alpha)$ at given $\beta$ and $\alpha$ and $\lambda = 1$, we only refer to this value by $r_1$ in our discussion.

### 6.5.2 Grid Pattern Based Schemes

In case of grid pattern based schemes, we will use the numerical method described in §6.4.1 to compute the maximum transmission range. For our numerical simulations, we will use the same network map as was described in §4.5 and the transmitters are spread in this network area in square, rectangular, hexagonal or triangular grid pattern. Here also, we set the parameter $d$, for all grid patterns, equal to 25 meters although it will have no effect on the validity of our conclusions as normalized maximum transmission range $r_1$ is independent of $\lambda$. We will only compute the maximum transmission range of the transmitter $i$, located in the center of the network area, *i.e.*, $\mathbf{z}_i = (x_i, y_i) = (0, 0)$. The network area is large enough so that the reception area of transmitter $i$, and hence its maximum transmission range, is close to its reception area and maximum transmission range in an infinite map. In case of rectangular grid pattern, we vary the values of the factors $k_1$ and $k_2$ in the ratio of $\frac{1}{2}$ and $\frac{1}{4}$. Note that the factors $k_1$ and $k_2$ are associated with the construction of the rectangular grid pattern as shown in Fig. 3.1. This allows us to derive the conclusions on the impact of these factors on the maximum transmission range of rectangular grid pattern based schemes. We can determine the value of $\lambda$ using the Voronoi tessellation of the network map and we derive its value for square, rectangular, hexagonal and triangular grid pattern to be equal to $\frac{1}{d^2}$, $\frac{1}{k_1 k_2 d^2}$, $\frac{4}{3\sqrt{3}d^2}$ and $\frac{2}{\sqrt{3}d^2}$ respectively.

### 6.5.3 Summary of Results

Figure 6.5 shows the plots of the normalized optimal transmission range $r_1$ with varying $\beta$ and $\alpha$ for all MAC schemes. In Fig. 6.5(a) and 6.5(b), $\beta$ is varying and $\alpha$ is fixed at 4.0. Similarly, in Fig. 6.5(c) and 6.5(d), $\beta$ is fixed at 10.0 and $\alpha$ is varying. These results show that under typical values of $\beta$, in the range of 1 to 20, and $\alpha$, in the range of 3 to 6, the normalized maximum transmission range of all grid pattern based schemes are almost similar and *at most* double the normalized optimal average transmission range of slotted ALOHA scheme. However, as the values of $\beta$ and $\alpha$ approach their extremities, certain grid pattern based schemes seem to outperform the others.

For example, as $\beta$ approaches zero, the maximum transmission range is influenced most by the closest source of interference and the most optimal scheme which maximizes the transmission range, in this case, is based on rectangular grid pattern with $k_2 \gg k_1$. However, as $\beta$ increases and approaches the value of 100, influence from more distant transmitters increase and the shape of the reception area approaches the shape of a small circular disk with transmitter at the center. Therefore, in this case, the most optimal scheme to maximize the transmission

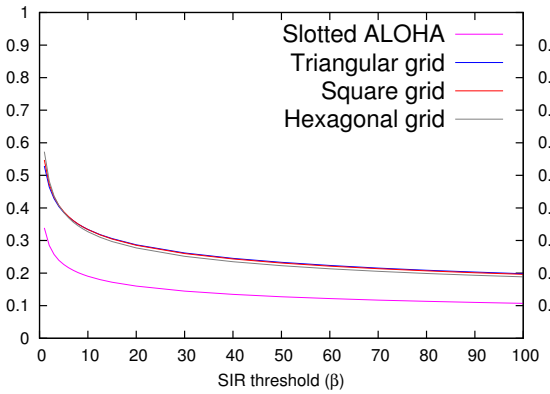


(a) $\beta$ is varying and $\alpha = 4.0$.

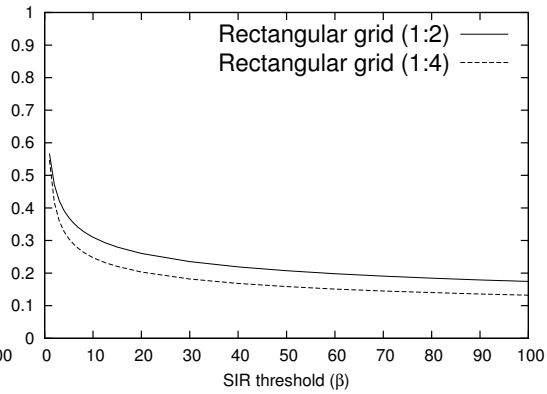


(b) $\beta$ is varying and $\alpha = 4.0$. Rectangular grid with given $(k_1 : k_2)$ ratio.

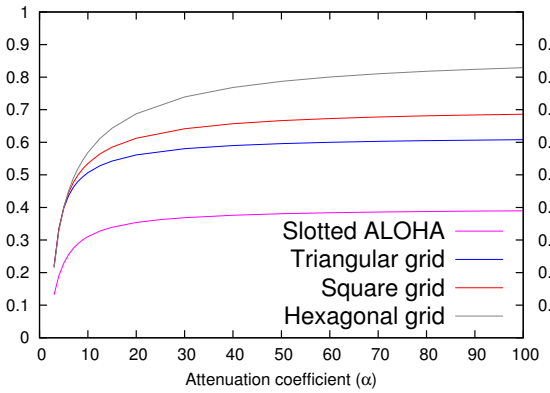


(c) $\beta = 10.0$ and $\alpha$ is varying.

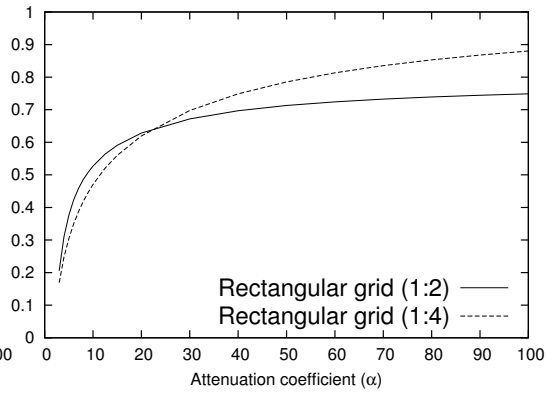


(d) $\beta = 10.0$ and $\alpha$ is varying. Rectangular grid with given $(k_1 : k_2)$ ratio.

Figure 6.5: Optimal $r_1 = \sqrt{\lambda} r_\lambda$ with $\lambda = 1$ of slotted ALOHA and grid pattern based schemes.

range is based on triangular grid pattern.

On the other hand, as $\alpha$ increases, the reception area is influenced most by the interference from the nearest interferer as compared to any other interferer and the area of correct reception tends to be the Voronoi cell. Therefore, in this case, the most optimal scheme should also be based on rectangular grid pattern with $k_2 \gg k_1$. We will discuss the asymptotic behavior of normalized maximum transmission ranges of grid pattern based schemes in detail in §6.6.

Figure 6.6 shows the plots of the optimized (minimized) number of retransmissions $\frac{1}{rp(\lambda,r,\beta,\alpha)}$ required to transport a packet through multiple relays from its source node to its destination node located at unit distance with $\lambda = 1$ and varying $\beta$ and $\alpha$. In Fig. 6.6(a) and 6.6(b), $\beta$ is varying and $\alpha$ is fixed at 4.0 whereas in Fig. 6.6(c) and 6.6(d), $\beta$ is fixed at 10.0 and $\alpha$ is varying.

Note that, in case of grid pattern based schemes, $p(\lambda, r, \beta, \alpha)$ is equal to one as, under

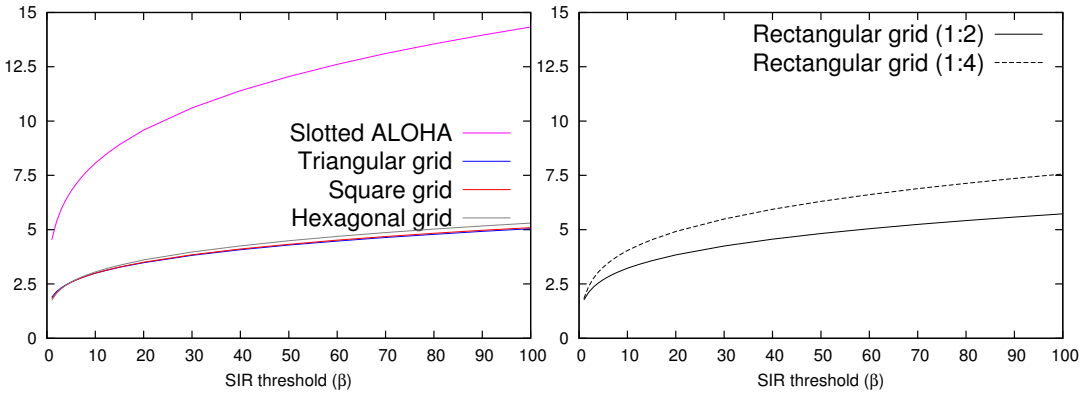


(a) $\beta$ is varying and $\alpha = 4.0$.

(b) $\beta$ is varying and $\alpha = 4.0$. Rectangular grid with given $(k_1 : k_2)$ ratio.

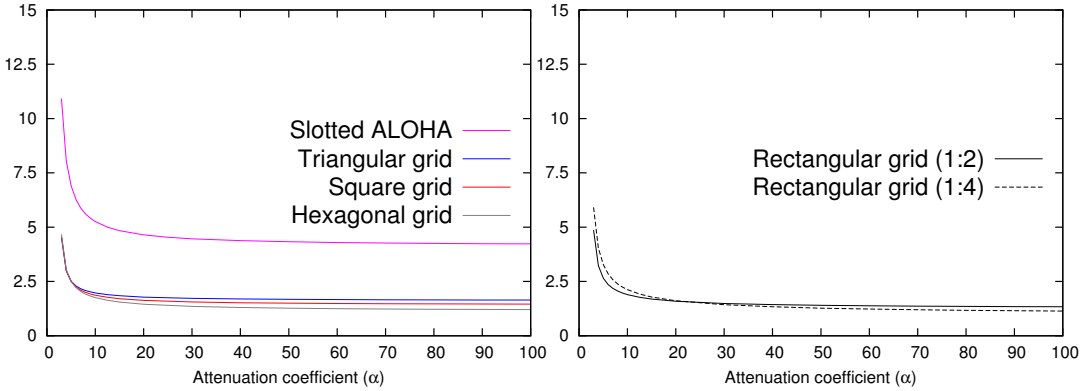


(c) $\beta = 10.0$ and $\alpha$ is varying.

(d) $\beta = 10.0$ and $\alpha$ is varying. Rectangular grid with given $(k_1 : k_2)$ ratio.

Figure 6.6: Optimal (minimized) $\frac{1}{rp(\lambda,r,\beta,\alpha)}$ with $\lambda = 1$ of slotted ALOHA and grid pattern based schemes.

*no fading* channel model, the reception area of a transmitter remains the same *modulo* a rotation. Therefore, in case of grid pattern based schemes, $\frac{1}{rp(\lambda,r,\beta,\alpha)} = \frac{1}{r}$. In order to quantify the improvement in the quantity $\frac{1}{rp(\lambda,r,\beta,\alpha)}$ by grid pattern based schemes over slotted ALOHA scheme, we perform a scaled comparison of slotted ALOHA and all grid pattern based schemes which is obtained by dividing the optimized quantity $\frac{1}{rp(\lambda,r,\beta,\alpha)}$ of all these schemes with the minimized quantity $\frac{1}{rp(\lambda,r,\beta,\alpha)}$ of triangular grid pattern based scheme. The reason of choosing triangular grid pattern based scheme as the reference here is twofold. First is that, under typical values of $\beta$ and $\alpha$, it can achieve the most optimal normalized transmission range in the wireless network although it is almost similar to other grid pattern based schemes. Second reason is that, triangular grid pattern based scheme can be visualized as the most optimal node

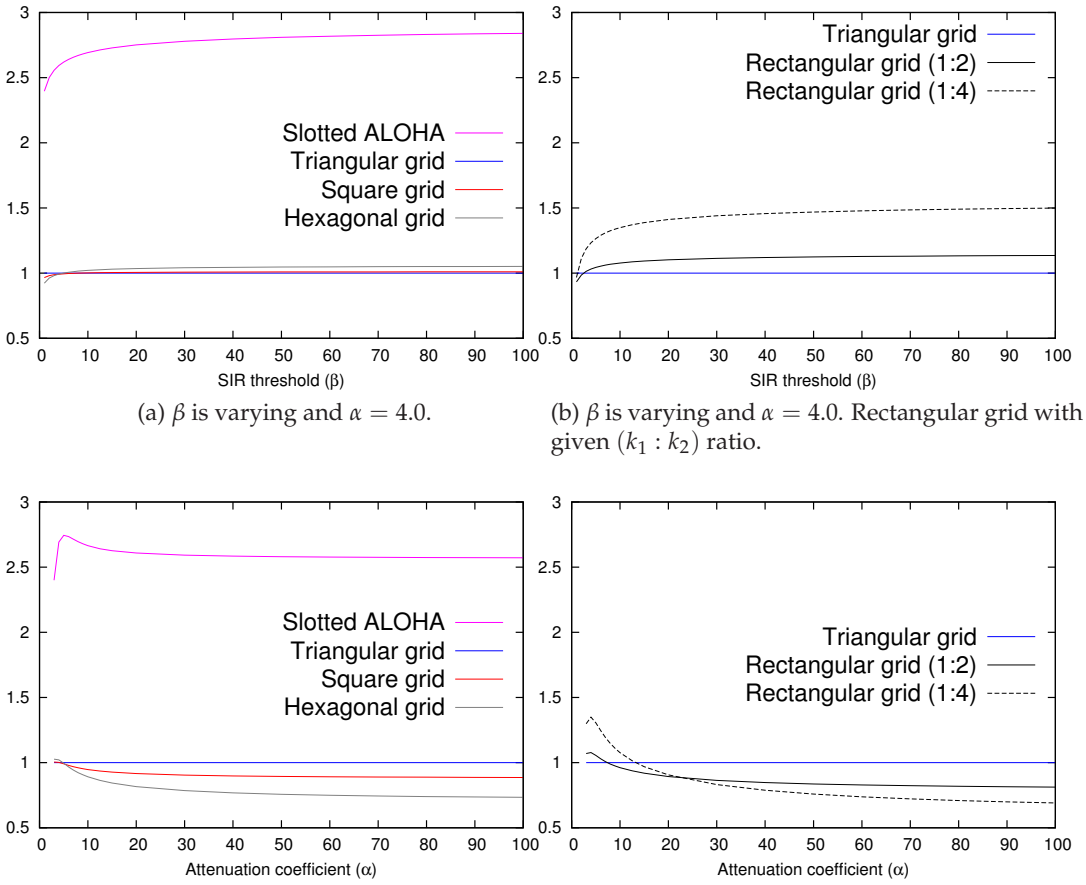


(a) $\beta$ is varying and $\alpha = 4.0$.

(b) $\beta$ is varying and $\alpha = 4.0$. Rectangular grid with given $(k_1 : k_2)$ ratio.

(c) $\beta = 10.0$ and $\alpha$ is varying.

(d) $\beta = 10.0$ and $\alpha$ is varying. Rectangular grid with given $(k_1 : k_2)$ ratio.

Figure 6.7: Optimal (minimized) $\frac{1}{rp(\lambda,r,\beta,\alpha)}$ with $\lambda = 1$ of slotted ALOHA and grid pattern based schemes normalized *w.r.t.* triangular grid pattern based scheme.

coloring scheme which ensures that neighboring transmitters are located at exactly the distance $d$ from each other. Figure 6.7 shows the scaled comparison with $\beta$ and $\alpha$ varying. It can be observed that the grid pattern based schemes can reduce the number of transmissions required to deliver a packet to its destination to *at most* one-third of the optimal average number of transmissions required with slotted ALOHA scheme. In other words, end-to-end network throughput in wireless networks with grid pattern based schemes can *at most* be three times the throughput with slotted ALOHA scheme. It is also interesting to note that when we only consider the single-hop simultaneous transmissions as in Chapter 4, the most optimal node coloring scheme, *i.e.*, the scheme based on triangular grid pattern may achieve the most optimal local capacity. However, it may not achieve the most optimal end-to-end network throughput in multi-hop wireless networks as the values of $\beta$ and $\alpha$ approach their extremities.

## 6.6 Asymptotic Analysis of Grid Pattern Based Schemes

In this section, we will analyze the asymptotic behavior of the normalized maximum transmission range of grid pattern based schemes as $\beta$ and $\alpha$ approach extreme values.

The unexpected result is that when $\beta$ approaches zero or $\alpha$ approaches infinity, the most optimal grid pattern to maximize the normalized transmission range is the *linear* pattern, *i.e.*, transmitters are equidistantly spaced on a line.

### 6.6.1 With Respect to SIR Threshold

In this section, we will again assume that the transmitter $i$ is located at origin and our aim is to find its maximum transmission range as $\beta$ approaches infinity.

From (6.3), we can write

$$\frac{\|\mathbf{z}-\mathbf{z}_i\|^{-\alpha}}{\sum\limits_{j\neq i,\mathbf{z}_j\in\mathcal{S}}\|\mathbf{z}-\mathbf{z}_j\|^{-\alpha}} = \frac{\|\mathbf{z}^{-\alpha}\|}{\sum\limits_{j\neq i,\mathbf{z}_j\in\mathcal{S}}\|\mathbf{z}-\mathbf{z}_j\|^{-\alpha}} = \frac{r_{\mathbf{z}}^{-\alpha}}{I(x,y)} = \beta\,,$$

where $r_{\mathbf{z}}$ is the distance of point $\mathbf{z}$ from the location of the transmitter $i$ and $I(x,y)$ is the signal level of the interference at point $\mathbf{z}$. As $\beta$ approaches infinity, the reception area of a transmitter shrinks to a circular disk of an infinitesimally small radius with the transmitter at its center, *i.e.*, the transmission radius of transmitter $i$ also shrinks to an infinitesimally small value.

Therefore, we can write the above equation as

$$\frac{r_0(0,0)^{-\alpha}}{\beta} = I(0,0)\,,$$

where $r_0(0,0)$ is the transmission range of transmitter $i$ at origin when $\beta$ approaches infinity and $I(0,0)$ is the received signal level, at the location of transmitter $i$, from all transmitters except $i$, *i.e.*,

$$I(0,0) = \sum_{j\neq i,\mathbf{z}_j\in\mathcal{S}}\|\mathbf{z}_i-\mathbf{z}_j\|^{-\alpha} = \sum_{j\neq i,\mathbf{z}_j\in\mathcal{S}}\|\mathbf{z}_j\|^{-\alpha}\,.$$

Our goal is to determine the *normalized* maximum transmission range $r_1'$ which is defined as

$$r_1' = \beta^{\frac{1}{\alpha}} r_0(0,0) = (I(0,0))^{-\frac{1}{\alpha}}\,.$$

Note that, in the above expression, we also normalize the transmission range with respect to (*w.r.t.*) $\beta$ as, when $\beta$ approaches infinity, the transmission range $r_0(0,0)$ will also approach zero. Therefore, we will compute $\beta^{\frac{1}{\alpha}} r_0(0,0)$ for various grid pattern based schemes in the same network setting, as described in §6.5.2, and identity the scheme which maximizes the normalized maximum transmission range in the wireless network under the asymptotic condition when $\beta$ approaches infinity. Table 6.1 shows the values of the normalized maximum transmission

| | | $r'_1 = \beta^{\frac{1}{\alpha}} r_0(0,0)$ | $c'(\infty, 4.0) = \pi(r'_1)^2 = \pi\beta^{\frac{2}{\alpha}} r_0^2(0,0)$ |
|---|---|---|---|
| *Square* | | 0.638232 | 1.279696 |
| *Rectangular* | $\frac{k_1}{k_2} = \frac{1}{2}$ | 0.554905 | 0.967357 |
| | $\frac{k_1}{k_2} = \frac{1}{4}$ | 0.409452 | 0.526690 |
| *Hexagonal* | | 0.609856 | 1.168434 |
| *Triangular* | | 0.644845 | 1.306352 |

Table 6.1: Normalized maximum transmission range $r'_1$ and local capacity $c'(\beta, \alpha)$ of various grid pattern based schemes as $\beta$ approaches infinity. $\alpha = 4.0$ and $\lambda = 1.0$.

range of various grid pattern based schemes as $\beta$ approaches infinity with $\alpha = 4.0$ and $\lambda = 1.0$. It is evident that as $\beta$ approaches infinity, the most optimal maximum transmission range is obtained with triangular grid pattern based scheme. In Chapter 4, we evaluated the local capacity $c(\beta, \alpha)$ of single-hop wireless networks with various MAC schemes. It will also be interesting to compute its value for grid pattern based schemes when $\beta$ approaches infinity. In this case, $\sigma(\lambda, \beta, \alpha)$ will be equal to the surface area of the reception area of a transmitter which is a circular disk. We know that the normalized area of this circular disk is equal to $\pi(r'_1)^2$ and the results in Table 6.1 prove that, as $\beta$ approaches infinity, the most optimal scheme to maximize local capacity is also based on triangular grid pattern.

It is also interesting to see what happens when $\beta$ approaches zero.

We know that for $\beta$ equal or greater than one, the reception areas of the transmitters do not overlap as there is only one transmitter that can be received successfully at any location in the plane. Figure 4.2 shows such an example where the reception areas of randomly distributed transmitters are shown for $\beta$ greater or equal to one. However, as the value of $\beta$ decreases and approaches an infinitesimally small value, the reception areas of transmitters start to overlap.

In Fig. 6.8, nodes in the network use square grid pattern based scheme and this figure shows the transformation of the reception area of a transmitter (marked in red) in the same network setting, as described in §6.5.2, as the value of $\beta$ approaches an infinitesimally small

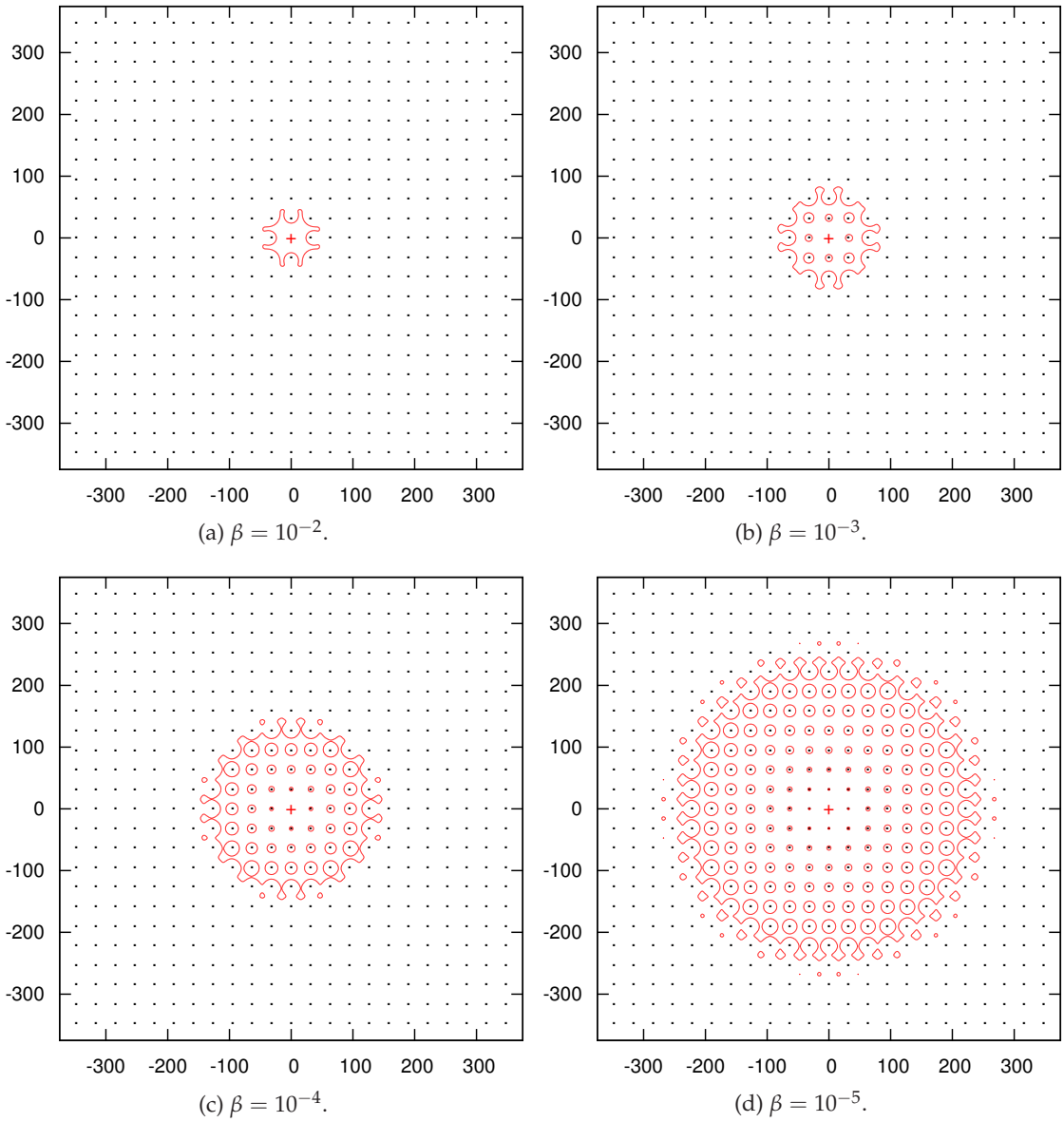


(a) $\beta = 10^{-2}$. (b) $\beta = 10^{-3}$.

(c) $\beta = 10^{-4}$. (d) $\beta = 10^{-5}$.

Figure 6.8: Reception area of a transmitter with square grid pattern based scheme as $\beta$ approaches an infinitesimally small value. $\alpha = 4.0$, $d = \sqrt{1000}$ and $\lambda = \frac{1}{d^2} = \frac{1}{1000}$.

value. Note that, as $\beta$ approaches an infinitesimally small value, reception area of the transmitter becomes *non-contiguous* and also excludes the locations of the interferers where the signal level of interference is infinite. We can see that as $\beta$ approaches zero, the reception area tends to an infinite plane though excluding the points of the locations of the interferers.

Our results in Fig. 6.5(b) and 6.6(b) also hint that as $\beta$ decreases, the most optimal trans-

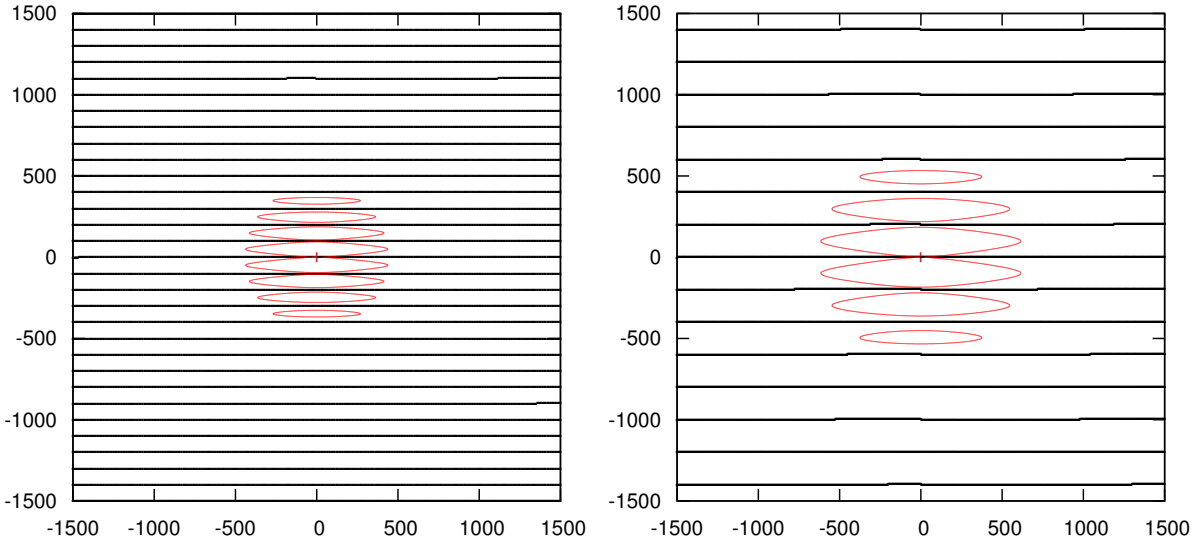


(a) $\frac{k_1}{k_2} = \frac{10}{100}$.




(b) $\frac{k_1}{k_2} = \frac{5}{200}$.

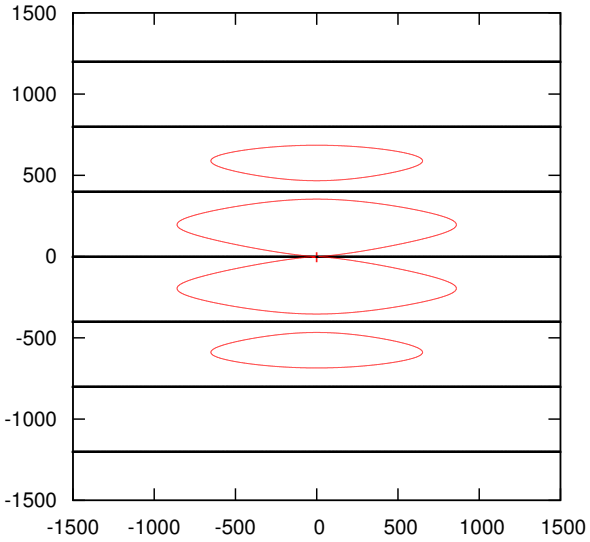


(c) $\frac{k_1}{k_2} = \frac{2.5}{400}$.

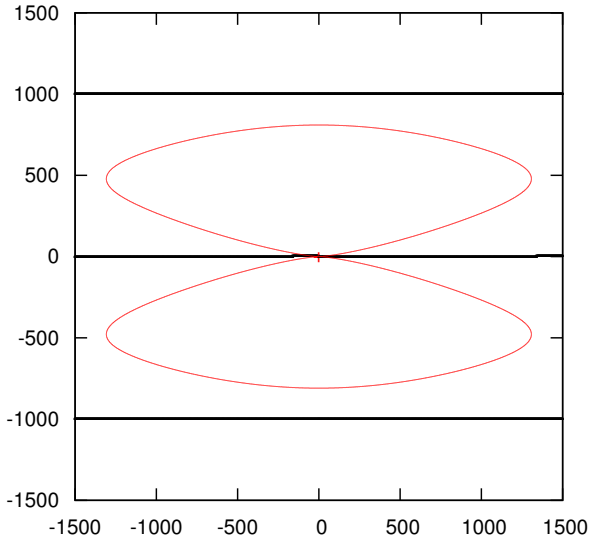


(d) $\frac{k_1}{k_2} = \frac{1}{1000}$.

Figure 6.9: Reception area of a transmitter with rectangular grid pattern based scheme as $\frac{k_1}{k_2}$ approaches an infinitesimally small value. $\beta = 10^{-5}$, $\alpha = 4.0$, $d = 1$ and $\lambda = \frac{1}{k_1 k_2 d^2} = \frac{1}{1000}$ is kept *constant*.

mission scheme to maximize the transmission range is based on rectangular grid pattern with $k_2 > k_1$. Figure 6.9 shows the transformation of the reception area of a transmitter when nodes, in the network setting of §6.5.2, use rectangular grid pattern based scheme and the value of

$k_1/k_2$ approaches an infinitesimally small value. Note that because of a very small $k_1$, the transmitters in this figure appear to be densely packed on lines. It can be noticed that as the value of $k_1/k_2$ decreases, the reception area of the transmitter becomes *contiguous* and its maximum transmission range also increases. For example, at $\beta = 10^{-5}$, the results in Fig. 6.8(d) and 6.9(d) show that, as compared to square grid pattern, rectangular grid pattern based scheme can achieve longer transmission range. Note that, in Fig. 6.9, values of the factors $k_1$ and $k_2$ are varied such that $\lambda$ remains constant and we observed their impact on the maximum transmission range. From our results, we conjecture that as $\beta$ approaches zero, the most optimal MAC scheme to maximize the normalized transmission range in multi-hop wireless networks, such that the reception area of a transmitter also remains connected, is based on rectangular grid pattern with $k_2$ approaching infinity or, in other words, *linear* pattern with transmitters equidistantly placed on a straight line and, as the density of nodes in the network approach infinity, $k_1$ (*i.e.* the distance in-between simultaneous transmitters on the line) approaching an infinitesimally small value.

### 6.6.2 With Respect to Attenuation Coefficient

As $\alpha$ approaches infinity, the reception area of a transmitter tends to be the Voronoi cell around this transmitter. This is true for all values of $\beta$. This is because the reception area is influenced most by the interference from the nearest transmitter as compared to any other transmitter. The average area of the Voronoi cell is equal to the inverse of the density of the set of simultaneous transmitters, *i.e.*, $1/\lambda$. Figure 6.10 shows the reception area of a transmitter in the network setting of §6.5.2 where nodes employ square, rectangular, hexagonal and triangular grid pattern based schemes with $\beta = 1.0$ and $\alpha = 100.0$. In this figure, the arrows represent the directions of the maximum transmission range of a transmitter with each scheme. We have used the numerical method described in §4.3.1 to plot these reception areas and we can see that at very high value of $\alpha$, the reception areas tend to be the Voronoi cell of a specific shape which depends on the positioning of simultaneous transmitters by the grid pattern based schemes.

As $\alpha$ approaches infinity, reception area of a transmitter in square grid pattern based scheme approaches the shape of a square with area $d^2$ and this is irrespective of the value of $\beta$. This can also be observed in Fig. 6.10(a). From Voronoi tessellation of the network map, we can see that the density of the set of simultaneous transmitters $\lambda$ is equal to $1/d^2$ and the maximum transmission range is along the diagonals of the square reception area, given by $r_\lambda = d/\sqrt{2}$. Therefore, as $\alpha$ approaches infinity, the normalized maximum transmission range of a transmitter in square grid pattern based scheme approaches the value of

$$r_1 = \sqrt{\lambda} r_\lambda = \frac{1}{\sqrt{2}} \approx 0.707 \, .$$

This result can also be verified by the plot in Fig. 6.5(c) when $\alpha = 100.0$.

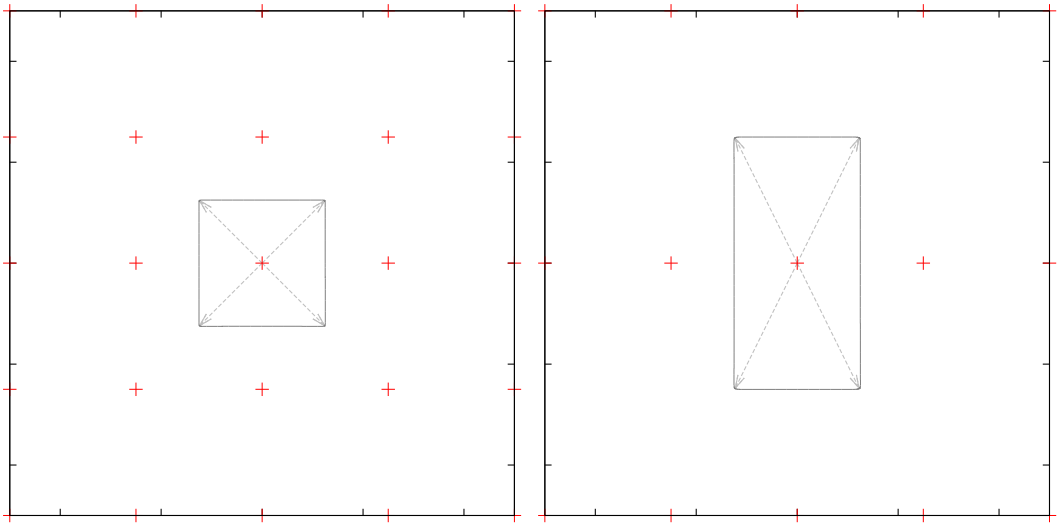

(a) Square grid.

(b) Rectangular grid with $\frac{k_1}{k_2} = 0.5$.

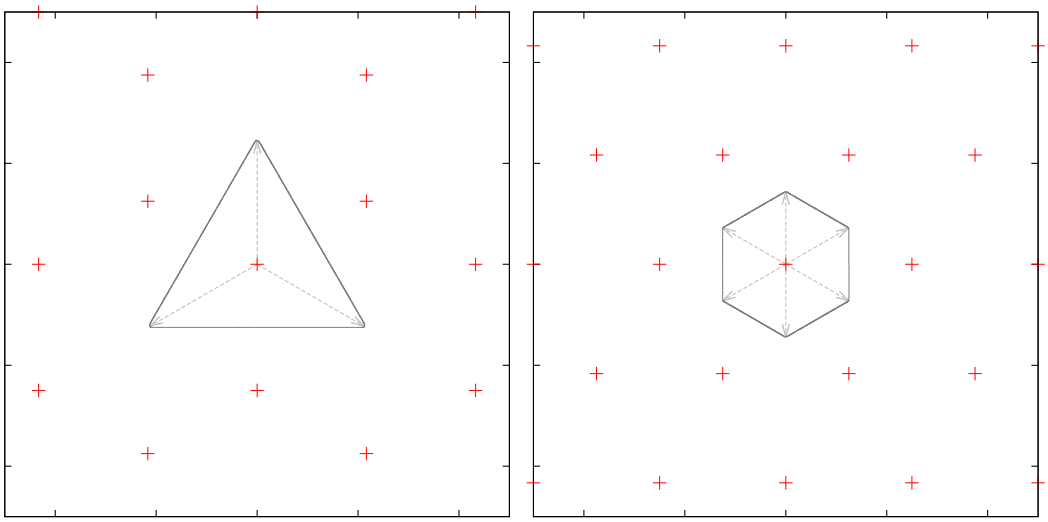

(c) Hexagonal grid.

(d) Triangular grid.

Figure 6.10: Reception area of a transmitter with various grid pattern based schemes. Grids are constructed with parameter $d$. $\beta = 1.0$ and $\alpha = 100.0$.

In case of rectangular grid pattern based scheme, as $\alpha$ approaches infinity, the reception area approaches the shape of a rectangle with area equal to $k_1 k_2 d^2$ and $\lambda = 1/k_1 k_2 d^2$ where $k_1$ and $k_2$ are the factors associated with the dimensions of the rectangular grid pattern as shown in Fig. 3.1. In this case also, the maximum transmission range is along the diagonals of the

rectangular reception area and is given by

$$r_\lambda = \frac{d}{2}\sqrt{k_1^2 + k_2^2}$$
$$= \frac{d}{2}\sqrt{k_1 k_2}\sqrt{\frac{\left(\frac{k_1}{k_2}\right)^2 + 1}{\left(\frac{k_1}{k_2}\right)}},$$

and therefore,

$$r_1 = \sqrt{\lambda} r_\lambda = \frac{1}{2}\sqrt{\frac{\left(\frac{k_1}{k_2}\right)^2 + 1}{\left(\frac{k_1}{k_2}\right)}}.$$

It is interesting to note that in case of rectangular grid pattern based scheme, the maximum transmission range depends on the factors $k_1$ and $k_2$. Note that, in case of square grid pattern, $k_1/k_2 = 1$. However, in case of rectangular grid pattern, $k_1/k_2$ can be any value less than one and as $k_2$ approaches infinity, $k_1/k_2$ approaches zero and $r_1$ approaches infinity. Our results in Fig. 6.5(d) also verify that, with $\alpha$ approaching 100, as $k_1/k_2$ decreases, $r_1$ increases.

Similarly, we can also repeat the calculations and derive the maximum transmission ranges with hexagonal and triangular grid pattern based schemes under asymptotic conditions.

Table 6.2 shows the normalized maximum transmission range of all grid pattern based schemes as $\alpha$ approaches infinity. The asymptotic behavior of maximum transmission range of various grid pattern based schemes shows that as $\alpha$ increases, the normalized maximum transmission range in the wireless network can be achieved when simultaneous transmitters are positioned in a rectangular grid pattern with $k_2 \gg k_1$. This also allows us to conjecture that asymptotically, as $\alpha$ approaches infinity, the most optimal positioning of simultaneous transmitters, to maximize the normalized transmission range in multi-hop wireless networks, is in a rectangular grid pattern with $k_2$ approaching infinity or, in other words, *linear pattern* with transmitters equidistantly spaced on a straight line. Moreover, as the density of nodes in the network approaches infinity, $k_1$ (the distance in-between simultaneous transmitters on the line) approaches an infinitesimally small number.

## 6.7 Conclusions

We evaluated the performance of multi-hop wireless networks under the framework of normalized optimum transmission range and computed the optimized number of retransmissions required to transport a packet over multi-hop path to its final destination. We used analytical tools, based on realistic interference model, to evaluate the performance of slotted ALOHA and

| | $\lambda$ | $r_\lambda$ | $r_1 = \sqrt{\lambda} r_\lambda$ |
|---|---|---|---|
| *Square* | $\frac{1}{d^2}$ | $\frac{d}{\sqrt{2}}$ | $\frac{1}{\sqrt{2}} \approx 0.707$ |
| *Rectangular* $\left(\frac{k_1}{k_2} < 1\right)$ | $\frac{1}{k_1 k_2 d^2}$ | $\frac{d}{2}\sqrt{k_1 k_2}\sqrt{\frac{\left(\frac{k_1}{k_2}\right)^2+1}{\left(\frac{k_1}{k_2}\right)}}$ | $\frac{1}{2}\sqrt{\frac{\left(\frac{k_1}{k_2}\right)^2+1}{\left(\frac{k_1}{k_2}\right)}}$ |
| *Hexagonal* | $\frac{4}{3\sqrt{3}d^2}$ | $d$ | $\frac{2}{\sqrt{3\sqrt{3}}} \approx 0.877$ |
| *Triangular* | $\frac{2}{\sqrt{3}d^2}$ | $\frac{d}{\sqrt{3}}$ | $\sqrt{\frac{2}{3\sqrt{3}}} \approx 0.620$ |

Table 6.2: Maximum transmission range of a transmitter with various grid pattern based schemes as $\alpha$ approaches infinity.

grid pattern based schemes. Our results show that designing of the MAC scheme to optimize these quantities shall take into account the system parameters like SIR threshold and attenuation coefficient. Our results also show that at typical values of SIR threshold equal to 10.0 and attenuation coefficient equal to 4.0, most optimal scheme is based on triangular grid pattern and compared to slotted ALOHA, which does not use any significant protocol overhead, triangular grid pattern based scheme can only improve the normalized optimum transmission range and network throughput by the factors of *at most* 2 and 3 respectively. However, we still need to quantify the network throughput capacity of these MAC schemes in multi-hop wireless networks.

# Chapter 7

# Throughput Capacity in Wireless Network

In the previous chapter, we used analytical methods to lay the ground work for the analysis of the throughput capacity in multi-hop wireless networks. We derived the optimal normalized transmission range and compared slotted ALOHA with grid pattern based schemes. We also studied the optimized number of retransmissions required to deliver a packet to its final destination with these schemes. However, we have not yet evaluated the actual throughput capacity of various MAC schemes in a realistic wireless network under various channel fading models. In this chapter, we will quantify the throughput capacity of multi-hop wireless networks with various MAC schemes under *no fading* and *Rayleigh fading* channel models.

## 7.1 Model and Assumptions

In this chapter, we will consider a wireless network consisting of $n$ nodes which are distributed in a planar disk of radius $r$ and centered at origin $(0, 0)$. We have used the following models for uniformly distributing nodes on the planar disk:

- *uniform distribution* model and
- *random grid distribution* model.

The *uniform distribution* model takes $n$ as an argument and uniformly distributes $n$ nodes in the planar disk.

Note that uniformly distributed nodes may not give the maximum throughput capacity with grid pattern based schemes especially at low density of nodes because many points of the virtual grid, formed during the construction of the set of simultaneous transmitters $\mathcal{S}$ (see §3.4), may not overlap any node and hence the number of active transmitters in the network, in any given slot, maybe lower than the optimal number possible with grid pattern based schemes.

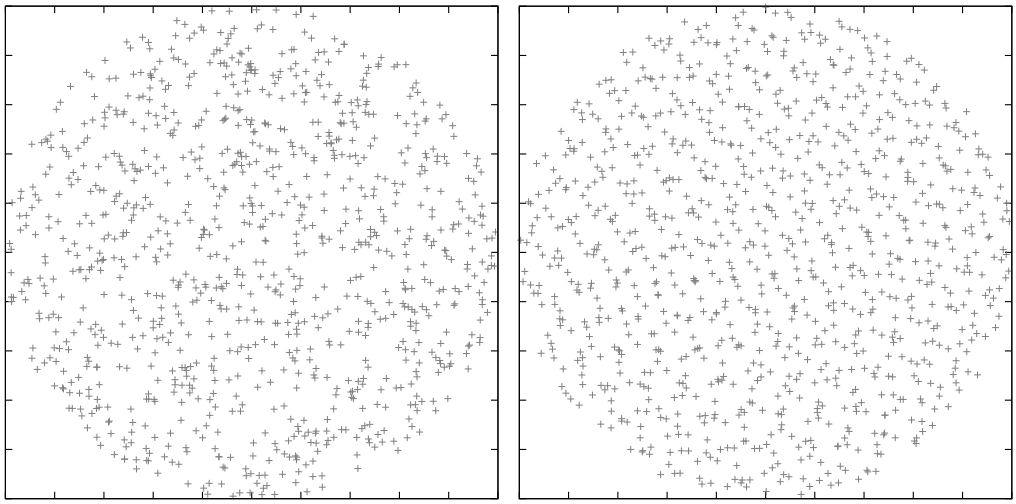

(a) *Uniform distribution.* (b) *Random grid distribution.*

Figure 7.1: Types of node distributions we have used in our Monte Carlo simulations.

As we are interested in finding the optimal throughput capacity, we have devised the *random grid distribution* model. The *random grid distribution* model takes two arguments, $n$ and $d$. Here is how this model uniformly distributes $n$ nodes on the planar disk. Consider a triangular grid pattern[1] of nodes spread in an infinite area also containing the planar disk. Depending on the parameter $d$, let us say that at least $m$ number of nodes lie within the planar disk. Here $d$ is the distance between neighboring nodes in the triangular grid pattern. We may call this triangular grid pattern, with $m$ nodes in the planar disk, a grid frame. There shall be at least $n/m$ such grid frames with each frame contributing a maximum of $m$ nodes to the network. All these grid frames shall be superimposed over each other such that each frame is randomly rotated about the origin $(0, 0)$ and also randomly displaced along $x$-axis and $y$-axis. The random rotation is uniformly selected from the interval $[0, \frac{\pi}{6}]$ and the random displacement along $x$-axis and $y$-axis is uniformly selected from the interval $[0, d]$. Now using the model in §3.4 which describes the construction of the set of simultaneous transmitters $\mathcal{S}$ under grid pattern based scheme and considering that the virtual triangular grid formed from the position of a randomly selected node also overlaps the grid frame to which this node belongs, the set $\mathcal{S}$ will consist of all nodes in this frame which lie within the planar disk. Figure 7.1 shows the distribution of 1000 nodes on the planar disk with both types of node distribution models.

Our main parameter of interest is the end-to-end throughput capacity, denoted by $\zeta(n, \beta, \alpha)$, which is defined as the average maximum rate of successful end-to-end transmissions in a multi-hop wireless network. We will develop an analytical model which we will use with

[1] Because, the only grid pattern based scheme with which we will evaluate the throughput capacity in this chapter is the triangular grid pattern based scheme.

Monte Carlo simulations to compute the *achievable* throughput capacity.

The throughput capacity depends on the number of nodes $n$, SIR threshold $\beta$, attenuation coefficient $\alpha$ as well as the following factors:

– the MAC scheme employed by nodes in the network and

– the average slot occupancy rate of node $i$, $\Omega_i(n)$.

In §7.2, we will identify the parameters of various MAC schemes to tune their respective throughput capacity. Note that $\Omega_i(n)$ also depends on the tuning parameters of the MAC schemes.

We have not yet spoken about the routing protocol as it may also impact the slot occupancy rate $\Omega_i(n)$. As nodes are uniformly distributed in a planar disk and if each node sends data to a randomly selected destination node, it can be argued that routing hot spots may form at the center of the disk. We assume that routing will not be impacted by the throughput capacity because we assume that $\Omega_i(n)$ are given and do not depend on the actual node throughput. We also recall from §3.1.5 that nodes always transmit on the medium when allowed by the MAC layer. For example, with slotted ALOHA scheme, each node transmits with a slot occupancy rate of $p_n$, irrespective of whether it has packets in its buffer or not. In other words, routing will have no impact on the slot occupancy rate of nodes and packets travel approximately along the straight lines from source to destination nodes. Therefore, we can ignore any routing protocol and it is considered beyond the scope of this thesis. Note that some works, *e.g.*, the articles [Georgiadis *et al.* 2006, Stamatiou *et al.* 2009] have investigated delay minimizing routing and optimal throughput back-pressure routing respectively. In this chapter, we will only measure the average maximum rate of successful end-to-end transmissions in a multi-hop wireless network with various MAC schemes. Therefore, our results should compliment the protocol design, *e.g.*, designing protocols based on the results of articles [Georgiadis *et al.* 2006, Stamatiou *et al.* 2009].

The allowed number of retransmissions per packet are also unlimited and we do not take into account any constraints on the packet delivery delay. Therefore, if the multi-hop wireless network is connected, end-to-end delivery is guaranteed. Note that a multi-hop wireless network is connected if there are no isolated nodes in the network, or in other words, at least one path (route) exists between any pair of nodes as discussed in the article [Gupta & Kumar 2000].

If $p_{ij}$ is the probability of successful transmission from node $i$ to node $j$, the average number of transmissions required to deliver a packet from node $i$ to node $j$ is

$$t_{ij} = \frac{1}{p_{ij}} .$$

Note that the value of $t_{ij}$ is an approximation as in case of *no fading*, interference may be correlated from one slot to another slot, *e.g.*, in case of a typical node coloring scheme. However, in our models of MAC schemes, the state information of medium access layer is independent

from one slot to another slot, *i.e.*, the set of simultaneous transmitters $\mathcal{S}$ is constructed independently in each slot. In order to further minimize the correlation of interference from one slot to another, we will also compute the throughput capacity under *Rayleigh fading*.

Consequently, the average minimum number of transmissions required to deliver a packet from node $i$ to node $j$, either directly (single-hop) or over a multi-hop path, is given by

$$m_{ij} = \min_{k} \left\{ m_{ik} + t_{kj} \right\} , \ \forall \ (i,j) , \tag{7.1}$$

such that $m_{ii} = 0$.

In our model, we will consider that all nodes send equal traffic to every other node. Note that this model may not be realistic as nodes have in general a *favorite* destination but, if these destinations are randomly distributed in the network, this model is equivalent since the traffic will be continuous in the network.

**Theorem 7.1.1.** *The throughput capacity $\zeta(n,\beta,\alpha)$ of multi-hop wireless networks consisting of $n$ randomly distributed nodes, where each node sends data to a randomly selected node, is bounded by*

$$\zeta(n,\beta,\alpha) \leq \frac{(n-1)n \sum\limits_{i} \Omega_i(n)}{\sum\limits_{ij} m_{ij}} . \tag{7.2}$$

*Proof.* During $T$ slots, there are on average $T \sum_i \Omega_i(n)$ packet transmission attempts in the network. By the definition of the throughput capacity, the number of successfully delivered packets is $\zeta(n,\beta,\alpha)T$. Since each node sends equal traffic to every other node and there are $n(n-1)$ source-destination pairs, the number of packets delivered from a source node $i$ to a destination node $j$ during $T$ slots is $\frac{\zeta(n,\beta,\alpha)}{n(n-1)}T$. We know that the average minimum number of transmissions required to deliver a packet from node $i$ to node $j$ is $m_{ij}$. Therefore

$$\zeta(n,\beta,\alpha) \frac{\sum\limits_{ij} m_{ij}}{n(n-1)} T ,$$

is less than or equal to the average number of transmission attempts in the network during $T$ slots and should be equal to $T \sum \Omega_i(n)$. This completes the proof of (7.2). □

The challenge here is to compute $p_{ij}$ and $m_{ij}$ for all pairs of nodes and a satisfactory analytical formulation, with all MAC schemes discussed in §7.2, is not feasible. Therefore, we will use Monte Carlo simulation method to compute $p_{ij}$ and $m_{ij}$. If node $i$ is isolated, $m_{ij}$ for all $j$ is equal to infinity and $\zeta(n,\beta,\alpha)$ collapses to zero. Therefore, wireless network of $n$ nodes must be connected and it is a *necessary* condition for the feasibility of the throughput capacity as discussed in the article [Gupta & Kumar 2000]. A wireless network consisting of $n$ randomly distributed nodes is connected *w.h.p.*, that approaches one as $n$ approaches infinity, if $\Omega_i(n)$

scales as $c_1/\log n$ and, consequently, throughput capacity $\zeta(n,\beta,\alpha)$ scales as $c_2\sqrt{n/\log n}$, for some $c_1 > 0$ and $c_2 > 0$ depending on the MAC scheme, interference model, physical layer parameters *etc*. Equation (7.2) incorporates $c_1$ and $c_2$ and, therefore, their values can also be determined.

**Theorem 7.1.2.** *The throughput capacity $\zeta(n,\beta,\alpha)$ has a refined bound, given by*

$$\overline{\zeta}(n,\beta,\alpha) \leq n(n-1)\min_i\left(\frac{\Omega_i(n)}{\Theta_i(n)}\right), \tag{7.3}$$

*where $\Theta_i(n)$ is the traffic load at node $i$ and it is computed as the sum of the average minimum number of transmissions by node $i$, for each packet of a route (flow) passing through $i$.*

*Proof.* During $T$ slots, the number of packets successfully delivered to their destinations are $\zeta(n,\beta,\alpha)T$. As every node sends data to every other node, there are $n(n-1)$ routes in the network and the traffic load (share) of each route during $T$ slots is $\frac{\zeta(n,\beta,\alpha)}{n(n-1)}T$.

Therefore, the slot occupancy of node $i$ during $T$ slots for routing purposes is equal to $\Theta_i\frac{\zeta(n,\beta,\alpha)}{n(n-1)}T$ and its value should be less than or equal to $\Omega_i(n)T$, *i.e.*,

$$\Theta_i\frac{\zeta(n,\beta,\alpha)}{n(n-1)}T \leq \Omega_i(n)T\,.$$

Thus, we arrive at

$$\overline{\zeta}(n,\beta,\alpha) \leq n(n-1)\min_i\left(\frac{\Omega_i(n)}{\Theta_i(n)}\right).$$

□

The values of $\Omega_i(n)$ are almost the same for all $i$ except the slightly higher slot occupancy rate of nodes on the border of the network area because of the border effects, *e.g.*, in case of CSMA and node coloring schemes. However, asymptotically, the difference is negligible.

Therefore, the nodes with minimum average $\Omega_i(n)/\Theta_i(n)$ or, in other words, maximum average $\Theta_i(n)$ lie in the neighborhood of the center of the network area. The bound given by (7.3) is lower than the bound given by (7.2) because the average of $\Theta_i(n)$ in the center is approximately equal to

$$c_3\frac{\sum\limits_i \Omega_i(n)}{n} = c_3\frac{\sum\limits_{ij} m_{ij}(n)}{n},$$

where $c_3$ is a constant and it depends on the shape of the network area. Note that, in this chapter, we will only compute the throughput capacity $\zeta(n,\beta,\alpha)$ given by (7.2) as the refined bound $\overline{\zeta}(n,\beta,\alpha)$ in (7.3) is within the factor $1/c_3$ of $\zeta(n,\beta,\alpha)$ and the constant multiplicative factor $1/c_3$ can be derived from the results on traffic density in ad hoc networks, using node distribution of random waypoint mobility model, as discussed in the article [Hyytiä *et al.* 2006].

For example, in case of rectangular network area, we can compute the value of $c_3$ from the article [Bettstetter *et al.* 2003] to be $c_3 = 2 + \frac{1}{4}$.

## 7.2 Optimization Parameters of MAC Schemes

In this section, we will identify the parameters of various MAC schemes which can be tuned to optimize the throughput capacity with these schemes.

### 7.2.1 Slotted ALOHA Scheme

In case of slotted ALOHA scheme, the throughput capacity $\zeta(n, \beta, \alpha)$ at given values of $n$, $\beta$ and $\alpha$ can be optimized by tuning the medium access probability $p$. We recall that the set of simultaneous transmitters $\mathcal{S}$ with slotted ALOHA scheme is elected using the evaluation model described in §3.2 and the value of $p$ has an impact on the density $\lambda$ of the set $\mathcal{S}$. We will determine its optimized value $p^*(n, \beta, \alpha)$ by using the Monte Carlo simulations we will perform in §7.3, where we will employ the evaluation model of §3.2, and feeding these results into our analytical model, described in §7.1, to compute the throughput capacity $\zeta(n, \beta, \alpha)$.

### 7.2.2 MAC Schemes Based on Exclusion Rules

In this section, we will discuss the tuning of the throughput capacity $\zeta(n, \beta, \alpha)$ of exclusion rules based MAC schemes, *i.e.*, node coloring and CSMA based schemes.

We discussed the evaluation model of node coloring scheme in §3.3.1.1. In that model, the value of $d$, *i.e.*, the minimum Euclidean distance in between simultaneous transmitters controls the selection of the set of simultaneous transmitters $\mathcal{S}$ and its density $\lambda$. Therefore, $d$ can be tuned at its optimized value $d^*(n, \beta, \alpha)$ such that the throughput capacity of node coloring scheme in wireless network consisting of $n$ nodes is maximized under given values of $\beta$ and $\alpha$. Here also, we would like to mention that the throughput capacity $\zeta(n, \beta, \alpha)$ can be computed using the results of Monte Carlo simulations in our analytical model developed in §7.1.

Similarly, we can tune the value of the carrier sense threshold parameter $\theta_{cs}$ of CSMA based scheme using the Monte Carlo simulations with the evaluation model discussed in §3.3.1.2. In other words, the value of $\theta_{cs}$ can be tuned at $\theta^*_{cs}(n, \beta, \alpha)$ to optimize the throughput capacity $\zeta(n, \beta, \alpha)$ of CSMA based scheme under given values of $n$, $\beta$ and $\alpha$.

### 7.2.3 Grid Pattern Based Schemes

The model of grid pattern based schemes is discussed in §3.4. In this chapter, we will only consider the triangular grid pattern based scheme for two reasons. First, it can be visualized as the most optimal packing of simultaneous transmitters with exclusion rules based MAC

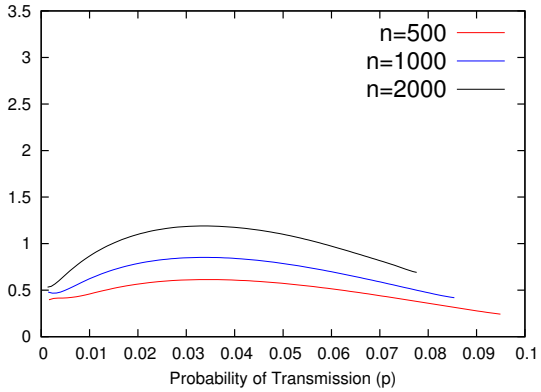


Figure 7.2: Optimization of the throughput capacity $\zeta(n, 20.0, 4.0)$ (packets per slot) with slotted ALOHA scheme in network with *uniform distribution* of nodes under *no fading*. $\beta = 20.0$ and $\alpha = 4.0$.

schemes like node coloring or CSMA and second, under typical values of $\beta$ and $\alpha$, it can achieve the maximum normalized transmission range as shown in Chapter 6.

As described with other MAC schemes, for given values of $n$, $\beta$ and $\alpha$, the value of the parameter $d$ of triangular grid pattern based scheme is varied to find the most optimal $d^*(n, \beta, \alpha)$ which maximizes the throughput capacity $\zeta(n, \beta, \alpha)$ with this scheme. Note that here we will use *random grid distribution* model to distribute $n$ nodes on the planar disk with parameter $d$ of the triangular grid pattern based scheme as the second argument of the model. We will also recompute the optimum throughput capacity of slotted ALOHA, node coloring and CSMA based schemes with *random grid distribution* of nodes.

## 7.3 Evaluation and Results

It does not appear feasible to build a satisfactory and tractable analytical formulation to derive the accurate values of the tuned parameters $p^*(n, \beta, \alpha)$, $d^*(n, \beta, \alpha)$ and $\theta^*_{cs}(n, \beta, \alpha)$ that maximize the throughput capacity $\zeta(n, \beta, \alpha)$ with slotted ALOHA, node coloring, CSMA and triangular grid pattern based schemes. Therefore, we determine these values using the hybrid of analytical model and Monte Carlo simulations. With all MAC schemes, the set of simultaneous transmitters $\mathcal{S}$, in each slot, is constructed using the models described in Chapter 3. In order to compute the probability of successful transmission from each node to every other node, we consider that nodes employ broadcast transmissions and probability of successful transmission is obtained from the number of received and transmitted packets obtained over 25000 slots. With this information, the throughput capacity $\zeta(n, \beta, \alpha)$ can be computed using (7.1) and (7.2).

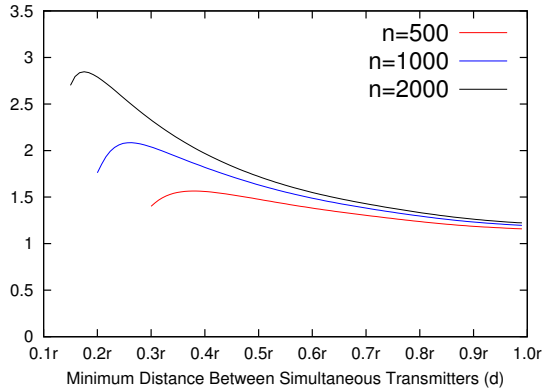


Figure 7.3: Optimization of the throughput capacity $\zeta(n, 20.0, 4.0)$ (packets per slot) with node coloring scheme in network with *uniform distribution* of nodes under *no fading*. $\beta = 20.0$ and $\alpha = 4.0$.

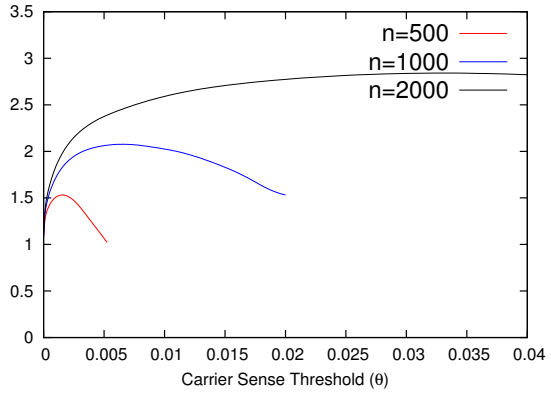


Figure 7.4: Optimization of the throughput capacity $\zeta(n, 20.0, 4.0)$ (packets per slot) with CSMA based scheme in network with *uniform distribution* of nodes under *no fading*. $\beta = 20.0$ and $\alpha = 4.0$.

### 7.3.1 Optimization of the Throughput Capacity

In case of slotted ALOHA, we vary the value of probability of transmission $p$ to determine the optimal $p^*(n, \beta, \alpha)$ which maximizes the throughput capacity $\zeta(n, \beta, \alpha)$ with given values of $n$, SIR threshold $\beta$ and attenuation coefficient $\alpha$. Figure 7.2 shows the throughput capacity $\zeta(n, 20.0, 4.0)$ with slotted ALOHA, in network with *uniform distribution* of nodes, averaged over 100 samples of node distributions. The value of $n$ is varied whereas $\beta = 20.0$ and $\alpha = 4.0$. It can be observed that as $p$ increases, the throughput capacity $\zeta(n, \beta, \alpha)$ increases with rate in $O(\sqrt{n})$ and a maximum occurs at

$$p = p^*(n, 20.0, 4.0) \approx \frac{c_1}{\log n} \approx \frac{0.25}{\log n} .$$

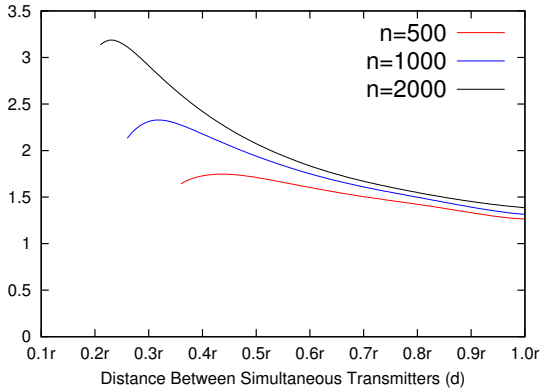


Figure 7.5: Optimization of the throughput capacity $\zeta(n, 20.0, 4.0)$ (packets per slot) with triangular grid pattern based scheme in network with *random grid distribution* of nodes under *no fading*. $\beta = 20.0$ and $\alpha = 4.0$.

In other words, setting the average slot occupancy rate of each node $\Omega_i(n)$ equal to $p^*(n, \beta, \alpha)$ gives the approximate value of the optimal throughput capacity $\zeta(n, \beta, \alpha)$ with slotted ALOHA under given values of $n$, $\beta$ and $\alpha$. Similarly, Fig. 7.3 and 7.4 show the tuning of node coloring and CSMA based schemes respectively in network with *uniform distribution* of nodes under given values of $n$, $\beta = 20.0$ and $\alpha = 4.0$. The optimal values of $d^*(n, \beta, \alpha)$ and $\theta^*_{cs}(n, \beta, \alpha)$ can be determined to obtain the approximate values of the optimal throughput capacity $\zeta(n, \beta, \alpha)$ with these schemes respectively. Note that, in these cases, $\Omega_i(n)$ is the proportion of slots that each node is expected to be active and transmitting under the given values of $d$ and $\theta_{cs}$.

Figure 7.5 shows the optimization of triangular grid pattern based scheme under given values of $n$, $\beta = 20.0$ and $\alpha = 4.0$. The parameter $d$ of the triangular grid pattern based scheme is optimized by varying the argument $d$ of the *random grid distribution* model to distribute $n$ nodes on the planar disk (described in §7.1). This allows the construction of the set of simultaneous transmitters $\mathcal{S}$ which are arranged in a triangular grid pattern with parameter $d$, as shown in Fig. 3.1, which is varied to find the optimal $d^*(n, \beta, \alpha)$.

### 7.3.2 Summary of Results

Figure 7.6 shows the throughput capacity $\zeta(n, 20.0, 4.0)$ versus $n$ at optimized values of tuning parameters $p^*(n, 20.0, 4.0)$, $d^*(n, 20.0, 4.0)$ and $\theta^*_{cs}(n, 20.0, 4.0)$, depending on the MAC scheme, and we can observe that as $n$ increases, the throughput capacity $\zeta(n, \beta, \alpha)$ appears to scale as $c_2\sqrt{n/\log n}$. For example, in case of slotted ALOHA, under *no fading* channel model and $\beta = 20.0$ and $\alpha = 4.0$, $c_2 \approx 0.0715$. Similarly, the approximate values of constants $c_1$ and $c_2$ can also be determined for node coloring, CSMA and triangular grid pattern based schemes. Figure 7.7 shows the throughput capacity $\zeta(1000, \beta, 4.0)$ for all MAC schemes with $\alpha = 4.0$ and $\beta$ varying and Fig. 7.8 shows the comparison of the throughput capacity $\zeta(1000, 20.0, \alpha)$ for all

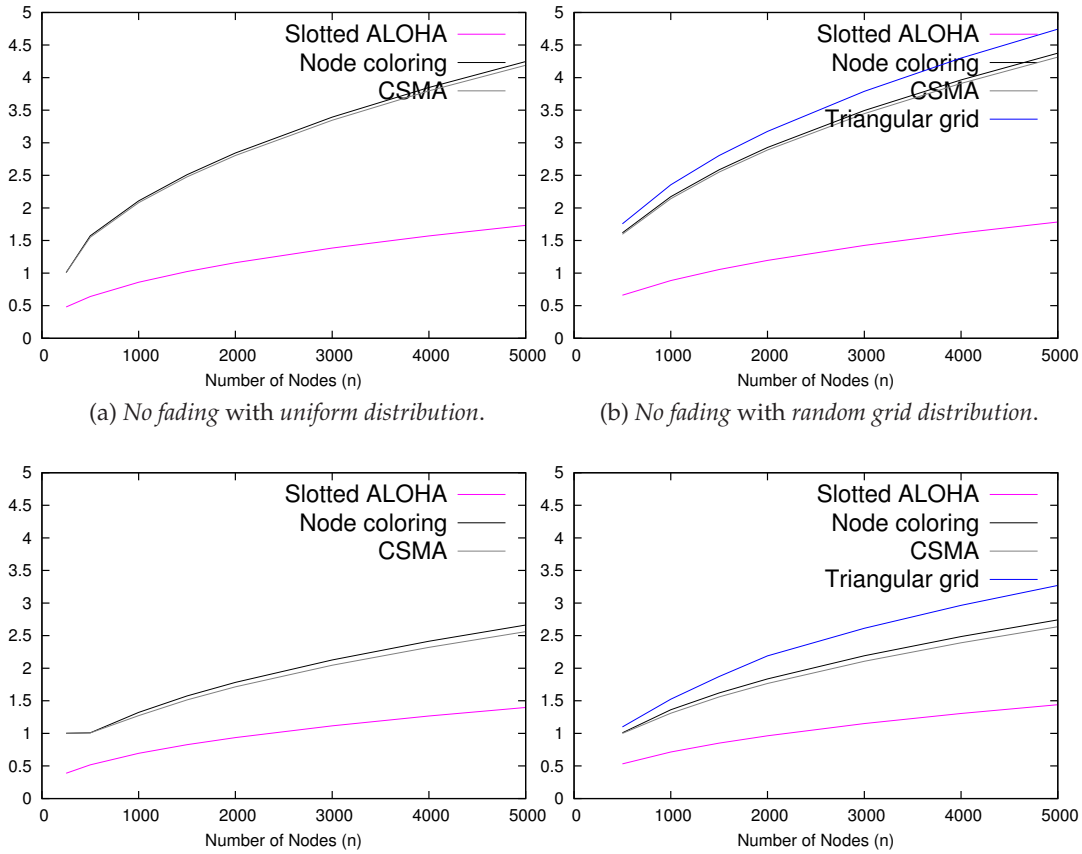


(a) *No fading* with *uniform distribution*. (b) *No fading* with *random grid distribution*.

(c) *Rayleigh fading* with *uniform distribution*. (d) *Rayleigh fading* with *random grid distribution*.

Figure 7.6: Optimal throughput capacity $\zeta(n, 20.0, 4.0)$ (packets per slot) of slotted ALOHA, node coloring, CSMA and triangular grid pattern based schemes. $n$ is varied, $\beta = 20.0$ and $\alpha = 4.0$.

MAC schemes with $\beta = 20.0$ and $\alpha$ varying. Note that we computed the throughput capacity $\zeta(n, \beta, \alpha)$ of triangular grid pattern based scheme with *random grid distribution* of nodes only whereas, we computed the throughput capacity $\zeta(n, \beta, \alpha)$ of slotted ALOHA, node coloring and CSMA based schemes with *uniform distribution* as well as *random grid distribution* of nodes. From the results, we can see that the optimal throughput capacities of these schemes (slotted ALOHA, node coloring and CSMA) are almost similar with both models of nodes distributions, *i.e.*, the difference is within the margin of $2 \sim 3\%$ of each other.

#### 7.3.2.1 Results under *No Fading* and *Rayleigh Fading*

The optimal tuning of all MAC schemes appears to remain insensitive to the fading on the channel. As the values of $n$, $\beta$ and $\alpha$ are varied, the optimized values of the tuning parameters

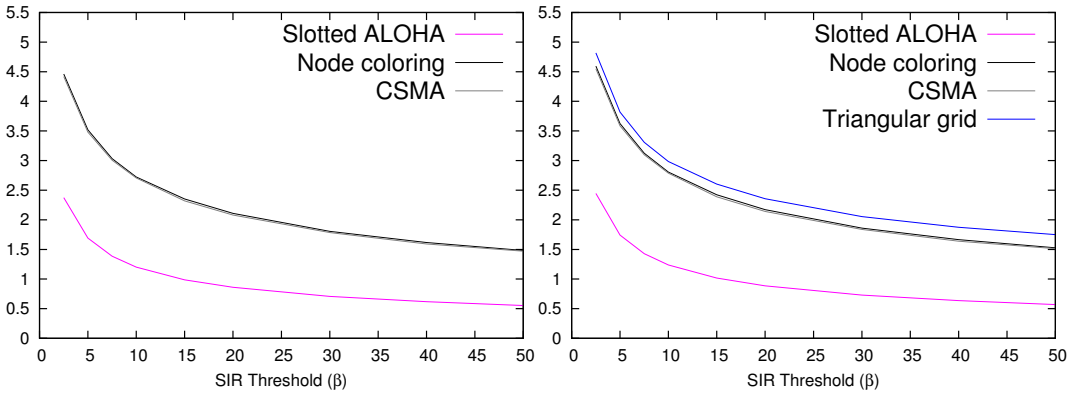


(a) *No fading* with *uniform distribution*. (b) *No fading* with *random grid distribution*.

(c) *Rayleigh fading* with *uniform distribution*. (d) *Rayleigh fading* with *random grid distribution*.

Figure 7.7: Optimal throughput capacity $\zeta(1000, \beta, 4.0)$ (packets per slot) of slotted ALOHA, node coloring, CSMA and triangular grid pattern based schemes. $n = 1000$, $\beta$ is varied and $\alpha = 4.0$.

$p^*(n, \beta, \alpha)$, $d^*(n, \beta, \alpha)$ and $\theta^*_{cs}(n, \beta, \alpha)$ are similar under *no fading* and *Rayleigh fading* of mean one. However, under *Rayleigh fading* and with low values of $n$, we observed that the parameters of node coloring (and grid pattern based schemes) and CSMA, $d$ and $\theta_{cs}$ respectively, should be tuned at values such that only one transmitter is active in each slot and therefore achieve higher throughput capacity $\zeta(n, \beta, \alpha) = 1$ in this case (see Fig. 7.6(c-d), $n < 500$). As $n$ becomes greater than 500, $d^*(n, \beta, \alpha)$ and $\theta^*_{cs}(n, \beta, \alpha)$ of node coloring (and grid pattern based schemes) and CSMA appear to be similar under *no fading* and *Rayleigh fading* channel models.

Figures 7.7(a-b) and 7.8(a-b) show that under *no fading* channel model, slotted ALOHA can achieve *at least* one-third or more of the throughput capacity of triangular grid pattern based scheme. However, under *Rayleigh fading* of mean one, *i.e.* Fig. 7.7(c-d) and 7.8(c-d), this factor improves to almost one-half. From Fig. 7.7 and 7.8, we can see that *Rayleigh fading* of mean one

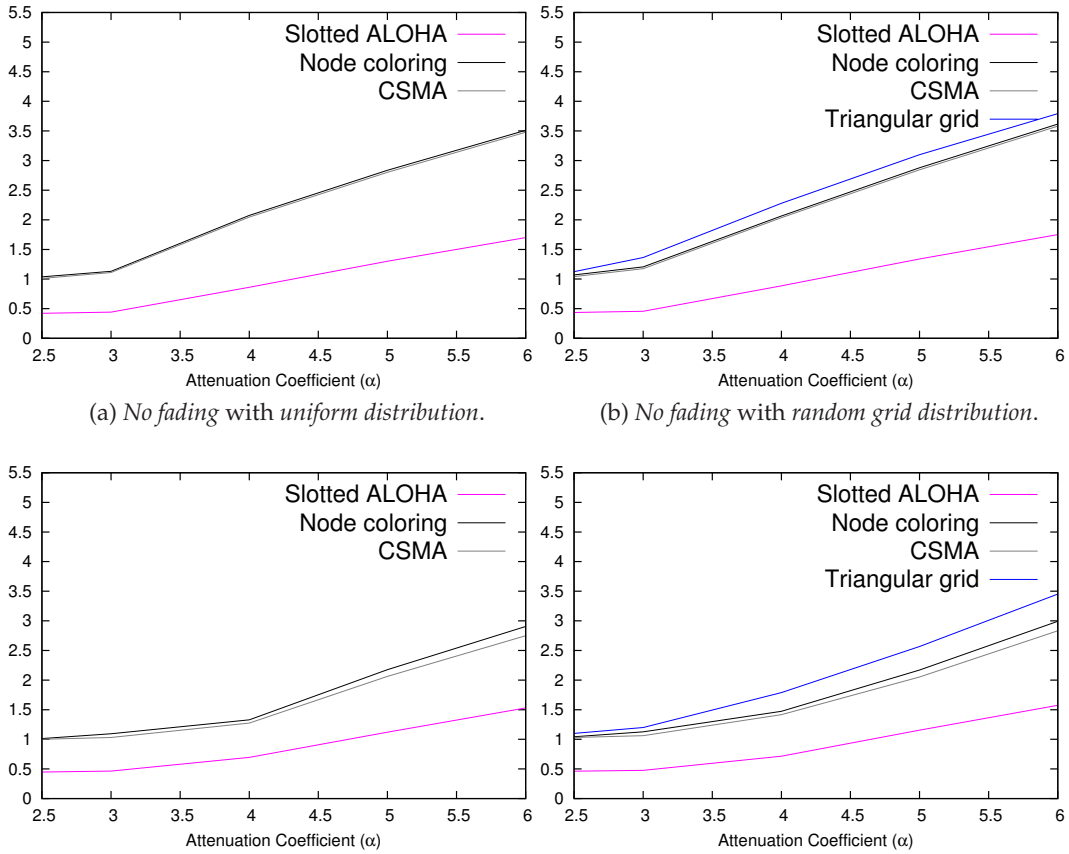


(a) *No fading* with *uniform distribution*. (b) *No fading* with *random grid distribution*.

(c) *Rayleigh fading* with *uniform distribution*. (d) *Rayleigh fading* with *random grid distribution*.

Figure 7.8: Optimal throughput capacity $\zeta(1000, 20.0, \alpha)$ (packets per slot) of slotted ALOHA, node coloring, CSMA and triangular grid pattern based schemes. $n = 1000$, $\beta = 20.0$ and $\alpha$ is varied.

reduces the throughput capacity $\zeta(1000, \beta, \alpha)$ with slotted ALOHA by $10 \sim 25\%$ when compared with *no fading* case. In contrast, fading reduces the throughput capacity $\zeta(1000, \beta, \alpha)$ of node coloring, CSMA and triangular grid pattern based schemes by approximately 35%.

#### 7.3.2.2 Optimality of Grid Pattern Based Schemes

Figures 7.6, 7.7 and 7.8 show that the optimal throughput capacity in multi-hop wireless networks can be achieved with triangular grid pattern based scheme and, under *no fading* channel model, this optimal throughput capacity is almost three times the throughput capacity of slotted ALOHA. This factor is slightly higher as compared to the result we obtained in §6.5.3 where we compared the optimized minimum number of transmissions required to deliver a packet, with various MAC schemes, along the straight line from its source to its destination node. In

contrast, here we used realistic distribution of nodes on the network area and therefore routes of packets are only an *approximation* of straight lines. Also note that, in case of *Rayleigh fading* channel model, the optimal throughput capacity is only twice the throughput capacity of slotted ALOHA.

#### 7.3.2.3 Observations on Node Coloring Schemes

As mentioned earlier, triangular grid pattern based scheme can be visualized as an optimal node coloring scheme because neighboring simultaneous transmitters are exactly at distance $d$ from each other. The comparison of the results of both schemes in Fig. 7.6, 7.7 and 7.8 show that the optimal packing of simultaneous transmitters in triangular grid pattern based scheme can only increase the throughput capacity in the range of $10 \sim 20\%$ depending on the value of $\beta$ and $\alpha$. For example, as $\beta$ increases from 2.5 to 50, the improvement factor increases from 10% to 18%. Similarly, as $\alpha$ increases from 2.5 to 6.0, the improvement factor of triangular grid pattern based scheme as compared to node coloring scheme drops from 15% to 8%.

#### 7.3.2.4 Observations on CSMA Based Schemes

Figures 7.6, 7.7 and 7.8 show that the throughput capacity of CSMA based scheme is slightly lower than node coloring scheme. The reason is that CSMA uses exclusion rule base on carrier sense and this results in lower density (packing) of simultaneous transmitters as compared to node coloring scheme. We also pointed out this observation during our discussion on the evaluation of local capacity in §4.5.4.3 and this can also be observed from the comparison of results on packing densities with $SSI$ and $SSI_k$ point processes in the article [Busson & Chelius 2009]. Moreover, under *Rayleigh fading* of mean one, this difference is exacerbated but by a very small margin.

## 7.4 Conclusions

In this chapter, we evaluated the throughput capacity of multi-hop wireless networks with various MAC schemes. Because of the lack of any satisfactory analytical model, we used a hybrid of an analytical model and Monte Carlo simulations to evaluate the throughput capacity of slotted ALOHA, node coloring, CSMA and triangular grid pattern based schemes. Our results show that compared to slotted ALOHA, triangular grid pattern based scheme can increase throughput capacity by a factor of 3 (or less). However, this factor reduces to only 2 (or less) under more realistic channel model with *Rayleigh fading*. Moreover, node coloring and CSMA can achieve almost similar throughput capacity as obtained with the triangular grid pattern based scheme.

# Part III

# Mobile Multi-hop Wireless Networks

# Chapter 8

# Capacity-Delay Tradeoff in Wireless Networks

So far, we have only analyzed the capacity of fixed wireless network with various MAC schemes. First, we took into account only single-hop simultaneous transmissions in the network and evaluated local capacity. Later, we extended our analysis to take into account the multi-hop communication between nodes and evaluated the transmission range and network throughput capacity with various MAC protocols. In this case, nodes relay packets toward their respective destinations like *hot potatoes* (and, therefore, packet delivery delay is negligible) which is the basis of Gupta & Kumar protocol framework.

We also discussed in Chapter 2 that if nodes are allowed to move in the network, we can improve the network capacity by designing a scheme that relay packets toward their final destinations by exploiting the mobility of nodes. The main idea is to allow mobile nodes to carry packets in their buffer while moving, before forwarding them. However, this improved network capacity comes at the expense of increased packet delivery delay. Indeed Grossglauser & Tse designed a *postman* routing scheme that achieves a total network capacity of $O(n)$ with packet delivery delay of $O(\sqrt{n}L/v)$ where $L$ is the length of network area and $v$ is the average speed of nodes. In this chapter, we aim to maximize the capacity of mobile networks while keeping the mean packet delivery delay bounded with increasing number of nodes. For relaying packets towards their destinations, mobile nodes use our proposed georouting strategy called the *Constrained Relative Bearing* (CRB) scheme. We will show that, in a random walk mobility model, this scheme achieves a network throughput capacity of $O(\frac{n}{\log n \log\log n})$ packets per slot with a time to delivery of $O(L/v)$. Note that, in random walk mobility models, nodes have free space motion and move in straight lines with constant speed. This mobility model is a subclass of the free space motion mobility model. Therefore, we can also extend our result to mobility models where average free space distance is non zero.

Our main contribution is summarized in Table 8.1.

Consider an example of an urban area network in a fixed square area of length $L$ with

| | *Network Capacity* | *Delivery Delay* |
|---|---|---|
| Gupta & Kumar [Gupta & Kumar 2000] | $O\left(\sqrt{\frac{n}{\log n}}\right)$ | *negligible* |
| Grossglauser & Tse [Grossglauser & Tse 2002] | $O(n)$ | $O\left(\frac{\sqrt{n}}{v}\right)$ |
| *Our work* | $O\left(\frac{n}{\log n \log\log n}\right)$ | $O\left(\frac{1}{v}\right)$ |

Table 8.1: Network Capacity vs. Delivery Delay Trade-off.

number of nodes $n = 10^6$, nominal bandwidth of 100 kbps and delay per store-and-forward operation of one ms. The average packet delivery delay for Gupta & Kumar's case would be around one second but with a network capacity of 10 Mbps. In case of Grossglauser & Tse, the network capacity would increase to about 100 Gbps but if the straight line crossing time $L/v$ is about one hour, *e.g.* with cars as mobile nodes, the time to delivery would be around one month. However, our model of using mobility of nodes along with the proposed CRB scheme, to relay packets to their destinations, would lead to a network capacity of 10 Gbps with time to delivery of about one hour.

## 8.1 Model and Assumptions

We consider a network of $n$ mobile nodes with their initial positions uniformly distributed in a square area. Each mobile node transmits packets to a randomly chosen fixed node, called its destination node, which is also randomly located in the network area. We assume that mobile nodes are aware of their own cartesian coordinates, *e.g.*, by using GPS or from the initial position, a mobile node could use the knowledge of its motion vector to compute its cartesian coordinates at any given time.

Initially we consider that only mobile nodes participate in the relay process to deliver packet to its destination node. The case where the fixed nodes may also participate in the relay process is discussed in §8.5. A mobile node should be aware of the cartesian coordinates of the destination node of a packet it carries. Indeed it can be assumed that this information is included in all packets or is relayed with the packets. Hence our model only requires that a source or relay node is aware of the cartesian coordinates of the destination node which is assumed fixed. Note

that if the destination node is mobile, a mechanism to disseminate its updated cartesian coordinates in the network can be used, *e.g.*, mechanisms proposed in articles [Stojmenovic 1999, Li *et al.* 2000]. However, this is beyond the scope of this thesis as we particularly focus on the capacity-delay tradeoff.

With the available information, a mobile relay can determine:

- its heading vector which is the motion vector when its speed is non zero,
- its bearing vector which is the vector between its position and the position of a packet's destination; and,
- the relative bearing angle, *i.e.*, the absolute angle between its heading and bearing vectors.

In the example of Fig. 8.1, node $A$ is carrying a packet for node $D$. This figure also shows the heading vector of mobile node $A$ and its bearing vector and relative bearing angle for destination node $D$. Note that a mobile relay may carry packets for multiple destinations but can easily determine the bearing vector and relative bearing angle for each destination node.

## 8.2 The Constrained Relative Bearing Georouting Scheme

In this section, we will present the parameters and specifications of the model of our georouting scheme. We will specify our scheme in the following two cases:

- the simplified case where the radio range is known at the node level and
- the realistic case where the radio range is unknown.

### 8.2.1 Parameters

We define the parameters $\theta_c$, called the carry angle, and $\theta_e$, called the emission angle. Each mobile node carries a packet to its destination node as long as its relative bearing angle $\theta$ is smaller than $\theta_c$ which is strictly smaller than $\pi/2$. When this condition is not satisfied, the packet is transmitted to the next relay.

### 8.2.2 High-Level Specification With Radio Range Awareness

In the following description, we initially assume that each node is aware of the effective range of transmission $r_n$. This means that there is a periodic beaconing that allows this estimate to be made. In §8.2.3, we will investigate how to specify our model without an estimate of the effective range $r_n$.

Assume that node $A$ is carrying a packet for node $D$. The velocity of node $A$ is denoted by $\mathbf{v}(A)$.

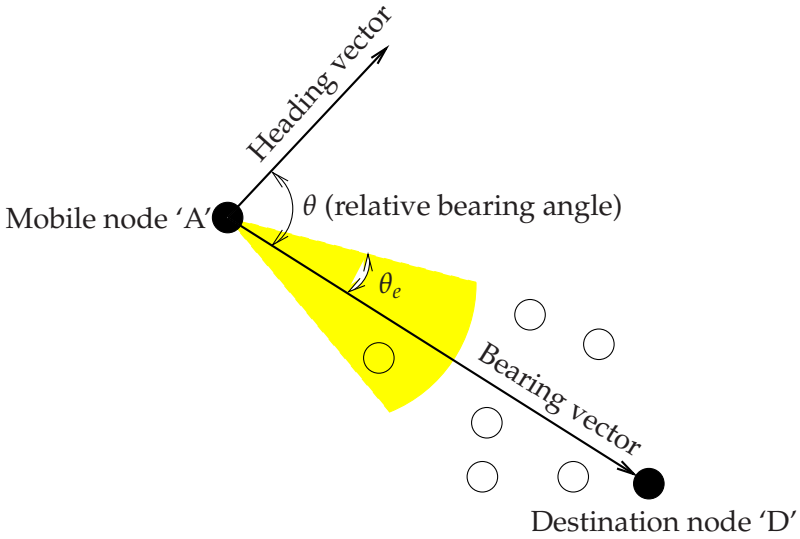


Figure 8.1: Figurative representation of our model. Unfilled circles represent the potential mobile relays for packet transmitted by node $A$ for node $D$.

- If node $A$ is within range of node $D$, it transmits the packet to $D$; otherwise,
- if the relative bearing angle is smaller than $\theta_c$, node $A$ continues to carry the packet; otherwise,
- node $A$ transmits the packet to a random neighbor mobile node inside the cone of angle $\theta_e$, with bearing vector as the axis, and then forgets the packet.

In order to better understand the model of our georouting scheme, consider the example in Fig. 8.1. Assume that node $A$ is out of range of node $D$ and, because of that, it cannot deliver the packet directly. Now, if $\theta < \theta_c$, node $A$ will continue to carry the packet for node $D$. Otherwise, it transmits the packet to one of the random mobile relays, represented by unfilled circles in the figure, within its effective range of transmission $r_n$.

#### 8.2.2.1 Transmission Procedure

To transmit the packet towards another mobile node, node $A$ shall proceed as follows:

- it first transmits a *Call-to-Receive* packet containing the positions of nodes $A$ and $D$;
- a random mobile node $B$ which receives this *Call-to-Receive* packet can compute the angle $(AB, AD)$. If this angle is smaller than $\theta_e$, it replies with an *Accept-to-Receive* packet containing an identifier of node $B$;
- node $A$ sends the packet to the first mobile node which replied with an *Accept-to-Receive* packet.

The first node which sends its *Accept-to-Receive* packet notifies the other receivers of the *Call-to-Receive* packet, to cancel their transmissions of *Accept-to-Receive* packets. There may be more than one (but finite) transmissions of *Accept-to-Receive* packets in case two or more receivers are at a distance greater than $r_n$ from each other.

Note that this transmission procedure does not need any beaconing or periodic transmission of hello packets. The back-off time of nodes, transmitting their *Accept-to-Receive* packet, can also be tuned in order to favor the distance or displacement towards $D$, depending on any additional optional specifications.

### 8.2.3 High-Level Specification Without Radio Range Awareness

The estimation of $r_n$ would require that nodes employ a periodic beaconing mechanism. If such a mechanism is not available or desirable, the CRB scheme relies on SINR for transmitting packets to their destinations or random mobile relays. In other words, a mobile node can relay a packet to its destination node or another mobile node only if the SINR at the receiver is above a given threshold.

#### 8.2.3.1 Transmission Procedure

In this case, the specification of the transmission procedure is also modified so that it terminates when the final destination receives the packet. To transmit the packet towards its destination node or another mobile node, node $A$ shall proceed as follows:

- it first transmits a *Call-to-Receive* packet containing the positions of nodes $A$ and $D$;
- if node $D$ receives this packet, it responds immediately with an *Accept-to-Receive* packet with highest priority. Node $A$, on receiving this packet, relays the packet to node $D$; otherwise,
- the procedure of selecting a random mobile node, as the next relay, is similar to the procedure described in §8.2.2.1. A random mobile node $B$, which receives the *Call-to-Receive* packet, computes the angle $(AB, AD)$. If this angle is smaller than $\theta_e$, it responds with an *Accept-to-Receive* packet;
- node $A$ relays the packet to the first mobile node which sent its *Accept-to-Receive* packet successfully. The first node which transmits its *Accept-to-Receive* packet also makes the other receivers to cancel their transmissions of *Accept-to-Receive* packets.

## 8.3 Performance Analysis

We assume that the network area is a square area and *w.l.o.g.* we assume that it is a square unit area. The mobile nodes move according to *i.i.d.* random walk: from a uniformly distributed

initial position, nodes move in a straight line with a certain speed and randomly change direction. The speed is randomly distributed in an interval $[v_{\min}, v_{\max}]$ with $v_{\min} > 0$. To simplify the analysis, we assume that $v_{\min} = v_{\max} = v$. We also assume that each node changes its direction with a Poisson point process of rate $\tau$. When a mobile node hits the border of the network, it simply bounces like a billiard ball. This leads to the *isotropic property*, discussed in the article [Jacquet *et al.* 2010], *i.e.*, at any given time the mobile nodes are uniformly distributed in the square and move in uniformly selected direction independently of their position.

In our georouting scheme, the average number of transmissions per slot is supposed to be the same for all mobile nodes and equal to

$$p_n = \frac{1}{\log\log n}\,.$$

Therefore, the radius of efficient transmission $r_n$ can be derived from the value of $p_n$ using (2.1) and is given by

$$r_n = \sqrt{\kappa \frac{\log\log n}{\pi n}}\,,$$

for some $\kappa > 0$ when $n$ approaches infinity. The average number of neighbors of an arbitrary node at an arbitrary time is $\kappa \log\log n$. Note that the value of $p_n$ is such that the average cumulated load is finite and the actual density of simultaneous transmitters is $\frac{n}{\kappa \log\log n}$.

In the following analysis, we will show that the number of transmissions per packet is of $O(\log n)$ and this would lead to a useful network capacity of $O(\frac{n}{\log n \log\log n})$. Note that, our scheme could lead to packet loss because of transmission failure, *e.g.*, because of no relay in the emission cone but we will show that the probability of this packet loss is inverse power of $\log n$ and it tends to zero as $n$ approaches infinity.

### 8.3.1 Methodology

Our parameters of interest are the following:

- the delay $D_n(r)$ of delivering a packet to the destination when the packet is generated in a mobile node at distance $r$ from its destination node and

- the average number of times $F_n(r)$ the packet changes relay before reaching its destination when it has been generated in a mobile node at distance $r$ from its destination node.

In order to exhibit the actual performance of our proposed CRB scheme, we aim to derive an upper-bound on the parameters $D_n(r)$ and $F_n(r)$. In the next two sub-sections, we assume *w.l.o.g.* that there is always a relay node, to receive the packet, in the emission cone (as the node density and angle $\theta_e$ are sufficiently large) when a relay change must occur.

### 8.3.2 Delivery Delay

We ignore the queueing delays which can become apparent when several packets could be in competition in the same relay to be transmitted at the same time.

**Theorem 8.3.1.**

$$D_n(r) \leq \frac{r}{v\cos(\theta_c)} + \frac{F_n(r)}{v}\left(t_f v - \frac{r_n}{\cos(\theta_c)}\right) , \tag{8.1}$$

*where $t_f$ is the packet processing time (including receive and transmit) in a node.*

*Proof.* We can write $D_n(r)$ as

$$D_n(r) \leq F_n(r)t_f + \frac{r - F_n(r)r_n}{v\cos(\theta_c)} ,$$

where $F_n(r)t_f$ is the average total delay of store and forward operations and $\frac{r-F_n(r)r_n}{v\cos(\theta_c)}$ is an upper bound of the delay when mobile relays carry a packet at constant speed $v$ with a relative bearing angle always smaller than $\theta_c$. Rearranging this equation leads to (8.1). □

**Remark 8.3.1.** *If $r_n$ is greater than $t_f v$, second factor in (8.1) becomes negative which gives the upper bound of*

$$D_n(r) \leq \frac{r}{v\cos(\theta_c)} .$$

*However, if $r_n$ is less than $t_f v$, $D_n(r)$ will also include an $O(\log n)$ factor because of $F_n(r)$.*

### 8.3.3 Number of Relay Changes

There are two events that trigger relay changes.

1. Relay change due to turn, *i.e.*, the mobile node, carrying the packet, changes its heading vector such that the relative bearing angle becomes greater than $\theta_c$.

2. Relay change due to pass over, *i.e.*, the mobile node keeps its trajectory and the relative bearing angle becomes greater than $\theta_c$.

Consider a packet generated at distance $r$ from its destination. Let $F_n^t(r)$ be the average number of relay changes due to turn. Equivalently, let $F_n^p(r)$ be the average number of relay changes due to pass over. Therefore, we have

$$F_n(r) = F_n^t(r) + F_n^p(r) ,$$

and we expect that the main contribution of $O(\log n)$ in $F_n(r)$ will come from $F_n^p(r)$.

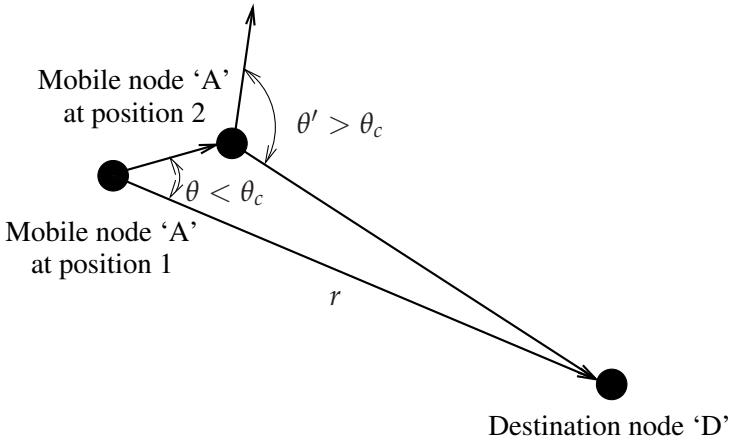


Figure 8.2: Figurative description of relay change due to turn. At position 1, $\theta < \theta_c$ and node $A$ carries the packet for node $D$. At position 2, node $A$ changes its heading vector and must transmit the packet.

#### 8.3.3.1 Number of Relay Changes Due to Turn

We prove the following theorem:

**Theorem 8.3.2.** *We have the bound*

$$F_n^t(r) \leq \frac{\pi - \theta_c}{\theta_c} \frac{\tau}{v \cos(\theta_c)} r \, .$$

*Proof.* We consider the case in Fig. 8.2 and assume that a mobile node is carrying a packet to its destination located at distance $r$. The node changes its direction with Poisson rate $\tau$. When the node changes its direction, it may keep a direction that stays within angle $\theta_c$ of the bearing vector and this will not trigger a relay change. This occurs with probability $\frac{\theta_c}{\pi}$. Otherwise, the packet must change relay. But the new relay may have relative bearing angle greater than $\theta_c$ which would result in an immediate new relay change. The probability that the relative bearing angle of a relay is equal or less than $\theta_c$ is $p = \frac{\theta_c}{\pi}$. If $k$ is the number of times a packet is relayed because the relative bearing angles of intermediate relays are greater than $\theta_c$, we have

$$\Pr(Y = k) = (1 - p)^k p \, ,$$

for $k = 0, 1, 2, \ldots$.

At each direction change, the average number of relay changes can be computed as

$$\mathbb{E}[Y] = \sum_{k=0}^{\infty} (1 - p)^k p.k = \frac{1 - p}{p} \, .$$

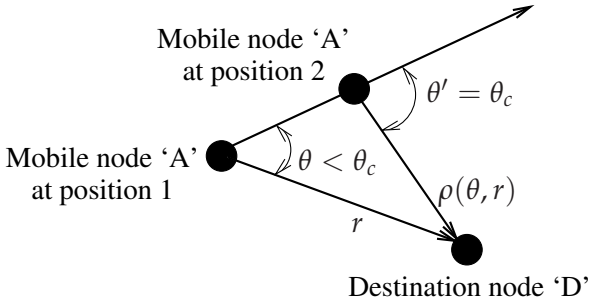


Figure 8.3: Figurative description of relay change due to pass over. At position 1, $\theta < \theta_c$ and node $A$ carries the packet for node $D$. At position 2, node $A$ has the same heading vector but $\theta' = \theta_c$ and it must transmit the packet.

Therefore, at each direction change, there is an average number of $\frac{\pi - \theta_c}{\theta_c}$ relay changes. For a packet generated at distance $r$ from its destination, the product of $D_n(r)$ and $\tau$ gives us the average maximum number of turns (which trigger possible change of relay) by the relays carrying it and multiplying this product with the average number of relays at each turn gives the upper-bound of $F_n^t(r)$.

Note that we have not considered the turn due to bounces on the borders of square map. But it is easy to see via straightforward geometric considerations that they cannot actually generate a relay change. □

#### 8.3.3.2 Number of Relay Changes Due to Pass Over

We prove the following theorem:

**Theorem 8.3.3.** *We have the bound*

$$F_n^p(r) \leq \frac{\pi \tan(\theta_c)}{\theta_c^2} \log\left(\frac{r}{r_n}\right) .$$

*Proof.* Here we consider the case of Fig. 8.3. We assume that a mobile node at distance $r$ from its destination has a relative bearing angle equal to $\theta$. If it keeps its trajectory (*i.e.*, does not turn), it will need to transmit to a new relay when it passes over the destination, *i.e.*, when it arrives at a distance of $\rho(\theta, r) = \frac{\sin(\theta)}{\sin(\theta_c)} r$ from the destination. The function of $\theta$ $\rho(\theta, r)$ is bijective from $[0, \theta_c]$ to $[0, r]$. For $x \in [0, r]$, let $\rho^{-1}(x, r)$ be its inverse.

Assume that $r$ is the distance to the destination when the relay receives the packet or just after a turn. Thus the angle $\theta$ is uniformly distributed on $[0, \theta_c]$, *i.e.*, with a constant probability density $\frac{1}{\theta_c}$. The probability density of the pass over event at $x < r$ (assuming no direction

change) is therefore

$$\frac{1}{\theta_c}\frac{\partial}{\partial x}\rho^{-1}(x,r) = \frac{\sin(\theta_c)}{\theta_c \cos(\rho^{-1}(x,r))r} = \frac{\tan(\rho^{-1}(x,r))}{\theta_c}\frac{1}{x}\,.$$

Since $\rho^{-1}(x,r) \leq \theta_c$, the point process where the packet would need a relay change due to pass over is upper bounded by a Poisson point process on the interval $[r_n, r]$ and of intensity equal to $\frac{\tan(\theta_c)}{\theta_c}\frac{1}{x}$ for $x \in [r_n, r]$.

Here also, the probability that the relative bearing angle of a new relay is equal or less than $\theta_c$ is $p = \frac{\theta_c}{\pi}$ and if $k$ is the number of times a packet is relayed, we have

$$\Pr(Y = k) = (1-p)^{k-1}p\,,$$

for $k = 1, 2, \ldots$. Note that $k \geq 1$, as a packet must always be relayed at least once due to pass over. Therefore, at each pass over, the average number of relay changes is equal to

$$\mathbb{E}[Y] = \sum_{k=1}^{\infty}(1-p)^{k-1}p.k = \frac{1}{p}\,,$$

or, in other words, equal to $\frac{\pi}{\theta_c}$ which is higher than the average number of relays in case of relay change due to turn. The reason of this higher number is the fact that, in case of relay change due to turn, a mobile relay may still move in a direction that stays within the angle $\theta_c$ and continue to carry the packet.

Neglecting the decrement of distance during each transmission phase, we can write

$$F_n^p(r) = \int_{r_n}^{r} \frac{\pi\tan(\theta_c)}{\theta_c^2}\frac{dx}{x} = \frac{\pi\tan(\theta_c)}{\theta_c^2}\log\left(\frac{r}{r_n}\right)\,.$$

□

We have thus

$$F_n(r) \leq \frac{\pi-\theta_c}{\theta_c}\frac{\tau}{\cos(\theta_c)v}r + \frac{\pi\tan(\theta_c)}{\theta_c^2}\log\left(\frac{r}{r_n}\right)\,.$$

Therefore, we have a main contribution of $O(\log n)$ relay changes that comes from $\log(1/r_n)$. The result holds because we assume that there is always a receiver in each relay change. In the next sub-section we remove will this condition to establish a result with high probability.

### 8.3.4 Number of Relay Changes With High Probability of Success

In the previous subsection we assumed that there is always a receiving relay in the emission cone at each relay change and we said that the relay change is always successful. The case

with failed relay change would introduce additional complications. For example one could use the fixed relays if the packet cannot be delivered to a mobile relay. Anyhow, to simplify the present contribution, we will show that *w.h.p.*, *i.e.* with probability approaching one when $n$ approaches infinity, every relay change succeeds.

**Theorem 8.3.4.** *W.h.p. on arbitrary packets, all relay changes succeed for this packet and are in average number $F_n(r)$ and the delay is $D_n(r)$.*

*Proof.* We use a modified stochastic system to cope with failed relay changes. The modification is the following: when there is no relay in the emission cone during a relay change a *decoy* mobile relay is created in the emission cone that will receive the packet. Each decoy relay is used only for one packet and disappear after use. Notice that the modified system is *not* a practical scheme in a practical network.

With this modified system, the analysis in the previous section still holds and in particular $F_n(r)$ is now the average unconditional number of relay changes (including those via decoy relays) for any packet starting at distance $r$ from destination.

Let $P_n(r)$ be the probability that a packet starting at distance $r$ has a failed relay change. The probability that a relay change fails is equal to

$$(1-\theta_e r_n^2)^{n-1} \sim e^{-n\theta_e^2 r_n^2} = (\log n)^{-\beta\frac{\theta_e}{\pi}} .$$

Therefore the average number of failed relay changes is

$$E_n(r) \leq F_n(r)(\log n)^{-\beta\frac{\theta_e}{\pi}} ,$$

which tends to zero when $\beta\frac{\theta_e}{\pi} > 1$, since $F_n(r)$ is of $O(\log n)$. The final result comes since $P_n(r) \leq E_n(r)$. □

## 8.4 Evaluation and Results

We performed simulations with the CRB georouting scheme under two contexts:

1. a simplified context where communication between nodes in the network is modeled using UDG model such that transmissions are collision free when the transmitters and the receivers are within radio range of each other and

2. a realistic context where the network employs slotted ALOHA scheme and a realistic SIR based communication model is considered.

Note that the simulations of the CRB scheme are stressed to the point that the motion timings are not so large compared to the duration of the slots.

### 8.4.1 Under UDG Model

In this section, we consider a network of $n$ mobile nodes. We assume that all nodes have the same radio range given by

$$r_n = \sqrt{\frac{\kappa \log \log n}{\pi n}} \, .$$

Each mobile node moves according to an *i.i.d.* random walk mobility model, *i.e.*, it starts from a uniformly distributed initial position, moves in straight line with constant speed and uniformly selected direction and reflects on the borders of the square area (like billiard balls).

In §8.4.2, we will further explore the effect of interference on the simulations, but for the moment we only consider a source mobile node and its randomly located destination node which is fixed. We adopt the UDG model of interference, *i.e.*, two nodes are connected or they can exchange information if the distance between them is smaller than a certain threshold called radio range, otherwise, they are disconnected. A mobile node relays the packet only if the relative bearing angle, *i.e.*, the absolute angle made by the heading vector and the bearing vector, becomes greater than $\theta_c$. Otherwise, it continues to carry the packet.

#### 8.4.1.1 Parameters and Assumptions

The purpose of our simulations is to verify the scaling behavior of average delay and number of hops per packet with increasing number of nodes in the network. Therefore, the number of mobile nodes $n$ in the network is varied from 10000 to two million nodes. The values of other parameters, which remain constant, and do not impact the scaling behavior are listed as follows:

1. the parameters of the CRB scheme, $\theta_c$ and $\theta_e$, are taken to be $\pi/6$,
2. the speed of all mobile nodes is constant, *i.e.*, 0.005 unit distance per slot,
3. all mobile nodes change their direction according to a Poisson point process with mean equal to 10 slots and
4. the value of the constant factor $\kappa$ is assumed to be equal to 40.

#### 8.4.1.2 Summary of Results

We have evaluated the following parameters:

1. average delay per packet and
2. average number of hops per packet.

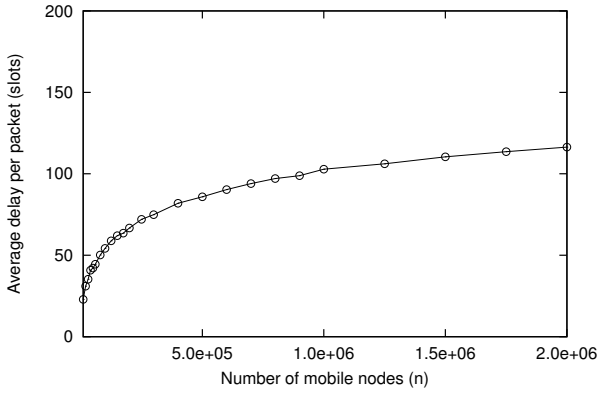


Figure 8.4: Average delay per packet.

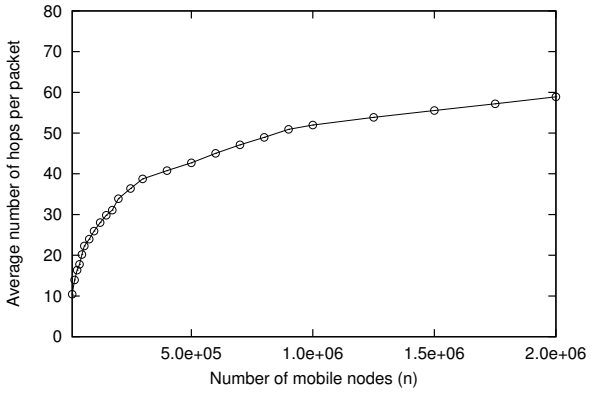


Figure 8.5: Average number of hops per packet.

We considered the Monte Carlo Method with 100 simulations. The delay of a packet is computed from the time when its processing started at its source mobile node until it reaches its destination node. Figure 8.4 shows the average delay per packet with an increasing number of nodes. We notice that as $n$ increases, the average delay per packet appears to approach a constant upper bound which can be computed from (8.1). Figure 8.5 shows the average number of hops per packet with increasing values of $n$.

### 8.4.2 Under SIR Model

In this section, we will present the simulations of the CRB georouting scheme with a transmission model which does not rely on the estimate of $r_n$ and is based on the required minimal SIR threshold. For our simulations, we will use the *no fading* channel model which is described in §3.1.4.

We assume that the nodes use slotted ALOHA scheme with medium access probability

equal to

$$p_n = \frac{1}{\kappa \log\log n} .$$

With this value of $p_n$, the effective range of successful transmission can be derived by using (2.1) as

$$r_n = \sqrt{\kappa \frac{\log\log n}{\pi n}},$$

for some $\kappa > 0$ which depends on the protocol and physical layer parameters. We assume that mobile nodes determine their relative bearing angles at the beginning of a slot and simultaneous transmitters in each slot emit a *Call-to-Receive* packet at the beginning of the slot. Moreover, we also assume that fixed nodes do not emit any packet except, maybe, an *Accept-to-Receive* packet in response to a transmission by a mobile node. In our simulation environment, $n$ mobile nodes start from a uniformly distributed initial position and move independently in straight lines and in randomly selected directions. They also change their direction randomly at a rate which is a Poisson point process. Each mobile node sends packets towards a unique destination (fixed) node, and all destinations nodes are also uniformly distributed in the network area. In order to keep load in the network finite, the packet generation rate at a node $\frac{\rho(n,\beta,\alpha)}{n}$ should be equal to $p_n / X_n$ where $X_n$ is the average number of transmissions per packet. From our theoretical analysis, we know that

$$X_n \leq \kappa \log(n) + c ,$$

where $c$ is a constant if $\theta_c$ is non-varying. Note that we have included $\beta$ and $\alpha$ as parameters of $\rho(n, \beta, \alpha)$ because, in our simulations, we have considered that it depends on the average number of hops required to reach the destination which in turn also depends on $r_n$ and consequently on $\beta$ and $\alpha$. However, we will keep $\beta$ and $\alpha$ constant as we are only interested in the scaling order of the throughput capacity when $n$ increases. In our simulations under SIR interference model, we assume that the knowledge of $r_n$ is not available and mobile nodes use the SIR threshold for successfully receiving a packet. We also assume that each mobile node generate packets, destined for its unique fixed destination node, at a uniform rate $\frac{\rho(n,\beta,\alpha)}{n}$ given by

$$\frac{\rho(n, \beta, \alpha)}{n} \geq \frac{1}{\kappa \log(n) \log\log n} . \tag{8.2}$$

Note that we ignored the value of constant $c$ and have observed that the simulation results are asymptotically correct because when $n$ increases, the value of $c$ should become insignificant as compared to the factor $\kappa \log(n)$.

#### 8.4.2.1 Parameters and Assumptions

The purpose of our simulations is to verify the scaling properties of network capacity, delay and number of transmissions per packet with increasing number of nodes in the network. The number of mobile nodes $n$ in the network is varied from 250 nodes to 100,000 nodes. The values of simulation parameters are listed as follows:

1. the parameters of the CRB scheme $\theta_c$ and $\theta_e$ are taken to be $\pi/6$,
2. the speed of all mobile nodes is constant, *i.e.*, 0.01 unit distance per slot,
3. all mobile nodes change their direction independently and randomly according to a Poisson point process with mean equal to 10 slots,
4. the value of the constant factor $\kappa$ is assumed equal to 500,
5. the SIR threshold $\beta$ is assumed equal to 1 and
6. the attenuation coefficient $\alpha$ is assumed equal to 2.5.

In our simulations, we make the following assumptions.

1. Each mobile node generates an infinite number of packets, at rate $\frac{\rho(n,\beta,\alpha)}{n}$, for its respective destination node.
2. A mobile node may carry, in its buffer, its own packets as well as the packets relayed from other mobile nodes. Therefore, it may have more than one packet in its buffer which it must transmit because their respective relative bearing angles become greater than $\theta_c$. In such a case, it first transmits the packet which is furthest from its destination.

#### 8.4.2.2 Summary of Results

We have examined the following parameters:

1. the throughput capacity per node $\frac{\zeta(n,\beta,\alpha)}{n}$,
2. average number of hops $h(n)$ and transmission attempts $t(n)$ per packet and
3. average delay per packet.

The throughput capacity per node $\frac{\zeta(n,\beta,\alpha)}{n}$ is the average number of packets arriving at their destinations per slot per mobile node. With $n$ increasing, throughput capacity per node should follow the following relation

$$\frac{\zeta(n,\beta,\alpha)}{n} = \frac{\eta}{\kappa \log(n) \log\log n}\,, \tag{8.3}$$

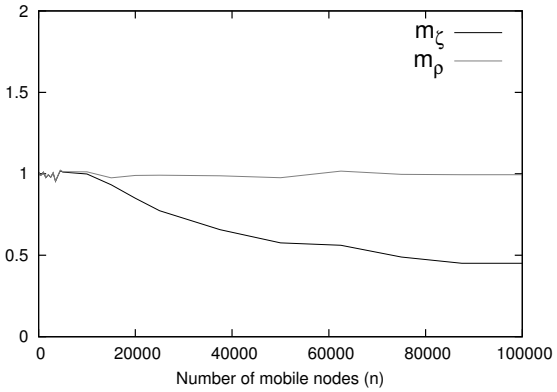


Figure 8.6: Verification of network throughput capacity with plots of $m_\zeta$ and $m_\rho$.

for some $0 < \eta < 1$ which depends on the protocol, physical layer and simulation parameters. Note that the values of these constants do not affect the scaling behavior of $\zeta(n, \beta, \alpha)$ *w.r.t.* $n$ which is also observed in our simulation results.

In order to verify the scaling behavior of simulated packet generation rate and throughput capacity, we have analyzed the parameters $m_\rho$ and $m_\zeta$ which are given by

$$\begin{aligned} m_\rho &= \frac{\rho(n, \beta, \alpha)}{n} \left(\kappa \log(n) \log\log(n)\right) , \\ m_\zeta &= \frac{\zeta(n, \beta, \alpha)}{n} \left(\kappa \log(n) \log\log(n)\right) . \end{aligned}$$

From the definition of $\rho(n, \beta, \alpha)$ in (8.2), the value of $m_\rho$ should be constant at one whereas, when $n$ increases, value of $m_\zeta$ should converge to a constant $\eta$. Note that we ran our simulations for a finite time and a proportion of packets may not have arrived at their destinations, *i.e.*, packets may have been flying when the simulation ended. The reason is that there is a delay between the time when packets are generated and when they are delivered to their destinations and the average of this delay appears to be a constant. As we ran simulations for a fixed time which is an order to this delay, the throughput capacity also appears to approach the packet generation rate but within the factor $\eta$ which approaches a constant value. From Fig. 8.6, value of $\eta$ is found to be approximately equal to 0.45. Figure 8.7 shows the simulated and theoretical packet generation rate $\rho(n, \beta, \alpha)$ and throughput capacity $\zeta(n, \beta, \alpha)$ in the network. The theoretical values of $\rho(n, \beta, \alpha)$ and $\zeta(n, \beta, \alpha)$ are computed from (8.2) and (8.3).

Figure 8.8 shows the average number of hops $h(n)$ and transmission attempts $t(n)$ per packet. The value of $t(n)$ is slightly higher than the value of $h(n)$ because of the possibility that a successful receiver may not be found in each transmission phase, *i.e.*, in the emission cone formed with $\theta_e$. With $n$ increasing, $h(n)$ and $t(n)$ are expected to grow in $O(\log(n))$. To

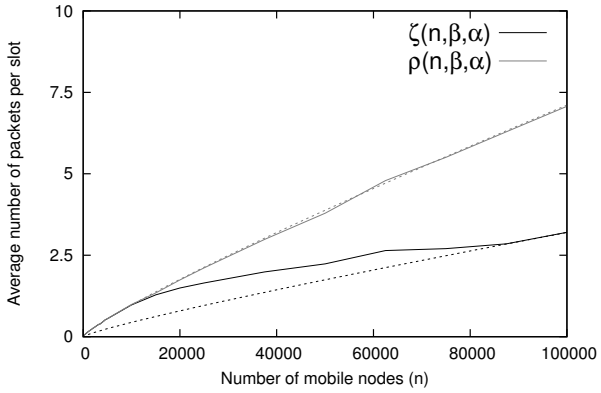


Figure 8.7: Simulated (solid lines) and theoretical (dotted lines) network throughput capacity $\zeta(n, \beta, \alpha)$ and network packet generation rate $\rho(n, \beta, \alpha)$.

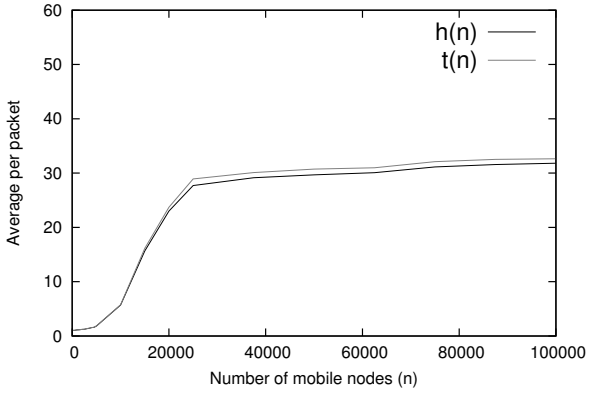


Figure 8.8: Average number of hops $h(n)$ and transmission attempts $t(n)$ per packet.

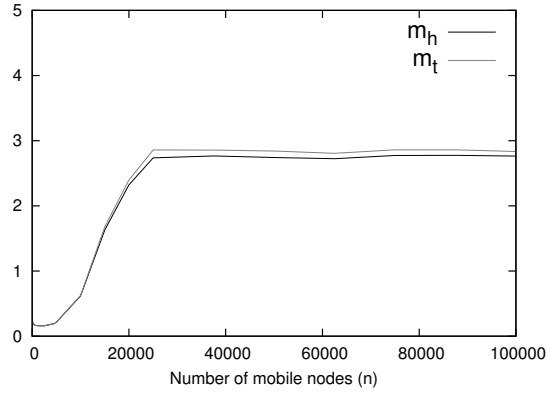


Figure 8.9: Verification of number of hops and transmission attempts with plots of $m_h$ and $m_t$.

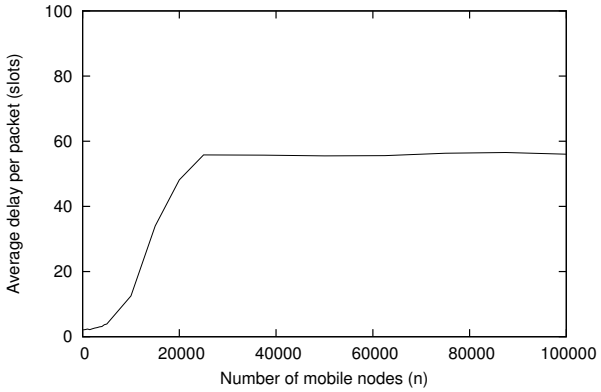


Figure 8.10: Average delay per packet.

verify this character in simulation results, we examine the parameters $m_h$ and $m_t$ given by

$$\begin{aligned} m_h &= h(n)\frac{1}{\log(n)}, \\ m_t &= t(n)\frac{1}{\log(n)}. \end{aligned}$$

If the values of $h(n)$ and $t(n)$ are in $O(\log(n))$, the values of $m_h$ and $m_t$ should approach a constant value which is the case in Fig. 8.9.

The delay of a packet is computed from the time when its processing started at its source mobile node until the time it arrives at its destination node. Figure 8.10 shows the average delay per packet. As the number of mobile nodes increase, the average delay appears to approach a constant value.

It can be observed that when $n$ is small, the average number of hops per packet is almost of $O(1)$ which also means that the average delay per packet is of $O(1)$ and the network throughput capacity is of $O(\eta n)$: although, in simulation results, it is bounded by the network packet generation rate which is of $O(\frac{n}{\log n \log\log n})$. This can be observed in Fig. 8.7, 8.8 and 8.10. The reason is that when $n$ is small, the number of simultaneous transmissions in the network is also small and packets can be delivered by the mobile nodes, directly to their destination nodes, in $O(1)$ hops. As $n$ increases, number of simultaneous transmitters increase and consequently the effective transmission range of each transmitter shrinks. Therefore, the dominant factor in the number of transmissions per packet comes from the fact that a mobile relay has to be close to the destination, to deliver a packet which has to be relayed $O(\log n)$ times. According to theoretical analysis, $h_n$ and $t_n$ grow in $O(\log n)$ which is also observed in the simulation results. Simulations also show that, asymptotically, network throughput capacity is of $O(\frac{n}{\log n \log\log n})$ and average delay per packet is of $O(1/v)$ which complies with our theoretical analysis.

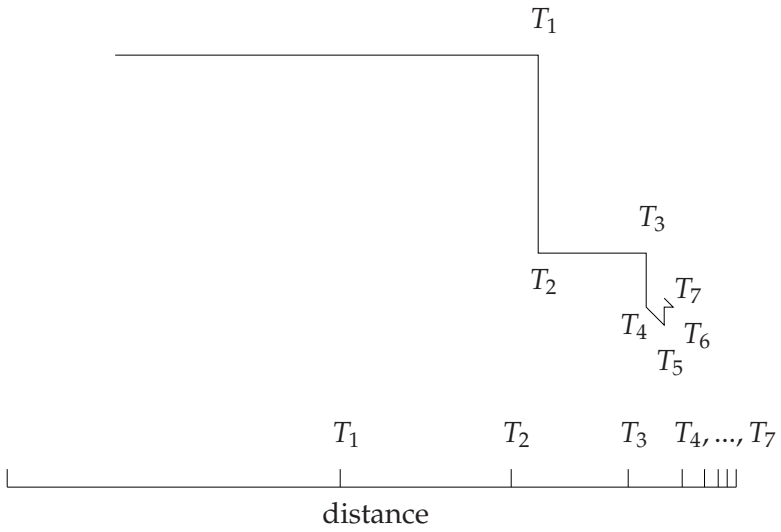


Figure 8.11: Illustration of self-similar trajectories in urban areas.

## 8.5 Extensions and General Mobility Models

In our discussion, we primarily focussed on the capacity-delay tradeoff and thus for the initial sake of clarity assumed that the fixed nodes can only receive packets destined for them. We could also consider a slight variation in the specification of the model of the CRB scheme such that the fixed nodes also participate in the routing of packets to their destination nodes. For example, during a transmission phase, if a packet cannot be transmitted to its destination node or relayed to a random mobile neighbor in the cone of transmission, it can be relayed to a fixed node. This fixed node must emit this packet immediately to its destination node or to any mobile relay in the neighborhood. Note that this will also help increase the connectivity of the network.

The condition about *i.i.d.* random walks can be relaxed and the result about the expected number of relay changes will still be valid. In other words, the *i.i.d.* random walk model can be seen as a worst case compared to realistic mobility models. If the mobile relays move like cars in an urban area, then we can expect that their mobility model will significantly depart from the random walk. Indeed cars move toward physical destinations and in their journey on the streets toward their destination, their heading after each turn is positively correlated with the heading before the turn. This implies that the probability that a relay change is needed after a turn is smaller than it would be under a random walk model where headings before and after turn are not correlated. Furthermore on a street, the headings are positively correlated (consider Manhattan one-way streets) and in this case a relay change due to a pass over will have more chances to arrive on a relay with good heading (one half instead of $\theta_c/\pi$). Again this would lead to less relay changes due to pass over.

The result still holds if we assume that the turn rate $\tau$ depends on $n$ and is equal to

$\tau = \tau_n = O(\log n)$. In this case, the mobility model would fit even better for the realistic mobility of an urban area. Indeed the trajectories of cars should be fractal or self-similar, showing more frequent turns when cars are close to their physical destination (different than packet destination) or when leaving their parking lot. In this case, the overall turn rate tends to be in $O(\log n)$ with a coefficient depending on the Hurst parameter of the trajectory. This would lead to the same estimate of $O(\log n)$ relay change per packet.

Figure 8.11 illustrates a self-similar trajectory in an urban area. It shows a two-dimensional trajectory (upper half) and its traveled distance (lower half). The successive turns are indicated by $T_1, \ldots, T_7$. The trajectory after any turn $T_i$ looks like a reduced copy of the original trajectory. The CRB scheme may need some adaptation to cope with some unusual street configurations, *e.g.*, to replace the cartesian distance with the Manhattan distance in the street map.

## 8.6 Conclusions

We study the scaling properties of a georouting scheme in a wireless network of $n$ mobile nodes. Our aim is to increase the network capacity quasi-linearly with $n$ while keeping the average delay bounded. In our model, mobile nodes move according to an *i.i.d.* random walk with velocity $v$ and transmit packets to randomly chosen destinations. The average packet delivery delay of our scheme is of $O(1/v)$ and it achieves the network capacity of $O(\frac{n}{\log n \log\log n})$. This shows a practical throughput-delay trade-off, in particular when compared with the seminal result of Gupta & Kumar which shows network capacity of $O(\sqrt{n/\log n})$ and negligible delay and the groundbreaking result of Grossglauser & Tse which achieves network capacity of $O(n)$ but with an average delay of $O(\sqrt{n}/v)$. The foundation of our improved capacity and delay trade-off relies on the fact that we use a mobility model that contains free space motion, a model that we consider more realistic than classic brownian motions. We confirm the generality of our analytical results using simulations under various interference models.

We have examined asymptotic capacity and delay in mobile networks with a georouting scheme, called the CRB, for communication between source and destination nodes. Our results show that the CRB allows to achieve the network capacity of $O(\frac{n}{\log n \log\log n})$ with packet delivery delay of $O(1)$ and transmissions per packet of $O(\log n)$. It is noticeable that this scheme does not need any sophisticated overhead for implementation. However, in this case, the mobile nodes must be aware of their position via a GPS system. We have shown the asymptotic performance via analytical analysis under a UDG model with random *i.i.d.* walks. The analytical results have been confirmed by simulations and in particular under ALOHA with SIR interference model. We have seen that the performance of the CRB can be maintained even with non *i.i.d.* random walks, the latter being a worst case scenario. However, this latter result would require that the mobile nodes stay within same heading for $O(1/\log n)$ time. A next step would be to analyze the performance of this scheme on real traffic traces in urban areas.

# Chapter 9

# Conclusions

This thesis has addressed the evaluation of various types of wireless networks via geometrical analyses. The main focus of our work is to study the impact of optimized medium access control on the performance of these networks. First, we laid the groundwork by discussing the models (network, propagation, transmission, node models, *etc*.) in Chapter 3. We also discussed the models of various MAC schemes that we used throughout our work. These models allowed us to capture the spatial distributions of simultaneous transmitters in the network with these schemes. In this chapter, we will summarize our results and contributions and later we will also discuss some of the future directions for research.

## 9.1 Summary of Contributions

In the first part of this thesis, we introduced the common framework of local capacity which is defined as the information rate received by a receiver which is randomly located in the network. Our results showed the limits of improvement in local capacity by a highly managed MAC scheme like grid pattern based schemes, which may require complicated protocol overhead, over a low managed MAC scheme like ALOHA which requires minimal protocol overhead. We first showed that the most optimal scheme in single-hop networks is based on triangular grid pattern and it can at most double the local capacity of slotted ALOHA. We also showed that node coloring and CSMA can achieve almost the same local capacity as triangular grid pattern based scheme. Under *Rayleigh* fading channel model, we established bounds on the local capacity with grid pattern based schemes and our results showed that though fading degrades the performance of these schemes, triangular grid pattern has the highest upper bounds under fading as well.

We also studied the problem of locating additional base stations to optimize the capacity and coverage of an existing cellular network. We showed that this is an NP-Hard problem. For our analysis, we considered a realistic model of cellular network and took into account the SIR and attenuation coefficient. We evaluated heuristics to locate a given number of additional

base stations, to optimize the Shannon capacity and coverage, in a given area of the cellular network defined by the service provider.

In the second part, we shifted our focus to multi-hop wireless networks. Evaluating throughput capacity of multi-hop networks is an extremely challenging task because of the inter-related factors like transmission range, spatial distribution of simultaneous transmitters and the impact of routing. Therefore, we divided our analysis into two chapters. In Chapter 6, we studied the normalized transmission range of slotted ALOHA and grid pattern based schemes. We showed that under typical values of $\beta$ and $\alpha$, the most optimal scheme for optimizing maximum transmission range is also based on triangular grid pattern. However, we also showed an unexpected result under asymptotic conditions, *i.e.*, when $\beta$ is very low and approaches zero or when $\alpha$ is very high and approaches infinity, the most optimal MAC scheme is based on *linear* pattern. In Chapter 7, we extended our analysis and evaluated throughput capacity. In our analysis, we considered that routing has no impact on the slot occupancy rate of nodes and our results confirmed that performance improvements above ALOHA are limited.

The last part of this thesis dealt with mobile wireless networks. In this case, we presented a georouting scheme, called the Constrained Relative Bearing (CRB) scheme, and studies its scaling properties when the number of nodes in the network increases. We showed that it is possible to achieve a bounded packet delivery delay while still having a network capacity which increases *almost* linearly when the number of nodes in the network increases. For our analysis of the CRB scheme, we used a realistic mobility model with free space portions and also showed that the performance holds on fractal trajectories. In future, we can also extend this analysis to the case where destinations are also mobile and to network maps with holes, *e.g.*, lake, parks, *etc*.

## 9.2 Perspectives and Future Directions

An important question in the design and implementation of protocols is to understand the tradeoff between performance and protocol overhead costs. The schemes we evaluated in this thesis represent particular points on this tradeoff curve and provide useful insights for network and protocol designers. In case of multi-hop networks, we have ignored the impact of routing as the focus of this work is on the medium access control and its impact on the geometry of simultaneous transmitters. However, these results can also provide useful insights for designing scheduling mechanisms such as back pressure routing or delay minimizing routing techniques, *etc*. as they may also impact the spatial distribution of simultaneous transmitters in the network.

Many of the MAC schemes presented in this thesis are based on high-level description and do not take into account the packet management or issues related to synchronization and distributed implementation of these protocols. Therefore, it would be interesting to devise realistic specifications where actual distribution of nodes in the network and shadowing effects

also have to be taken into consideration for the placement of simultaneous transmitters. For instance, under shadowing effects, the most optimal placement of simultaneous transmitters may not be a regular pattern. An idea to cope with the impact of actual node distribution and shadowing effects on the optimal placement of transmitters in the network is to introduce a fast training period which would enable the nodes to perform channel measurements. The information gained during this fast training period can serve two purposes:

- nodes can use a distributed algorithm to derive a scheduling scheme that approaches the optimal placement under the restrictions imposed by given network settings and channel conditions and
- utilize the information, gained in the fast training period, during the routing process.

This thesis discussed the limits on the performance of an optimized MAC scheme and, therefore, promotes the idea of cross-layer optimization between MAC and routing layers and perhaps application layer as well, *e.g.*, in case of content centric networks. Our results show that focus of designing new schemes and protocols for wireless networks requires renewed focus on the optimization of existing schemes and design of new routing protocols. For example, design of an intelligent routing protocol that can control the transmission range depending on the network settings or a routing protocol that uses the knowledge of the fast training period, discussed above, that is available at the MAC layer to route packets on optimal paths.

In case of cellular networks, we discussed heuristics to locate additional base stations in an existing network while considering the criteria of optimizing the capacity and coverage only. In our work, we presented heuristics which essentially locate additional base stations sequentially. For example, if the service provider decides to add multiple base stations in the network, these heuristics will add these base stations sequentially where the addition of one base station does not take into account the potential performance improvement by the addition of another base station. The performance of our heuristics can be further improved if we cooperatively locate additional base stations in the network. An important extension in this line of work would be to take into account the costs incurred for locating additional base stations in a cellular network. For simplifying our analysis, we also assumed that the users (customers) are uniformly distributed in the network area. Therefore, it would be interesting to devise a trade-off mechanism which takes into account competing factors like installation and maintenance costs, customer demands and improvements in performance, *etc*. for locating additional base stations.

# Appendix A

# Appendix

## A.1 Locating the Starting Point z on the Closed Curve Bounding the Reception Area

The SIR $S_i(\mathbf{z})$ at point $\mathbf{z}$ should be greater or at least equal to $\beta$. We assume that it is equal to $\beta$. Therefore, we have the following identity under *no fading* channel model

$$\frac{\|\mathbf{z}-\mathbf{z}_i\|^{-\alpha}}{\sum\limits_{j\neq i,\mathbf{z}_j\in\mathcal{S}}\|\mathbf{z}-\mathbf{z}_j\|^{-\alpha}}=\beta\,.$$

Our aim is to find the coordinates of point $\mathbf{z}$ which satisfy the above relation. To simplify computation of point $\mathbf{z}$ on the closed curve, bounding reception area of transmitter $i$ located at $\mathbf{z}_i$, its $y$ coordinate can be fixed such that $\mathbf{z}=(x,y)=(x,y_i)$. This reduces the above equation to

$$\frac{\|x-x_i\|^{-\alpha}}{\sum\limits_{j\neq i,\mathbf{z}_j\in\mathcal{S}}\|\mathbf{z}-\mathbf{z}_j\|^{-\alpha}}-\beta=0\,. \tag{A.1}$$

Equation (A.1) is a function of variable $x$ and can be solved using Newton's Method.

> *Remark: Newton's Method: Given a function $f(x)$ and its derivative $f'(x)$, begin with a first guess $x_0$. Provided the function is reasonably well-behaved, a better approximation $x_1$ is $:= x_0-\frac{f(x_0)}{f'(x_0)}$. The process is repeated until a sufficiently accurate value is reached:*

$$x_{n+1}=x_n-\frac{f(x_n)}{f'(x_n)}\,. \tag{A.2}$$

From (A.1)

$$f(x)=\frac{\|x-x_i\|^{-\alpha}}{\sum\limits_{j\neq i,\mathbf{z}_j\in\mathcal{S}}\|\mathbf{z}-\mathbf{z}_j\|^{-\alpha}}-\beta\,,$$

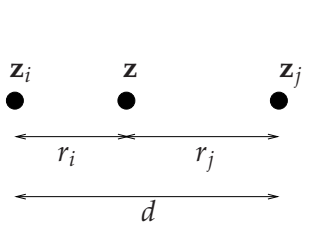


(a) Square and Triangular grid based schemes.

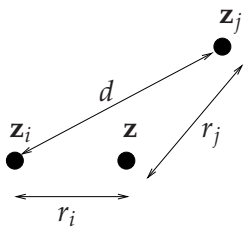


(b) Hexagonal grid pattern based scheme.

Figure A.1: Geometric representation of finding the first approximation of point $\mathbf{z} = (x_0, y_i)$.

We assume that $u = r_i^{-\alpha}$ and $g = \sum_{j \neq i, \mathbf{z}_j \in \mathcal{S}} r_j^{-\alpha}$ where $r_i = \|x - x_i\|$ and $r_j = \|\mathbf{z} - \mathbf{z}_j\|$.

Newton's Method requires the derivative of $f(x)$ which is computed as below.

$$\frac{d}{dx}u = -\alpha \frac{x - x_i}{r_i^{\alpha+2}} .$$

$$\frac{d}{dx}g = \sum_{j \neq i, \mathbf{z}_j \in \mathcal{S}} -\alpha \frac{\mathbf{z} - \mathbf{z}_j}{r_j^{\alpha+2}} .$$

The first derivative of the function $f(x)$ is

$$\begin{aligned} f'(x) &= \frac{1}{g^2}(g\frac{d}{dx}u - u\frac{d}{dx}g) \\ &= \frac{\left( (\sum_{j \neq i, \mathbf{z}_j \in \mathcal{S}} r_j^{-\alpha})(-\alpha \frac{x - x_i}{r_i^{\alpha+2}}) - (r_i^{-\alpha})(-\alpha \frac{\mathbf{z} - \mathbf{z}_j}{r_j^{\alpha+2}}) \right)}{\frac{1}{\left[ \sum_{j \neq i, \mathbf{z}_j \in \mathcal{S}} r_j^{-\alpha} \right]}} . \end{aligned}$$

Newton's Method also requires first approximation of the root, $x_0$. An approximate value, closer to the actual root, can significantly reduce the number of iterations in Newton's Method.

In all three types of grid networks, the transmitter closest to $i$, hereafter referred to as $j$, lies at distance $d$ and hence can give the best estimate $x_0$. For first approximation $x_0$, we can ignore all other transmitters in the network. In this case

$$\begin{aligned} \frac{\|\mathbf{z} - \mathbf{z}_i\|^{-\alpha}}{\|\mathbf{z} - \mathbf{z}_j\|^{-\alpha}} &\geq \beta \\ \frac{r_i^{-\alpha}}{r_j^{-\alpha}} &\geq \beta : i \neq j , \end{aligned}$$

where $r_i = \|\mathbf{z} - \mathbf{z}_i\|$ and $r_j = \|\mathbf{z} - \mathbf{z}_j\|$ and we get

$$\frac{r_j}{r_i} \leq (\beta)^{\frac{1}{\alpha}} .$$

The location of transmitters $i$ and $j$ and point $\mathbf{z}$ in the plane form three corners of a triangle with angle $\theta$ equal to 0 in case of square and triangular grid and $\pi/6$ radians in case of hexagonal grid layout. Figure A.1 shows the location of transmitters $\mathbf{z}_i$ and $\mathbf{z}_j$, point $\mathbf{z}$ and distances $r_i$, $r_j$ and $d$. Using above relation between $r_i$ and $r_j$ and the Law of Cosines, we get the solution of $r_i$ as

$$r_i = \frac{-B \pm \sqrt{B^2 - 4AC}}{2A} ,$$

where $A = 1 - \beta^{\frac{2}{\alpha}}$, $B = -2.d.\cos(\theta)$ and $C = d^2$ where $d$ is the distance between transmitters $i$ and $j$ and is a known parameter of the grid layout.

*Remark: Select positive value of $r_i$ as the solution of the above quadratic equation. Using $x_0 = x_i + r_i$ as the first approximate solution in Newton's Method (A.2), and after a few iterations, we can get a sufficiently accurate value $x_{n+1}$ which will be the x coordinate of the point $\mathbf{z}$.*

*The coordinates of point $\mathbf{z}$ will be: $(x_{n+1}, y_i)$.*

# List of Notations

| | |
|---|---|
| $\alpha$ | Attenuation coefficient |
| $\beta$ | Minimum signal-to-interference ratio threshold required for successfully receiving a packet |
| $\gamma_i(\mathbf{z})$ | Channel gain between transmitter $i$ and a receiver at point $\mathbf{z}$ on the $2D$ plane |
| $\Omega_i(n)$ | Slot occupancy rate of node $i$ |
| $\sigma(\lambda, \beta, \alpha)$ | Average surface area of the reception area of an arbitrary transmitter in the network |
| $\theta_{cs}$ | Carrier sense threshold for carrier sense medium access control schemes |
| $\zeta(n, \beta, \alpha)$ | Throughput capacity (packets delivered per slot) of multi-hop wireless network |
| $c(\beta, \alpha)$ | Local capacity of single-hop wireless network |
| $d$ | Minimum Euclidean distance between simultaneous transmitters for node coloring and grid pattern based medium access control schemes |
| $n$ | Number of nodes in the network |
| $P_i$ | Transmit power of node $i$ |
| $r_1$ | Normalized optimum transmission range in the network |
| $r_n / r_\lambda$ | Optimum transmission range in the network |
| $S_i(\mathbf{z})$ | Signal-to-interference ratio of transmitter $i$ at point $\mathbf{z}$ on the $2D$ plane |
| $\mathbf{z}_i$ | Location of transmitter $i$ on the $2D$ plane: $\mathbf{z}_i = (x_i, y_i)$ |
| $\mathcal{A}_i(\mathcal{S}, \beta, \alpha)$ | Reception area of transmitter $i$ |
| $\mathcal{N}$ | Set of nodes in the network |
| $\mathcal{S}$ | Set of simultaneous transmitters in each slot |
| $\lambda$ | Spatial density of the set $\mathcal{S}$ |

# Bibliography


[3GPP 2005] 3GPP. *Third Generation Partnership Project, Radio Access Network Work Group 1 Contributions*. 3GPP, Sept. 2005.

[3GPP2 2007] 3GPP2. *Third Generation Partnership Project 2, Ultra Mobile Broadband Technical Specifications*. 3GPP2, Mar. 2007.

[802.11n 2009] IEEE 802.11n. *IEEE Standard for Information technology – Telecommunications and information exchange between systems – Local and metropolitan area networks – Specific requirements Part 11: Wireless LAN Medium Access Control (MAC) and Physical Layer (PHY) Specifications*. IEEE 802.11n Standard, Oct. 2009.

[802.16e 2009] IEEE 802.16e. *IEEE Standard for Local and Metropolitan Area Networks Part 16: Air Interface for Broadband Wireless Access Systems*. IEEE 802.16 Standard, May 2009.

[Aboolian *et al.* 2007] Robert Aboolian, Oded Berman and Dmitry Krass. *Competitive Facility Location and Design Problem*. European Journal of Operational Research, vol. 182, no. 1, pages 40–62, 2007.

[Adjih *et al.* 2004] Cédric Adjih, Emmanuel Baccelli, Thomas Heide Clausen, Philippe Jacquet and Georgios Rodolakis. *Fish Eye OLSR Scaling Properties*. Journal of Communications and Networks, vol. 6, no. 4, pages 352–361, Dec. 2004.

[Aeron & Saligrama 2007] S. Aeron and V. Saligrama. *Wireless Ad Hoc Networks: Strategies and Scaling Laws for the Fixed SNR Regime*. IEEE Transactions on Information Theory, vol. 53, no. 6, pages 2044–2059, June 2007.

[Ahmad *et al.* 2006] S.H.A. Ahmad, A. Jovicic and P. Viswanath. *On Outer Bounds to the Capacity Region of Wireless Networks*. IEEE Transactions on Information Theory, vol. 52, no. 6, pages 2770–2776, June 2006.

[Altman *et al.* 2009] Eitan Altman, Anurag Kumar, Chandramani Kishore Singh and Rajesh Sundaresan. *Spatial SINR Games Combining Base Station Placement and Mobile Association*. In INFOCOM, pages 1629–1637. IEEE, 2009.

[Andrews *et al.* 2010] J.G. Andrews, S. Weber, M. Kountouris and M. Haenggi. *Random Access Transport Capacity*. IEEE Transactions on Wireless Communications, vol. 9, no. 6, June 2010.

[Arfken 1985] G. Arfken. Lagrange Multipliers." chapter 17 in Mathematical Methods for Physicists, pp 945-950, volume 3rd ed. Academic Press, Orlando FL., 1985.

[Aurenhammer & Klein 2000] F. Aurenhammer and R. Klein. Voronoi Diagrams. Ch. 5 in Handbook of Computational Geometry (Ed. J.-R. Sack and J. Urrutia), pp. 201-290, volume 1st ed. Amsterdam, Netherlands: North-Holland, 2000.

[Baccelli & Blaszczyszyn 2000] François Baccelli and Bartek Blaszczyszyn. *On a Coverage Process Ranging from the Boolean Model to the Poisson Voronoi Tessellation With Applications to Wireless Communications*. Rapport technique RR-4019, INRIA, Oct. 2000.

[Baccelli & Blaszczyszyn 2009] François Baccelli and Bartek Blaszczyszyn. Stochastic Geometry and Wireless Networks, Volume II - Applications. Foundations and Trends in Networking: Vol. 4: No 1-2, pp 1-312. NoW Publishers, 2009.

[Baccelli *et al.* 2006] F. Baccelli, B. Blaszczyszyn and P. Muhlethaler. *An ALOHA Protocol for Multihop Mobile Wireless Networks*. IEEE Transactions on Information Theory, vol. 52, no. 2, Feb. 2006.

[Bao & Garcia-Luna-Aceves 2001] Lichun Bao and J.J. Garcia-Luna-Aceves. *A New Approach to Channel Access Scheduling for Ad Hoc Networks*. In International Conference on Mobile Computing and networking, 2001.

[Basagni *et al.* 1998] Stefano Basagni, Imrich Chlamtac, Violet R. Syrotiuk and Barry A. Woodward. *A Distance Routing Effect Algorithm for Mobility (DREAM)*. In MOBICOM, pages 76–84, 1998.

[Bertsekas 1999] D. P. Bertsekas. Nonlinear Programming. Athena Scientific, second édition, 1999.

[Bettstetter *et al.* 2003] C. Bettstetter, G. Resta and P. Santi. *The Node Distribution of the Random Waypoint Mobility Model for Wireless Ad Hoc Networks*. IEEE Transactions on Mobile Computing, vol. 2, no. 3, pages 257–269, July 2003.

[Blaszczyszyn *et al.* 2010] Bartek Blaszczyszyn, Paul Muhlethaler and Skander Banaouas. *A Comparison of ALOHA and CSMA in Wireless Ad Hoc Networks under Different Channel Conditions*. INRIA-00530093, 2010.

[Bölcskei *et al.* 2006] Helmut Bölcskei, Rohit U. Nabar, Ozgur Oyman and Arogyaswami Paulraj. *Capacity Scaling Laws in MIMO Relay Networks*. IEEE Transactions on Wireless Communications, vol. 5, no. 6, pages 1433–1444, June 2006.

[Bowyer 1981] Adrian Bowyer. *Computing Dirichlet Tessellations*. The Computer Journal, vol. 24, no. 2, pages 162–166, 1981.

[Brandenburg & Wyner 1974] L.H. Brandenburg and A.D. Wyner. *Capacity of the Gaussian Channel with Memory: The Multivariate Case.* Bell Syst. Tech. J., vol. 53, no. 5, pages 745–778, 1974.

[Busson & Chelius 2009] Anthony Busson and Guillaume Chelius. *Point Processes for Interference Modeling in CSMA/CA Ad Hoc Networks*. In PE-WASUN, 2009.

[Buttazzo & Santambrogio 2005] Giuseppe Buttazzo and Filippo Santambrogio. *A Model for the Optimal Planning of an Urban Area*. SIAM Journal on Mathematical Analysis, vol. 37, no. 2, pages 514–530 (electronic), 2005.

[Chen & Gans 2006] Biao Chen and Michael J. Gans. *MIMO Communication in Ad Hoc Networks.* IEEE Transactions on Signal Processing, vol. 54, no. 7, pages 2773–2783, July 2006.

[Chiani *et al.* 2010] M. Chiani, M.Z. Win and Hyundong Shin. *MIMO Networks: The Effects of Interference*. IEEE Transactions on Information Theory, vol. 56, no. 1, pages 336 –349, Jan. 2010.

[Choi & Murch 2004] Ruly Lai-U Choi and Ross D. Murch. *A Transmit Preprocessing Technique for Multiuser MIMO Systems Using a Decomposition Approach*. IEEE Transactions on Wireless Communications, vol. 3, no. 1, pages 20–24, 2004.

[Clausen & Jacquet 2003] T. Clausen and P. Jacquet. *Optimized Link State Routing Protocol (OLSR), IETF-RFC 3626*. In RFC 3626, United States, 2003.

[Deng *et al.* 2007] Jing Deng, Y.S. Han, Po-Ning Chen and P.K. Varshney. *Optimal Transmission Range for Wireless Ad Hoc Networks Based on Energy Efficiency*. IEEE Transactions on Communications, vol. 55, no. 9, pages 1772–1782, Sept. 2007.

[Derbel & Talbi 2010] Bilel Derbel and El-Ghazali Talbi. *Distributed Node Coloring in the SINR Model*. In ICDCS, 2010.

[Diggavi *et al.* 2005] S.N. Diggavi, M. Grossglauser and D.N.C. Tse. *Even One-Dimensional Mobility Increases The Capacity Of Wireless Networks*. In IEEE Transactions on Information Theory, volume 51, pages 3947–3954, Nov. 2005.

[Drezner 1995] Z. Drezner, editeur. Facility Location. A Survey of Applications and Methods. Springer Series in Operations Research. Springer Verlag, New York, 1995.

[Eiselt & Laporte 1997] H.A Eiselt and Gilbert Laporte. *Sequential Location Problems.* European Journal of Operational Research, vol. 96, no. 2, pages 217–231, 1997.

[Eiselt *et al.* 1993] H.A. Eiselt, Gilbert Laporte and Jacques-François Thisse. *Competitive Location Models: A Framework and Bibliography*. Transportation Science, vol. 27, pages 44–54, 1993.

[Foschini 1996] G. J. Foschini. *Layered Space-Time Architecture for Wireless Communication in a Fading Environment when Using Multi-Element Antennas.* Bell Labs Tech. J., vol. 3, no. 1, pages 20–24, 1996.

[Franceschetti *et al.* 2007] Massimo Franceschetti, Olivier Dousse, David N. C. Tse and Patrick Thiran. *Closing the Gap in the Capacity of Wireless Networks Via Percolation Theory*. IEEE Transactions on Information Theory, vol. 53, no. 3, March 2007.

[Gabszewicz & Thisse 1992] Jean J. Gabszewicz and Jacques-Francois Thisse. *Location*. In R.J. Aumann and S. Hart, editeurs, Handbook of Game Theory with Economic Applications, volume 1 of *Handbook of Game Theory with Economic Applications*, chapitre 9, pages 281–304. Elsevier, 1992.

[Gamal *et al.* 2004] Abbas El Gamal, James P. Mammen, Balaji Prabhakar and Devavrat Shah. *Throughput-Delay Trade-off in Wireless Networks*. In INFOCOM, volume 1, pages 4 (xxxv+2866), 2004.

[Ganti *et al.* 2011] Radha Krishna Ganti, Jeffrey G. Andrews and Martin Haenggi. *High-SIR Transmission Capacity of Wireless Networks with General Fading and Node Distribution*. IEEE Transactions on Information Theory, vol. 57, no. 5, pages 3100–3116, May 2011.

[Georgiadis *et al.* 2006] Leonidas Georgiadis, Michael J. Neely and Leandros Tassiulas. *Resource Allocation and Cross-Layer Control in Wireless Networks*. Foundations and Trends in Networking, vol. 1, April 2006.

[Gomez & Campbell 2004] J. Gomez and A.T. Campbell. *A Case for Variable-Range Transmission Power Control in Wireless Multi-hop Networks*. In IEEE INFOCOM 2004., volume 2, pages 1425–1436, Mar. 2004.

[Grossglauser & Tse 2002] Matthias Grossglauser and David N. C. Tse. *Mobility Increases the Capacity of Ad Hoc Wireless Networks*. IEEE/ACM Transactions on Networking, vol. 10, no. 4, pages 477–486, 2002.

[Gupta & Kumar 1998] Piyush Gupta and P. R. Kumar. *Critical Power for Asymptotic Connectivity in Wireless Networks*. In Stochastic Analysis, Optimization and Applications: A Volume in Honor of W. H. Felming, W. M. McEneany, G. Yin and Q. Zhang, pages 547–566, 1998.

[Gupta & Kumar 2000] Piyush Gupta and P. R. Kumar. *The Capacity of Wireless Networks*. IEEE Transactions on Information Theory, vol. 46, no. 2, 2000.

[Gupta & Kumar 2003] Piyush Gupta and P. R. Kumar. *Towards an Information Theory of Large Networks: An Achievable Rate Region*. IEEE Transactions on Information Theory, vol. 49, pages 1877–1894, Aug. 2003.

[Haas *et al.* 2002] Zygmunt J. Haas, Marc R. Pearlman and Prince Samar. *The Zone Routing Protocol (ZRP) for Ad Hoc Networks*. IETF Internet Draft, July 2002.

[Haenggi 2009] Martin Haenggi. *Outage, Local Throughput, and Capacity of Random Wireless Networks*. IEEE Transaction on Wireless Communication, vol. 8, Aug. 2009.

[Hasan & Andrews 2007] A. Hasan and J.G. Andrews. *The Guard Zone in Wireless Ad Hoc Networks*. IEEE Transactions on Wireless Communications, vol. 6, March 2007.

[Hochbaum 1997] D. S. Hochbaum. Approximating Covering and Packing Problems: Set Cover, Vertex Cover, Independent Set, and Related Problems, in Approximation Algorithms for NP-hard Problems. PWS Publishing Company, Boston, 1997.

[Hong & Hua 2007] Kezhu Hong and Yingbo Hua. *Throughput Analysis of Large Wireless Networks with Regular Topologies*. EURASIP Journal on Wireless Commununications and Networking, Jan. 2007.

[Hou & Li 1986] Ting-Chao Hou and Victor Li. *Transmission Range Control in Multi-hop Packet Radio Networks*. IEEE Transactions on Communications, vol. 34, no. 1, pages 38–44, 1986.

[Hyytiä *et al.* 2006] Esa Hyytiä, Pasi Lassila and Jorma Virtamo. *Spatial Node Distribution of the Random Waypoint Mobility Model with Applications*. IEEE Transactions On Mobile Computing, vol. 5, no. 6, pages 680–694, 2006.

[Jacquet *et al.* 2010] Philippe Jacquet, Bernard Mans and Georgios Rodolakis. *Information Propagation Speed in Mobile and Delay Tolerant Networks*. IEEE Transactions on Information Theory, vol. 56, no. 10, pages 5001–5015, 2010.

[Jacquet 2009] P. Jacquet. *Shannon Capacity in Poisson Wireless Network Model*. Problems of Information Transmission, vol. 45, 2009.

[Jiang *et al.* 2011] Canming Jiang, Yi Shi, Yiwei Thomas Hou and Sastry Kompella. *On the Asymptotic Capacity of Multi-Hop MIMO Ad Hoc Networks.* IEEE Transactions on Wireless Communications, vol. 10, no. 4, pages 1032–1037, April 2011.

[Jovicic *et al.* 2004] A. Jovicic, P. Viswanath and S.R. Kulkarni. *Upper Bounds to Transport Capacity of Wireless Networks*. IEEE Transactions on Information Theory, vol. 50, no. 11, pages 2555–2565, Nov. 2004.

[Karp & Kung 2000] Brad Karp and H. T. Kung. *GPSR: Greedy Perimeter Stateless Routing for Wireless Networks*. In MOBICOM, pages 243–254, 2000.

[Kaye & George 1970] A. Kaye and D. George. *Transmission of Multiplexed PAM Signals Over Multiple Channel and Diversity Systems*. IEEE Transactions on Communication Technology, vol. 18, no. 5, pages 520–526, Oct. 1970.

[Kaynia & Jindal 2008] M. Kaynia and N. Jindal. *Performance of ALOHA and CSMA in Spatially Distributed Wireless Networks*. In IEEE International Conference on Communications, May 2008.

[Kelif & Coupechoux 2009] J.-M. Kelif and M. Coupechoux. *Cell Breathing, Sectorization and Densification in Cellular Networks*. In WiOPT 2009, pages 1–7, June 2009.

[Keung *et al.* 2010] G.Y. Keung, Qian Zhang and Bo Li. *The Base Station Placement for Delay-Constrained Information Coverage in Mobile Wireless Networks*. In IEEE International Conference on Communications, pages 1–5, May 2010.

[Kleinrock & Tobagi 1975] L. Kleinrock and F. Tobagi. *Packet Switching in Radio Channels: Part 1 - Carrier Sense Multiple-Access Modes and Their Throughput-Delay Characteristics*. IEEE Transactions on Communications, vol. 23, no. 12, Dec. 1975.

[Ko & Vaidya 1998] Young-Bae Ko and Nitin H. Vaidya. *Location-Aided Routing (LAR) in Mobile Ad Hoc Networks*. In MOBICOM, pages 66–75, 1998.

[Kranakis *et al.* 1999] Evangelos Kranakis, Harvinder Singh and Jorge Urrutia. *Compass Routing on Geometric Networks*. In Canadian Conference On Computational Geometry, pages 51–54, 1999.

[Leveque & Telatar 2005] O. Leveque and I.E. Telatar. *Information-Theoretic Upper Bounds on the Capacity of Large Extended Ad Hoc Wireless Networks*. IEEE Transactions on Information Theory, vol. 51, no. 3, pages 858–865, Mar. 2005.

[Li *et al.* 2000] Jinyang Li, John Jannotti, Douglas S. J. De Couto, David R. Karger and Robert Morris. *A Scalable Location Service for Geographic Ad Hoc Routing*. In MOBICOM, pages 120–130, 2000.

[Lin & Sharrof 2004] Xiaojun Lin and Ness B. Sharrof. *The Fundamental Capacity-Delay Tradeoff in Large Mobile Ad Hoc Networks.* In Third Annual Mediteranean Ad Hoc Networking Workshop, June 2004.

[Liu & Haenggi 2005] Xiaowen Liu and Martin Haenggi. *Throughput Analysis of Fading Sensor Networks with Regular and Random Topologies*. EURASIP Journal on Wireless Communications and Networking, vol. 2005, Sept. 2005.

[Navas & Imielinski 1997] Julio C. Navas and Tomasz Imielinski. *GeoCast - Geographic Addressing and Routing*. In MOBICOM, pages 66–76, 1997.

[Neely & Modiano 2005] M.J. Neely and E. Modiano. *Capacity and Delay Tradeoffs for Ad Hoc Mobile Networks*. IEEE Transactions on Information Theory, vol. 51, no. 6, pages 1917–1937, June 2005.

[Nelson & Kleinrock 1984] Randolph Nelson and Leonard Kleinrock. *The Spatial Capacity of Slotted ALOHA Multihop Packet Radio Network with Capture*. IEEE Transactions on Communications, vol. 32, no. 6, pages 684 – 694, June 1984.

[Niesen *et al.* 2009] U. Niesen, P. Gupta and D. Shah. *On Capacity Scaling in Arbitrary Wireless Networks*. IEEE Transactions on Information Theory, vol. 55, no. 9, pages 3959–3982, Sept. 2009.

[Ozgur *et al.* 2007] A. Ozgur, O. Leveque and D.N.C. Tse. *Hierarchical Cooperation Achieves Optimal Capacity Scaling in Ad Hoc Networks*. IEEE Transactions on Information theory, vol. 53, no. 10, pages 3549–3572, Oct. 2007.

[Paulraj & Kailath 1993] Arogyaswami J. Paulraj and Thomas Kailath. *Increasing Capacity in Wireless Broadcast Systems Using Distributed Transmission/Directional Reception (DTDR)*. US Patent number 5,345,599, 1993.

[Perkins & Belding-Royer 1999] Charles E. Perkins and Elizabeth M. Belding-Royer. *Ad Hoc On-Demand Distance Vector (AODV) Routing*. In WMCSA, pages 90–100, 1999.

[Plastria 2001] Frank Plastria. *Static Competitive Facility Location: An Overview of Optimisation Approaches*. European Journal of Operational Research, vol. 129, no. 3, pages 461–470, 2001.

[Prommak *et al.* 2004] Chutima Prommak, Joseph Kabara and David Tipper. *Demand-Based Network Planning for Large Scale Wireless Local Area Networks*. In Broadnets, 2004.

[Ramanathan 1997] Ram Ramanathan. *A Unified Framework and Algorithm for (T/F/C)DMA Channel Assignment in Wireless Networks*. In IEEE INFOCOM, 1997.

[Rhee *et al.* 2009] Injong Rhee, Ajit Warrier, Jeongki Min and Lisong Xu. *DRAND: Distributed Randomized TDMA Scheduling for Wireless Ad Hoc Networks*. IEEE Transactions on Mobile Computing, vol. 8, no. 10, Oct. 2009.

[Rozovsky & Kumar 2001] R. Rozovsky and P. R. Kumar. *SEEDEX: a MAC Protocol for Ad Hoc Networks*. In MobiHoc, 2001.

[Santi & Blough 2003] P. Santi and D.M. Blough. *The Critical Transmitting Range for Connectivity in Sparse Wireless Ad Hoc Networks*. IEEE Transactions on Mobile Computing, vol. 2, no. 1, pages 25 – 39, Jan.-Mar. 2003.

[Santi 2005] P. Santi. *The Critical Transmitting Range for Connectivity in Mobile Ad Hoc Networks*. Mobile Computing, IEEE Transactions on, vol. 4, no. 3, pages 310 – 317, May-June 2005.

[Stamatiou *et al.* 2009] Kostas Stamatiou, Franceseo Rossetto, Martin Haenggi, Tara Javidi, James R. Zeidler and Miehele Zorzi. *A Delay Minimizing Routing Strategy for Wireless Multi-hop Networks*. In WiOPT, June 2009.

[Stojmenovic 1999] Ivan Stojmenovic. *Home Agent Based Location Update and Destination Search Schemes in Ad Hoc Wireless Networks*, 1999.

[Stolyar & Viswanathan 2008] Alexander L. Stolyar and Harish Viswanathan. *Self-Organizing Dynamic Fractional Frequency Reuse in OFDMA Systems*. In INFOCOM, pages 691–699. IEEE, 2008.

[Stolyar & Viswanathan 2009] Alexander L. Stolyar and Harish Viswanathan. *Self-Organizing Dynamic Fractional Frequency Reuse for Best-Effort Traffic Through Distributed Inter-Cell Coordination*. In INFOCOM, pages 1287–1295. IEEE, 2009.

[Takagi & Kleinrock 1984] H. Takagi and L. Kleinrock. *Optimal Transmission Ranges for Randomly Distributed Packet Radio Terminals*. IEEE Transactions on Communications, vol. 32, no. 3, pages 246 – 257, Mar. 1984.

[Tanemura 1979] Masaharu Tanemura. *On Random Complete Packing by Discs*. Annals of the Institute of Statistical Mathematics, vol. 31, 1979.

[Tanenbaum 2002] Andrew Tanenbaum. Computer networks. Prentice Hall Professional Technical Reference, 2002.

[Telatar 1999] E. Telatar. *Capacity of Multi-Antenna Gaussian Channels.* European Transactions on Telecommunications, vol. 10, pages 585–595, 1999.

[Toumpis & Goldsmith 2004] S. Toumpis and A.J. Goldsmith. *Large Wireless Networks Under Fading, Mobility, and Delay Constraints.* In IEEE INFOCOM, volume 1, Mar. 2004.

[Vergados *et al.* 2010] Dimitrios Vergados, Aggeliki Sgora, Dimitrios Vergados, Demosthenes Vouyioukas and Ioannis Anagnostopoulos. *Fair TDMA Scheduling in Wireless Multi-hop Networks*. Telecommunication Systems, Dec. 2010. 10.1007/s11235-010-9397-9.

[Watson 1981] David F. Watson. *Computing the n-Dimensional Tessellation with Application to Voronoi Polytopes*. The Computer Journal, vol. 24, no. 2, pages 167–172, 1981.

[Weber *et al.* 2005] S.P. Weber, X. Yang, J.G. Andrews and G. de Veciana. *Transmission Capacity of Wireless Ad Hoc Networks With Outage Constraints*. IEEE Transactions on Information Theory, vol. 51, no. 12, Dec. 2005.

[Weber *et al.* 2008] Steven Weber, Nihar Jindal, Radha Krishna Ganti and Martin Haenggi. *Longest Edge Routing on the Spatial ALOHA Graph*. In IEEE GLOBECOM, pages 223–227, 2008.

[Weber *et al.* 2010] S. Weber, J.G. Andrews and N. Jindal. *An Overview of the Transmission Capacity of Wireless Networks*. IEEE Transactions on Communications, vol. 58, Dec. 2010.

[Weisstein 2008] Eric W. Weisstein. *Triangle Interior.* Wolfram MathWorld, Aug. 2008.

[Xie & Kumar 2004] Liang-Liang Xie and P. R. Kumar. *A Network Information Theory for Wireless Communication: Scaling Laws and Optimal Operation*. IEEE Transactions on Information Theory, vol. 50, pages 748–767, May 2004.

[Xue & Kumar 2006] Feng Xue and P. R. Kumar. *Scaling Laws for Ad Hoc Wireless Networks: an Information Theoretic Approach*. In Foundations and Trends in Networking, volume 1, 2006.

[Zheng & Tse 2003] Lizhong Zheng and David N. C. Tse. *Diversity and Multiplexing: A Fundamental Tradeoff in Multiple-Antenna Channels*. IEEE Transactions on Information Theory, vol. 49, pages 1073–1096, May 2003.

[Zhu & Corson 2001] Chenxi Zhu and M. S. Corson. *A Five-Phase Reservation Protocol (FPRP) for Mobile Ad Hoc Networks*. Wireless Networks, 2001.

[Zorzi & Pupolin 1995] M. Zorzi and S. Pupolin. *Optimum Transmission Ranges in Multihop Packet Radio Networks in the Presence of Fading*. IEEE Transactions on Communications, vol. 43, no. 7, July 1995.